DOPED-MAGNESIUM MANGANESE OXIDE CATHODE FOR RECHARGEABLE MAGNESIUM BATTERIES

NURHIDAYU BINTI HAJI HARUDIN

FACULTY OF SCIENCE
UNIVERSITI MALAYA
KUALA LUMPUR

2021

Universiti Malaya

DOPED-MAGNESIUM MANGANESE OXIDE CATHODE FOR RECHARGEABLE MAGNESIUM BATTERIES

Universiti Malaya

NURHIDAYU BINTI HAJI HARUDIN

DISSERTATION SUBMITTED IN FULFILMENT OF
THE REQUIREMENTS FOR THE DEGREE OF MASTER
OF SCIENCE

DEPARTMENT OF PHYSICS
FACULTY OF SCIENCE
UNIVERSITI MALAYA
KUALA LUMPUR

2021

UNIVERSITI MALAYA

ORIGINAL LITERARY WORK DECLARATION

Name of Candidate: **NURHIDAYU BINTI HAJI HARUDIN**

Matric No: **SMA170058 / 17058861/1**

Name of Degree: **MASTER OF SCIENCE**

Title of Project Paper/Research Report/Dissertation/Thesis (“this Work”):

DOPED-MAGNESIUM MANGANESE OXIDE CATHODE FOR RECHARGEABLE MAGNESIUM BATTERIES.

Field of Study:

EXPERIMENTAL PHYSICS

I do solemnly and sincerely declare that:

(1) I am the sole author/writer of this Work;

(2) This Work is original;

(3) Any use of any work in which copyright exists was done by way of fair dealing and for permitted purposes and any excerpt or extract from, or reference to or reproduction of any copyright work has been disclosed expressly and sufficiently and the title of the Work and its authorship have been acknowledged in this Work;

(4) I do not have any actual knowledge nor do I ought reasonably to know that the making of this work constitutes an infringement of any copyright work;

(5) I hereby assign all and every rights in the copyright to this Work to the University of Malaya (“UM”), who henceforth shall be owner of the copyright in this Work and that any reproduction or use in any form or by any means whatsoever is prohibited without the written consent of UM having been first had and obtained;

(6) I am fully aware that if in the course of making this Work I have infringed any copyright whether intentionally or otherwise, I may be subject to legal action or any other action as may be determined by UM.

Candidate’s Signature Date:

Subscribed and solemnly declared before,

Witness’s Signature Date:

Name:

Designation:

Universiti Malaya

DOPED-MAGNESIUM MANGANESE OXIDE CATHODE FOR RECHARGEABLE MAGNESIUM BATTERIES

ABSTRACT

Magnesium has numerous good characteristics that make it attractive as an electrode material for rechargeable batteries. There are many advantages of Magnesium (Mg) such as available in abundance, ease of handling, low toxicity and environmental friendly. Due to its benefits, magnesium ion battery can be considered as an alternative to lithium in future. In the present work, the improvement electrochemical properties of magnesium-based cathode material, $MgMn_2O_4$ was done by adding calcium (Ca) and strontium (Sr) as dopant i.e $MgMn_{2-x}Ca_xO_4$ and $MgMn_{2-x}Sr_xO_4$. These materials with compositions of x=0.1,0.2,0.3,0.4,0.5 were synthesized by self-propagating combustion method using citric acid as a reducing agent. The precursors obtained were annealed at temperatures of 700°C and 800°C for 24 hours. The electrochemical studies were performed by using Linear Sweep Voltammetry (LSV) and Cyclic Voltammetry (CV) to determine electrochemical stability and properties of the prepared samples using 1M of magnesium trifluoromethane sulfonate $Mg(CF_3SO_3)_2$ electrolyte. The magnesium ion cells were fabricated using the optimized cathode materials and the cell performances were be studied by galvanostatic charge-discharge test. At temperature 700°C, the specific capacity obtained from $MgMn_{1.8}Ca_{0.2}O_4$ and $MgMn_{1.8}Sr_{0.2}O_4$ at first cycle was 60 mAh g^{-1} and 40 mAh g^{-1} respectively. At temperature 800°C, the fabricated cells conveyed the specific capacity of 138 mAh g^{-1} and 160 mAh g^{-1} for Ca and Sr doped samples respectively. Therefore, it can be stated that both Ca and Sr doped systems of $MgMn_2O_4$ based cathode materials enhances a good electrochemical properties thus improving the battery performances.

Keywords: Magnesium ion batteries, cathode materials, Ca doping, Sr doping, $MgMn_2O_4$

Universiti Malaya

KATOD TERDOP-MAGNESIUM MANGAN OKSIDA UNTUK BATERI MAGNESIUM BOLEH DICAS SEMULA

ABSTRAK

Magnesium mempunyai banyak ciri baik yang menjadikannya menarik sebagai bahan elektrod untuk bateri yang boleh dicas semula. Terdapat banyak kelebihan Magnesium (Mg) seperti tersedia dalam jumlah banyak, kemudahan pengendalian, ketoksikan rendah dan mesra alam. Kerana kelebihannya, bateri ion magnesium dapat dianggap sebagai alternatif untuk litium pada masa akan datang. Dalam karya ini, peningkatan sifat elektrokimia bahan katod berasaskan magnesium, $MgMn_2O_4$ dilakukan dengan menambahkan kalsium (Ca) dan strontium (Sr) sebagai dopan iaitu $MgMn_{2-x}Ca_xO_4$ dan $MgMn_{2-x}Sr_xO_4$. Bahan-bahan ini dengan komposisi (x = 0.1,0.2,0.3,0.4,0.5) disintesis dengan kaedah pembakaran menyebarkan sendiri menggunakan asid sitrik sebagai agen pengurangan. Prekursor yang diperoleh dianil pada suhu 700°C dan 800°C selama 24 jam. Kajian elektrokimia dilakukan dengan menggunakan Linear Sweep Voltammetry (LSV) dan Cyclic Voltammetry (CV) untuk menentukan kestabilan elektrokimia dan sifat sampel yang disediakan menggunakan 1M elektrolit magnesium trifluoromethane sulfonate $Mg(CF_3SO_3)_2$. Sel-sel ion magnesium dibuat menggunakan bahan katod yang dioptimumkan dan prestasi sel dikaji dengan ujian pengecasan muatan galvanostatik. Pada suhu 700°C, kapasiti spesifik yang diperoleh dari $MgMn_{1.8}Ca_{0.2}O_4$ dan $MgMn_{1.8}Sr_{0.2}O_4$ pada kitaran pertama masing-masing adalah 60 mAh g^{-1} dan 40 mAh g^{-1}. Pada suhu 800°C, sel-sel fabrikasi menyampaikan kapasiti spesifik 138 mAh g^{-1} dan 160 mAh g^{-1} untuk sampel doping Ca dan Sr. Oleh itu, dapat dinyatakan bahawa kedua-dua sistem doped Ca dan Sr dari bahan katod berasaskan $MgMn_2O_4$ meningkatkan sifat elektrokimia yang baik sehingga meningkatkan prestasi bateri.

Kata kunci: Bateri ion magnesium, bahan katod, dopan Ca, dopan Sr, $MgMn_2O_4$

Universiti Malaya

ACKNOWLEDGEMENTS

First and foremost, praises and thanks to God, the Almighty for His showers a blessings throughout my research work. Alhamdulillah finally, I was able to finish and complete this thesis successfully.

I would to express my sincere gratitude to my supervisors, Prof Dr. Zurina Osman and Prof Dr. Siti Rohana Binti Majid for their precious time, perfect supervision, caring, their patience, encouragement, excellent guidance, priceless advice and their support from the beginning until this final level of my research work, which help me to understand more on this project.

Special thank to my lab mates and friends, Dr Lisani Othman, Diyana Hambali, Dr Khairul Bahiyah Md.Isa and Rosnadiya Rosli who was always willing to help and always give support and assisting me in this project and not forgotten to members of Centre of Ionics (C.I.U.M), Dr Farhana Yusoff, Syaza Amira, Nurul Najla, Nurul shuhada, Nurul Adillah and other members who always give a moral support and their friendship.

I would like to convey thanks to Ministry of Education Malaysia and University of Malaya for provided a provisions of fund and laboratory facilities.

Finally, I would like to express my deeply love to my beloved families and my special best friend for their prayers, endless love and moral support throughout this project. Last but not least, appreciation is expressed to all individual who is directly and indirectly assist me during the preparation of my thesis.

Universiti Malaya

TABLE OF CONTENTS

Universiti Malaya

Universiti Malaya

Universiti Malaya

Universiti Malaya

LIST OF FIGURES

Universiti Malaya

Universiti Malaya

Universiti Malaya

Universiti Malaya

LIST OF TABLES

Universiti Malaya

LIST OF SYMBOLS AND ABBREVIATIONS

θ : theta

A : Ampere

$\mathring{A}$: Armstrong

K : Kelvin

mA : Miliampere

mV : Milivolt

nm : Nanometer

R_{ct} : Charge transfer resistance

V : Volt

ΔE_p : Peak separation

Ω : Ohm

Al : Aluminium

BET : Brunauer-Emmet-Teller

Ca : Calcium

CE : Counter electrode

Co : Cobalt

CV : Cyclic Voltammetry

DME : 1,2 - Dimethoxyethane

DFT : Density Functional Theory

DSC : Differential Scanning Calorimetry

EC : Ethylene Carbonate

EDX : Energy Dispersive X-ray

EIS : Electrochemical Impedance spectroscopy

FESEM : Field Emission Scanning Electron Microscopy

Universiti Malaya

LIB : Lithium Ion Batteries

$LiCoO_2$/LCO : Lithium cobalt Oxide

$LiMn_2O_4$: Lithium manganese Oxide

$LiPeFO_4$: Lithium ion phosphate

LSV : Linear Sweep Voltammetry

Mg : Magnesium

$Mg(CF_3SO_4)_2$: Magnesium trifluromethanesulfonate

$MgCl_2$: Magnesium chloride

$MgCo_2O_4$: Magnesium cobalt oxide

$MgMn_2O_4$: Magnesium manganese oxide

MIB : Magnesium Ion Batteries

Ni : Nickel

OCV : Open circuit voltage

ORR : Oxygen reduction reaction

PP : Polypropylene

Pt : Platinum

PTFE : Polytetrafluoroethylene

RE : Reference electrode

SPC : Self-propagating Combustion

Sr : Strontium

SS : Stainless steel

TEM : Transmission Electron Miscroscopy

TGA : Thermogravimetric analysis

WE : Working electrode

XRD : X-ray Diffraction

Universiti Malaya

CHAPTER 1: INTRODUCTION

1.1 Background of Research

The important field for rechargeable battery in large-scale energy storage includes power energy density, long cycle life, high-energy efficiency and high stability during operation. Since magnesium is abundant in the earth and receives attention in recent years, it can be classified as a secondary rechargeable battery as a promising alternative to lithium ion batteries (LIBs). Magnesium ion batteries (MIBs) offer several advantages over LIBs that are environmental friendliness, low material cost, safety and high rate capability (Aurbach et al., 2001). In battery applications, the most important part in the battery is the cathode as they are responsible for the initial step in the electrochemical process of the battery which can enhance power energy density, capacity of the cell and long life cycle that can give good structural stability (Jarusiripot, 2014; Son et al., 2018; Wang et al., 2018). Therefore, the research works is finding the suitable electrode materials in order to improve the performances of Mg ion batteries. In the effort to find potential host material for magnesium ion batteries, manganese oxide has been considered as an attractive active cathode material because of its low cost, environmental friendliness and good natural abundance (Huie et al., 2015). Manganese based binary oxides create attention due to its high specific capacity (up to 1000 mAh/g) which is much higher than the graphite (Zhao et al., 2015). Magnesium ion has two positive charges (Mg^{2+}), whereas lithium has only one charge (Li^{+}) and this means that it can stores almost twice energy in the same volume. Essentially, the correlation between crystallite size and electrochemical performance in manganese oxides are strongly connected (Yin et al., 2017). Mizuno & Mohtadi (2014) reported that the mobility of Mg^{2+} in compounds such as $MgMn_2O_4$ could be comparable to that of Li^{+} in a typical Li-ion battery (Mohtadi & Mizuno, 2014).

However, the $MgMn_2O_4$ have a poor tetragonal structural stability as a result of existence of high spin Mn^{3+} ion in $MgMn_2O_4$ leading to the Jahn-Teller effect thus

Universiti Malaya

delivered a low discharge capacity (Banu et al., 2019). Jin et.al stated that the effect of doping on the $MgMn_2O_4$ surface stability on the replacement of Ni instead of Mn effectively reduced the John-Teller distortion (Jin et al., 2016). Based on the literature, many research groups have reported that ion doping onto cathode materials could improve the electrochemical performance of the batteries. Liu et al. (2015) reported that doping of Sr^{2+} for Ba^{2+} in $LnBaCo_2O_{5+d}$ could potentially improve the electrochemical performance of cathode materials due to their higher electrical conductivity and catalytic activity for the oxygen reduction reaction (ORR) (Liu et al., 2015). Wang et al. (2018) stated that Ca-doped $Li_4Ti_5O_{12}$ (LTO) materials could improve the electrochemical performances at higher charge−discharge rates and assigned to the improved electronic conductivity (Wang et al., 2018). In the previous studies, Titanium (Ti), Nickel (Ni) and Cobalt (Co) have been used as the doping elements in $MgMn_2O_4$ (Zainol et al., 2018; Banu et al., 2019). In this study, Strontium (Sr) and Calcium (Ca) doped-$MgMn_2O_4$ based cathode materials are prepared and studied in order to stabilize the structural properties and to improved the electrochemical performances of the Magnesium battery.

The synthesis procedure is the one of the main important part in handling the materials. Various synthesis methods been used in material preparation like solid-state reaction, sol-gel method, self-propagating combustion (SPC), ion-exchange hydrothermal synthesis and ball milling (Glass, 2017; Liu et al., 2013; Mosa & Aparicio, 2015; Kim et al., 2008). SPC method is a simple method, fast and inexpensive that can produce fine particle size.

The cathode materials prepared by using self-propagating combustion method with a varied stoichiometry composition (x= 0.1,0.2,0.3,0.4,0.5). Structural, morphological and thermal properties was investigated using Thermogravimetric Anlaysis (TGA), X-Ray Diffraction (XRD), Field Emission Scanning Electron Microscopy (FESEM), Energy Dispersive X-ray (EDX), Electrochemical Impedance Spectroscopy (EIS) and Brunauer–

Universiti Malaya

Emmett–Teller (BET), Transmission Electron Microscope (TEM) and Raman Spectroscopy. Electrochemical properties of the cathode materials will be studied using Linear sweep voltammetry (LSV), Cyclic Voltammetry (CV) and charge discharge profiles.

1.2 Objectives of the Present Work

The objectives of this work are to study the battery performances using Mg-based cathode materials with strontium and calcium doped elements. More specifically, the detailed objectives are:

1) To study the effect of doping elements (Ca and Sr) on the structure of $MgMn_2O_4$ through XRD measurements.
2) To investigate the chemical and physical properties of doped–$MgMn_2O_4$ cathode materials using TGA, FESEM, EDX, EIS, TEM, Raman spectroscopy and BET.
3) To evaluate the electrochemical properties of optimized Ca and Sr doped $MgMn_2O_4$ as cathode materials for magnesium batteries.

1.3 Organization of the Dissertation

This dissertation is organized into eight chapters. The first chapter provides the background of research work and the objectives of the study.

Chapter two presents the overview of the Mg-based cathode materials in Mg battery application including the mechanism of the electron and ion transfer between anode, electrolyte and cathode part in the basic application of the battery.

Chapter three discusses the sample preparation including material synthesis done by the self-propagating combustion method. The characterization are done by using Thermogravimetric Anlaysis (TGA), X-Ray Diffraction (XRD), Field Emission Scanning Electron Microscopy (FESEM), Energy Dispersive X-ray (EDX), Electrochemical Impedance Spectroscopy (EIS), Brunauer–Emmett–Teller (BET), Transmission Electron Microscope (TEM) and Raman spectroscopy. The electrochemical studies such as Linear

Universiti Malaya

sweep voltammetry (LSV), Cyclic Voltammetry (CV) and battery performances profiles also be studied.

Chapter four until seven present the results and discussion of all the results in the experiment. The results of TGA, FESEM, TEM, XRD, EDX, EIS, BET and Raman spectroscopy were present in each of composition (x = 0.1, 0.2, 0.3, 0.4, 0.5) with different temperatures of 700°C and 800°C of the doped material (Sr and Ca) sample. The last part of this chapter is discussed about the electrochemical studies of LSV, CV and charge discharge profile of magnesium battery.

Chapter eight presents the summary and conclusion that have been made for the characteristics of $MgMn_2O_4$ - doped Sr and Ca and a few suggestions for future work.

Universiti Malaya

CHAPTER 2: LITERATURE REVIEW

2.1 Chapter Overview

This chapter presents the overview of Mg-battery application including the Mg-based cathode materials which are composed of many types of cathode materials such as $MgMn_2O_4$, $MgCO_2O_4$ and chevrel compounds. This work focuses on the $MgMn_2O_4$ with doping elements calcium and strontium. An overview of method on preparation of the cathode materials has been stated. The working principle and mechanism of Mg batteries application will be discussed.

Universiti Malaya

2.2 Introduction of Batteries

Battery is defined as an electrochemical storage device that transforms electrochemical energy directly into electrical energy. A battery consists of one or more of these cells, connected in series or parallel, or both, depending on the required output voltage and capacity. Figure 2.1 shows the basic major component of batteries which classified as positive electrode (Cathode), negative electrode (Anode) and electrolyte.

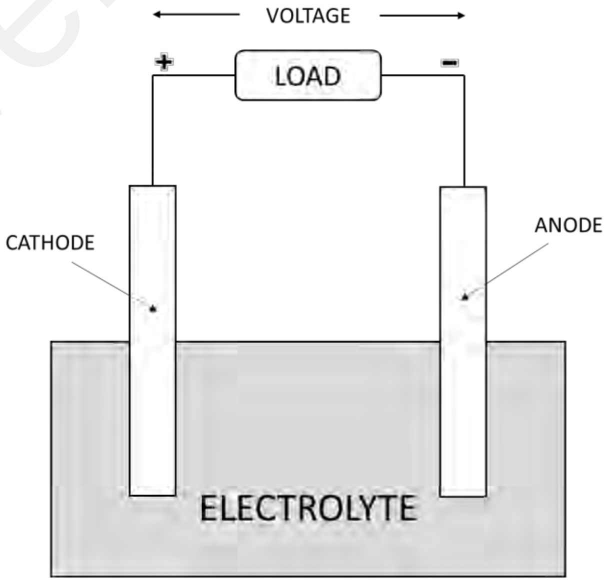

Figure 2.1: Schematic diagram of basic component of batteries.

2.3 Classification of Batteries

Based on the reversibility of electrochemical reactions, batteries can be specifically classified into primary or non-rechargeable batteries and secondary or rechargeable batteries.

2.3.1 Primary Batteries

In the primary batteries, the active materials undergo irreversible chemical reaction. Primary battery sometimes also called single-use or "throw away" batteries because they have to be disposed after used and cannot be recharged.

Disposable batteries are proposed to be used once and discarded. These batteries most commonly used in portable devices with low current drain, being used discontinuously. Disposable Primary Cells cannot be reliably recharged, since the chemical reactions are irreversible and active materials may not return to their original forms (Types of Battery- Primary & Secondary, 2018).

For primary batteries, the positive and negative active materials can be referred to as cathodic anodic reactants respectively. It is not to classify fuel cells as a primary batteries and consequently but an additional requirement of the definition is that reactants and products are contained within battery (Types of Battery- Primary & Secondary, 2018).A primary battery is thus a completely independent power source requiring neither an external power supply nor an external source of active materials.

2.3.2 Secondary / Rechargeable Batteries

Mostly secondary batteries are called rechargeable batteries because they can be recharged and reused multiple times. Discharged state is the main part for being assembled with active materials. Rechargeable batteries or secondary cells can be recharged by applying electric current, which the chemical reactions are reversible.

Universiti Malaya

Devices to supply the appropriate current are called chargers or rechargers (Types of Battery- Primary & Secondary, 2018).

Lithium batteries, magnesium batteries and sodium batteries can be classified as a secondary batteries. Lithium ion batteries already been practical as small power supplies for devices such as mobile phones and notebook computers. Secondary lithium batteries nowadays were famous in a research world as a candidate for secondary cells with a high energy density. In addition, high demand for large power supplies such as power supplies for automobiles, including electric vehicles, hybrid vehicles, and power supplies for distributed power storage and so on (Nishi, 2001).

What becomes a problem here is constraints on the annual production of lithium, which is the charge transporter within batteries, and transition metals such as cobalt for redox couples that have the function of maintaining charge neutrality for cathodes. In research and development for the next generation of secondary batteries, known as post-lithium ion secondary batteries, extensive investigations are being carried out on batteries that do not use rare metals. However, the dendritic formation of lithium during the charging process is predictable, and it causes several problems, such as poor safety characteristics, poor cyclability, and a requirement for a long charging time.

One of the candidates for the next generation of secondary batteries that has been proposed to meet this demand is the magnesium ion battery that uses magnesium instead of lithium as the charge carrier and iron, manganese and other transition metals instead of cobalt for redox couples, and such batteries are being investigated. We can expect that the environmental impact and cost will be greatly reduced.

Universiti Malaya

2.4 Magnesium Battery

Magnesium batteries can be categorized as secondary batteries or in other word can called as rechargeable batteries. Magnesium batteries are batteries with magnesium as the active element at the anode of an electrochemical cell with active topics of research nowadays specifically to replace Li-ion batteries (Mohtadi & Mizuno, 2014). Magnesium battery (MB) is a type of original batteries, which the negative electrode used is magnesium, and the positive electrode can be metal or non-metallic oxide. In the existing varieties, there are magnesium-manganese dry batteries, which are similar to the ordinary zinc-manganese batteries that can be discharged at any time. There are also reserve batteries, which can be stored for long time and the temporary use of water makes it possible to utilize (Tang et al., 2018). Magnesium-ion technology is capable for several reasons. Firstly, due to the natural abundance of magnesium in the earth's crust, approximately 104 times that of lithium, its incorporation into electrode materials is inexpensive. Secondly, magnesium is more atmosphere stable and has a higher melting (922 K) point than lithium (453.7 K), making it safer relative to lithium (Yoo et al., 2013). The divalent nature of magnesium ions also presents a potential advantage in terms of volumetric capacity (3833 mAh cm^{-3} for Mg vs. 2046 mAh cm^{-3} for Li).

2.5 Working Principle of Battery

A Mg-ion battery usually refers to a secondary battery in which energy is stored chemically through redox reactions that employ magnesium intercalation between the positive (cathode) and the negative (anode) electrodes i.e. as a battery is charged and discharged the magnesium ions move back and forth between the cathode and the anode because of this they are also referred as "Rocking-chair" batteries (Liden & Reddy, 2004). The cathode acts as a positive electrode which accepts the electrons while reducing and the anode acts as a negative electrode which donates the electrons and oxidizes during the

Universiti Malaya

discharge cycles. The electrodes do not touch each other but are electrically connected by the electrolyte while the separator prevents the mixing between them but allows ions to flow.

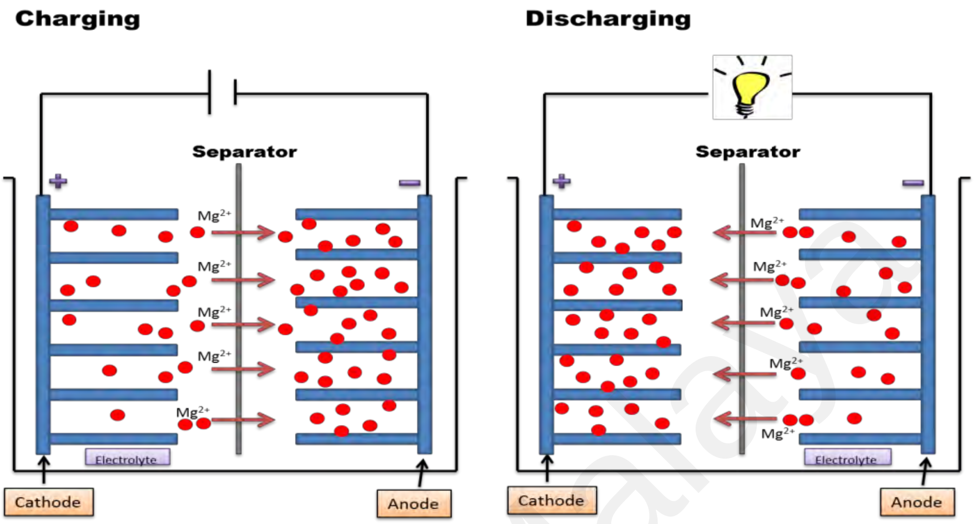

Figure 2.2: Working principle of magnesium ion batteries.

2.6 Cathode Materials

There are two electrodes in the ion battery, namely, the negative electrode which can also call anode that donate an electron during cell charge, and the cathode or the positive electrode, which accepts electrons during discharging process. Between these electrodes, the major role in ion battery performance described as cathode. The current and mostly used intercalation cathode is a solid host network with ability of storing guest ions via insertion and removing them reversely.

In order to achieve excellent electrochemical performances in batteries, several conditions on cathode materials should be satisfied as listed below (Whittingham, 2004):

1. It should offer a high electrode potential for a high output potential;
2. The electrode potential should be stable for a stable output potential;
3. High capacity and high energy density;

Universiti Malaya

4. High ion diffusion coefficient, highly stable electrode interface for high rate performance;

5. High structural stability during cycling, for perfect cycle performance;

6. High electronic conductivity and ion conductivity;

7. Low price and environmental-friendly.

2.6.1 Lithium-based Cathode Materials

2.6.1.1 $LiCoO_2$

John Goodenough was the person who recognized and introduced $LiCoO_2$ (LCO) which form a layered transition metal oxide cathodes (Mizushima et al., 1981). SONY Corporation originally discovered $LiCoO_2$ in 1991 and this material is still used in the majority of commercial Li-ion batteries. Its produce a layered structure which Co and Li, located in octahedral sites in layers and form a hexagonal symmetry as shown in Figure 2.3. LCO is a very famous cathode material because of its relatively high theoretical specific capacity of 274 mAh g^{-1} (Nitta et al., 2015). The major limitations of $LiCoO_2$ are low thermal stability, high cost and fast capacity fading during cycling at high current. LCO cathodes are expensive because of the Co are costly. The thermal stability of LCO is very low which refers to exothermic release of oxygen when a lithium metal oxide cathode is heated above a certain point, resulting in a runaway reaction in which the cell can burst into flames (Sarkar & Jou, 2002). Thermal runaway is an important role in the Li-ion batteries application resulting, for example, in the grounding of all Boeing 787 airplanes in 2013 (Williard et al., 2013). While this issue is general to transition metal oxide intercalation cathodes, LCO has the lowest thermal stability of any commercial cathode material (Shafey, 2018).

Universiti Malaya

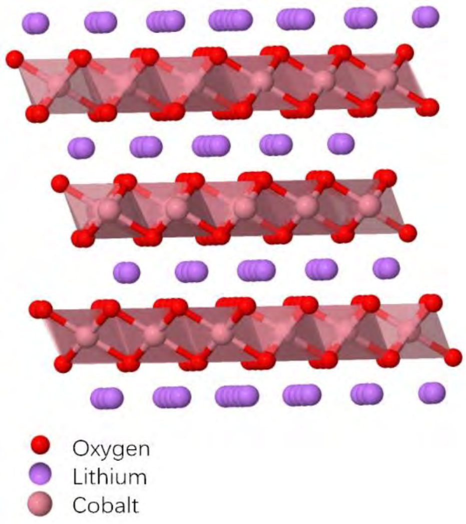

Figure 2.3: Structure of $LiCoO_2$ (“Lithium Cobalt Oxide – $LiCoO_2$,” 2020).

2.6.1.2 $LiMn_2O_4$ (Spinel)

$LiMn_2O_4$ spinel have been introduced by Thackery et al. in 1984. The structure of $LiMn_2O_4$ is a cubic spinel structure with a space group Fd-3m and lattice parameter of a = 8.2449 Å at room temperature. $LiMn_2O_4$ spinel is one of the attractive cathode material for Li-ion rechargeable batteries with a three-dimensional framework because of the advantages, such as environmental friendliness, cost efficiency, and low toxicity compared to other lithiated transition metal oxides, such as lithium cobalt oxide or lithium nickel oxide (Michalska et al., 2011; Iturrondobeitia et al., 2012; Arora et al., 1998). It consists of a cubic close-packing arrangement, which consist oxygen ions at the 32e sites, the Li ions at the tetrahedral 8a sites, and the Mn^{3+} and Mn^{4+} ions at the octahedral 16d sites. This kind of arrangement shows a cubic spinel-type structure (Anufrienko & Rojo, 2002).

Universiti Malaya

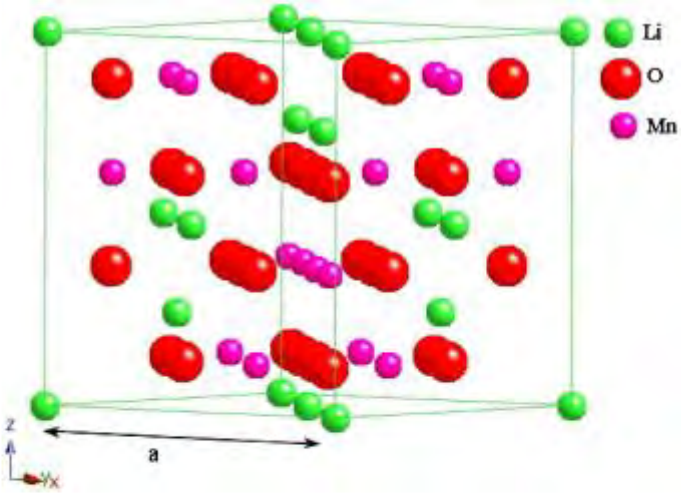

Figure 2.4: Structure of $LiMn_2O_4$ (Xia et al., 2012).

$LiMn_2O_4$ exhibits an operating voltage of 4.1 V and its theoretical capacity is 148 mAh g^{-1} (Julien & Massot, 2003). The reversible capacity is about 140 mAh g^{-1}. Li ions can also reversible in the $LiMn_2O_4$ structure with a potential of 3.0 V although working on the same Mn^{4+}/Mn^{3+} redox couple caused by a cooperative Jahn-Teller orbital order on Mn^{3+} ions (Yang et al., 2017). Even though $LiMn_2O_4$ spinel and its derivatives show promising features as the cathodes of high-power lithium batteries for transportation applications, a slow capacity fade has been encountered in the high voltage range, particularly at elevated temperatures (>50 °C). The loss of capacity can be attributed to several possible factors (Whittingham, 2004).

2.6.1.3 $LiPeFO_4$

$LiFePO_4$ was discovered as a cathode material by Padhi et al. (1997) which produce crystallizing in the olivine structure (Padhi et al., 1997). There have been exciting developments in $LiFePO_4$ cathode material for high-power lithium ion batteries in the past decade (Lee & Cho, 2011). Compared with the commercially used cathode material $LiCoO_2$, $LiFePO_4$ cathode material has several advantages, including low material cost, environmental friendliness, no toxicity, good chemical stability, high theoretical capacity and thermal stability at high temperature. This cathode material was applied for Li-ion

Universiti Malaya

batteries for high power applications. The discharge potential of pure $LiFePO_4$ is around 3.45 V versus (Li/Li^+), and the theoretical capacity is 170 mAh g^{-1} (Bi et al., 2013). It would therefore be advantageous to use large particles structure (of $LiFePO_4$ for practical manufacturing purposes if the intrinsic properties of the active material can be improved by new methods such as doping or surface coating (Satyavani et al., 2016).

Shuzhong et al. (2006) reported that in their work, they prepared Al-doped $LiFePO_4/C$ composite cathode materials using polymer-network synthesis technique (Shuzhong et al., 2006). They observed that Al-doped $Li\text{-}FePO_4/C$ composite cathode materials have a high initial capacity (124 mAh g^{-1}), good cycle stability and excellent low temperature performance. The electrical conductivity of $LiFePO_4/C$ materials obviously improved by doping Al. The better electrochemical performances of Al-doped $LiFePO_4/C$ composite cathode materials have a connection with its conductivity.

2.6.2 Magnesium-based Cathode Materials

Finding cathode materials with acceptable kinetics has become the major challenge for the development of rechargeable Mg batteries. In nowadays research, Mg based cathode materials for mg ion batteries is still in progress. So, the cathode materials from previous literature have been summarized in Table 2.1.

2.6.2.1 $MgMn_2O_4$

Manganese oxides are another promising family of magnesium ion batteries (MIB) cathode materials. Manganese oxides are a structurally rich class of materials providing layered, tunneled, or spinel structured materials (Sutin & Gütlich, 1985; Suib, 2008). The spinel magnesium manganese oxide ($MgMn_2O_4$) is one of the Mg based cathode materials with theoretical capacity of 272 mAh g^{-1} that promising cathode candidate for future application in high volumetric magnesium-ion batteries (Truong et al., 2017). $MgMn_2O_4$

Universiti Malaya

has a tetragonal structure different from the typical cubic structure of spinels, due to distortion induced by the strong Jahn-Teller effect of Mn^{3+} (Malavasi, Ghigna, et al., 2002). A cation migration is often observed in $MgMn_2O_4$, in which Mg^{2+} and Mn^{3+} exchange positions due to their similar ionic radii (0.63 Å for tetrahedral Mg^{2+} and 0.72 Å for octahedral Mn^{3+} respectively (Shannon & Prewitt, 1969). The exchange makes a changes of the structure from tetragonal to cubic, termed an under high temperature and high pressure conditions.

From previous studies, researchers have demonstrated strong correlations between crystallite size and electrochemical performance in manganese oxides (Truong et al., 2017). The first systematic study is $MgMn_2O_4$ as a cathode material in MIB. The materials were synthesized by a modified Pechini method and annealing temperature was used to control crystallite size of the products. The smaller crystallite sized material delivered higher capacity, which is 171 mAh g^{-1} after 30 cycle as tabulated in Table 2.1.

Cations doping has been proved as an effective method to improve the structural properties and cycle performances of cathode materials (Wang, Liu, Wang, Gao, & Zhang, 2013). Recently, Jin et al. (2016) studied the effect of Ni doping on the $MgMn_2O_4$ surface stability using density functional theory (DFT) and reported the replacement of Ni instead in Mn effectively reduced the John-Teller dis-tortion (Jin et al., 2016). There are several research related to doping $MgMn_2O_4$ such as Nickel (Ni), Cobalt (Co) and Titanium (Ti) that listed in Table 2.1.

Universiti Malaya

Table 2.1: Summary of the Mg-based cathode materials performances.

Cathode materials	**Electrolyte**	**Initial capacity (mAh g^{-1})**	**Operating voltage (V)**	**Cycle life**	**References**
$MgCoSiO_4$	0.25M $Mg(AlCl_2 EtBu)_2$ /THF	300	1.6	30 cycle	(Truong, Devaraju, & Honma, 2017)
$MgFeSiO_4$	0.1M $Mg(TFSI)_2$ in Acetonitrile (AN)	330	2.4	5 cycle	(Orikasa et al., 2014)
Ti-doped $MgMn_2O_4$	MgTFSI in 1:1 ethylene carbonate (EC) and propylene carbonate (PC)	52	3.0	10 cycle	(Zainol et al., 2018)
Three dimensional hollow spheres - $MgMn_2O_4$	1M $MgSO_4$	261.5	3.2	360 cycle	(Tao et al., 2018)
$MgMn_{2-x}M_xO_4$ (M = Ni,Co)	1M Magnesium nitrate ($Mg(NO_3)_2.6H_2O$)	Ni = 46 & Co = 24	1.0	-	(Banu et al., 2019)

Universiti Malaya

Table 2.1, continued,

Cathode materials	**Electrolyte**	**Initial capacity (mAh g^{-1})**	**Operating voltage (V)**	**Cycle life**	**References**
$MgMnSiO_4$	0.25 M $Mg(AlBu_2Cl_2)_2$/THF	164.1	2.0	20 cycle	(Sun & Jiang, 2014)
$MgFePO_4F$	0.5M TFSI in AN	55	2.2	10	(Murgia, 2018)
$MgMn_2O_4$	0.5 M $Mg(ClO_4)_2$ in acetonitrile	171	2.8	30	(Truong, Devaraju, Tran, et al., 2017)

2.6.2.2 $MgCo_2O_4$

Muldoon et al. (2014) surveyed some candidates among many cathode materials by chemical intercalation experiments using typical electrochemical methods (Muldoon et al., 2014). They proposed RuO_2 and Co_3O_4 as the candidates that expected to improved performances of Mg ions. These materials were also studied by Sutto & Duncan et al. (2012) to demonstrate the redox capability in a different non-aqueous electrolyte system (Sutto & Duncan, 2012; Shiga et al., 2013). According to their studies, Co_3O_4 did not allow for a sufficient magnesium insertion for several reasons, which are strong interactions between Mg^{2+} cations and oxygen atoms in the host lattice and a host structural changes and particle size after magnesiation. The initial capacity of 74 mAh g^{-1} was observed at around 1.5–2.0 V against Mg and a capacity retention of 60% after 30 cycles was reported. As such, the magnesiated Co_3O_4 did not show the high capacity obtained in the Li system.

Universiti Malaya

Ichitsubo et al. (2011) studied disordered $MgCO_2O_4$ (precisely, $(Mg_{1-x}Co_x)(Mg_{1-y}Co_yO_4)$ with high electrical conductivity. As they compared between spinel-phase Co_3O_4 and disordered spinel $MgCo_2O_4$, $MgCo_2O_4$ possess high open circuit voltage (OCV) by about 2.0 V at the initial stage just after a constant voltage. One reason for this increase could be resulting from an enhanced Mg^{2+} ion diffusion compared to the ordered structure (Ichitsubo et al., 2011).

The spinel material could not maintain high initial voltage (over 3.0 V vs Mg) during the rest time following charging as a continuous voltage decay was observed. This meant that these cathode materials possessed high polarization due to slow diffusion of Mg^{2+} in the host lattice. Thus, even for these materials it was not possible to discharge the battery at a higher voltage over 3.0 V vs Mg. Although the performance of these cathodes was not stable at high voltage, the introduction of the disordered structure into the Mg battery cathode is indeed a good idea to neutralize the local charge density occurring between inserted Mg^{2+} ions and the host lattice, and accelerate intrinsic Mg^{2+} ion diffusion (Mohtadi & Mizuno, 2014).

2.7 Calcium doping

Calcium is an alkaline earth metal that placed in group 2 in periodic table with the symbol Ca and atomic number of 20. Calcium is a reactive metal that forms a dark oxide-nitride layer when exposed to air. The physical and chemical properties are most similar to its heavier homologues strontium and barium. Calcium can react with water more quickly than magnesium and less quickly than strontium to produce calcium hydroxide and hydrogen gas.

Carbon coating and elemental doping are useful to improve the material weaknesses to a certain scope. However, nanostructures can also show weaknesses, including side reactions and volume swelling (Lefèvre et al., 2017; Zhao et al., 2016). Normally, the

Universiti Malaya

criteria of chosen dopant ions are should be either physically larger than the substituted ion, representing a strategy that can enhance the lithium-ion diffusion by means of lattice expansion and should possess higher oxidation states than that of the substituted ions themselves.

It is proven from the several studies that the metal doping can be used to stabilize the layered framework and improve the cyclability of layered materials. Elemental doping such as Mg^{2+}, Al^{3+}, Cr^{3+}, Ti^{3+}, or other ions is much more straightforward and useful for improving the properties of lithium-ion batteries (Feng et al., 2017). Chen et al. (2017) reported that Ca-doping into $LiNi_{0.8}Co_{0.1}Mn_{0.1}O_2$ can improve the electrochemical performance by decreasing the degree of Li/Ni cation maxing (Chen et al., 2017).

Wang et al. (2018) also reported calcium doping for lithium batteries. They stated that use of ionic doping in particular could effectively modify the intrinsic electronic conductivity and/or Li^+ ion diffusion coefficients within $Li_4Ti_5O_{12}$ structures, thereby leading to higher capacities and improved rate capabilities. The Ca doped $Li_4Ti_5O_{12}$ have a good electrochemical performance at high charge discharge rates and high electronic conductivity. They delivered capacity 122.4 mAh g^{-1} at 20C and fastest lithium-ion diffusivity (Wang et al., 2018). Therefore, in this work Ca doping have been used as our dopant for $MgMn_2O_4$ cathode material in order to get the better electrochemical performance and high rate of capability.

2.8 Strontium doping

Strontium is an alkaline earth metal placed in a group 2 in periodic table with the chemical element of Sr and atomic number of 38. Strontium is a soft silver-white yellowish metallic element that is highly chemically reactive. The metal forms a dark oxide layer when it is exposed to air. Strontium has physical and chemical properties similar to those of its two vertical neighbors in the periodic table, calcium and barium.

Universiti Malaya

Strontium also has a relatively large ionic radius, which is 255 ppm as compared to magnesium (Mg) which is 173 ppm. Qu et al. (2017) stated that if strontium are substitutional doping into the Li_2FeSiO_4 lattice, it could expand the lattice volume and provide more space for Li^+ mobility, which can improve Li^+ diffusion. It would be expected that strontium cation doping can enhance the electrochemical performance of Li_2FeSiO_4/C more significantly compared with magnesium cation doping (Qu et al., 2017).

Nie et al. (2006) reported that the Sr-doped $A_{2-\alpha}A'_{\alpha}BO_4$ (A = Pr, Sm, A' =Sr; B=Mn, Ni) has better cathodic properties than the undoped materials (Nie et al., 2006). Some researchers have investigated strontium-doped $AA'B_2O_{5+\delta}$ potentially improve the conductivity of layered perovskite oxides with good aspects of $LnBaCo_2O_{5+\delta}$ oxides (Zhao et al., 2010). In these studies, Sr doping is used as a dopant for magnesium based cathode materials ($MgMn_2O_4$) with different composition or amount (x=0.1, 0.2, 0.3, 0.4, 0.5) and being synthesized using self-propagating combustion method.

2.9 Methods of synthesizing cathode materials

2.9.1 Self-propagating combustion method

Self-propagating combustion (SPC) is a method for producing both inorganic and organic compounds by exothermic combustion reactions in solids of different nature. Reactions can occur between a solid reactant coupled with either a gas, liquid, or other solid. If the reactants, intermediates, and products are all solids, it is known as a solid flame (Borovinskaya et al., 2012). If the reaction occurs between a solid reactant and a gas phase reactant, it is called infiltration combustion. Since the process occurs at high temperatures, the method is ideally suited for the production of refractory materials including powders, metallic alloys, or ceramics.

Universiti Malaya

Kamarulzaman et al. (2013) reported that SPC is a simple, fast and inexpensive synthesis method, which yields fine particle size without the need for grinding (Kamarulzaman et al., 2013). In SPC, a huge amount of exothermic energy is produced during the reaction between the oxidizing agents and an appropriate reducing agent; therefore, there is no need for large amounts of external energy supplied to the reactants in the process. The total amount of the component nitrates used is less than 5 g based on stoichiometry calculations. The limitation with regard to the amount of material is clue to safety reasons, as the reaction is violent and occurs at high temperatures; it will only be safe if the reactants are prepared in small amounts.

2.9.2 Solid state reaction

Solid-state reaction is a technique used to deliver chemical structures by reactions carried out at extreme conditions, such as high temperature and pressure. This technique is generally used for the mass production advanced structures. The method is simple and easy to industrialize. However, the prepared product has non-uniform particles in non-crystalline form and the synthesis time is long. The lengthy and complex procedures requiring repeated grinding and calcination lead to the formation of larger particles with lower electrochemical performance (Satyavani et al., 2016).

2.9.3 Sol gel method

Sol-gel synthesis is a synthesis that can make particles smaller and spread more homogeneously (Purwamargapratala et al., 2019). In sol-gel synthesis, the surfaces of the powder products are controlled from the starting process. In addition, sol-gel synthesis is a low cost process and does not require high processing temperature and powders produced have the advantages of precise stoichiometry control, high purity, uniform structure and very small size. In sol-gel synthesis, a slow heating rate during calcination

Universiti Malaya

causes rougher and relatively less porous structure. On the other hand, with a high heating rate, more porous structure can be obtained (Satyavani et al., 2016; Hench & West, 1990).

Some researchers used sol gel method as their synthesis techniques. Daochuan Jiang et al. (2015) studied the $LiNi_{0.9}Co_{0.05}Mn_{0.025}Mg_{0.025}O_2$ cathode material by a sol–gel method for lithium-ion batteries. They stated that sol–gel method can be highly homogenous polycrystalline material and it is produced because of the molecular level mixing of the starting materials, and the lower temperature and shorter preparation time are required. The synthetic route of the sol–gel method is simple and straightforward compared with solid-state method (Jiang et al., 2015).

Universiti Malaya

CHAPTER 3: METHODOLOGY

The overall research methodology used in this work was summarized as flowchart in Figure 3.1. The first step was the sample preparation by using self-propagating combustion method. Then, followed by annealing process by using Thermogravimetric analysis (TGA). Then, the characterizations were carried out on the samples which include X-Ray Diffraction (XRD), Field Emission Scanning Electron Microscopy (FESEM), Energy Dispersive X-ray (EDX), Brunauer–Emmett–Teller (BET) testing, Raman spectroscopy and Transmission Electron Microscopy (TEM) analysis. The electrochemical studies include Linear sweep voltammetry (LSV), Cyclic Voltammetry (CV), charge discharge and Electrochemical impedance spectroscopy (EIS) of fabricated Mg batteries were also be carried out.

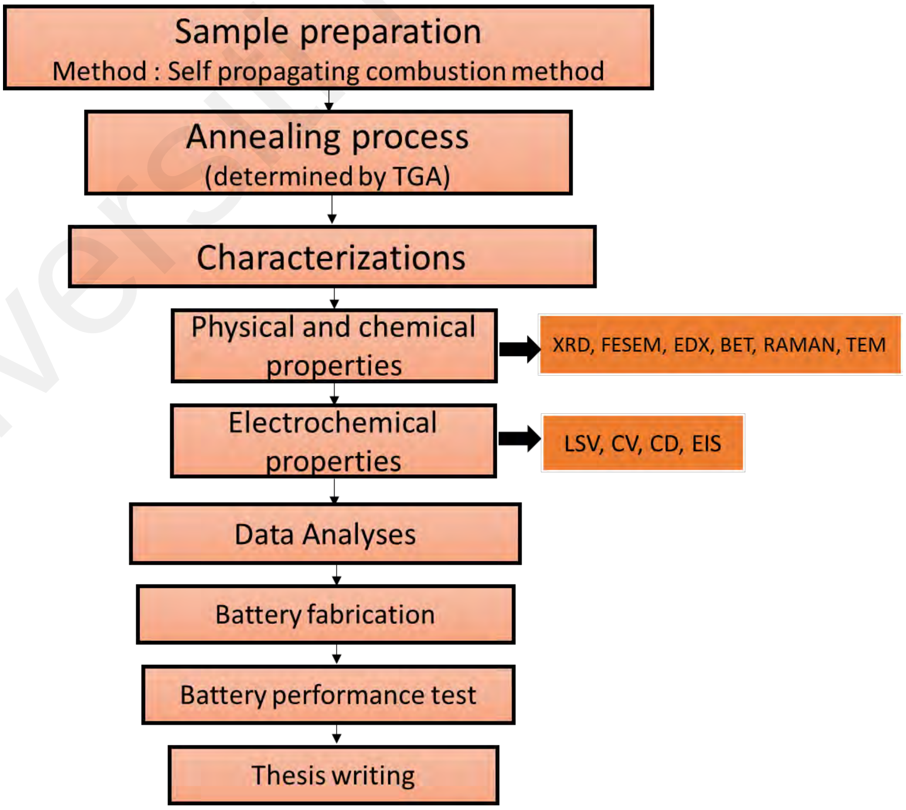

Figure 3.1: Research methodology flowchart.

University of Malaya

3.1 Sample preparation (Self - propagating combustion method)

Cathode material of $MgMn_{2-x}O_4$, $MgMn_{2-x}Sr_xO_4$ and $MgMn_{2-x}Ca_xO_4$ ($x = 0.1, 0.2, 0.3, 0.4, 0.5$) were synthesized by self-propagating combustion method with adjustable temperature of 200°C-250°C. The self-propagating combustion method involves the dissolution of starting materials in deionized water. Starting materials which are Mg nitrate hexahydrate ($Mg(NO_3)_2.6H_2O$), Manganese (II) nitrate hydrate ($Mn(NO_3)_2.xH_2O$), Calcium Nitrate Tetrahydrate, $CaN_2O_6.4H_2O$ (Ca-doped) and Strontium (II) nitrate, Sr $(NO_3)_2$ (Sr-doped) were dissolved in a deionized water and form a mixture. The mixture will be slow heated after adding a citric acid ($C_6H_8O_7$) which act as combusting agent with an adjustable temperature around 200°C - 250°C. The mixtures will combust when it has reached its ignition conditions. The method is summarized in the Figure chart 3.2 below.

Universiti Malaya

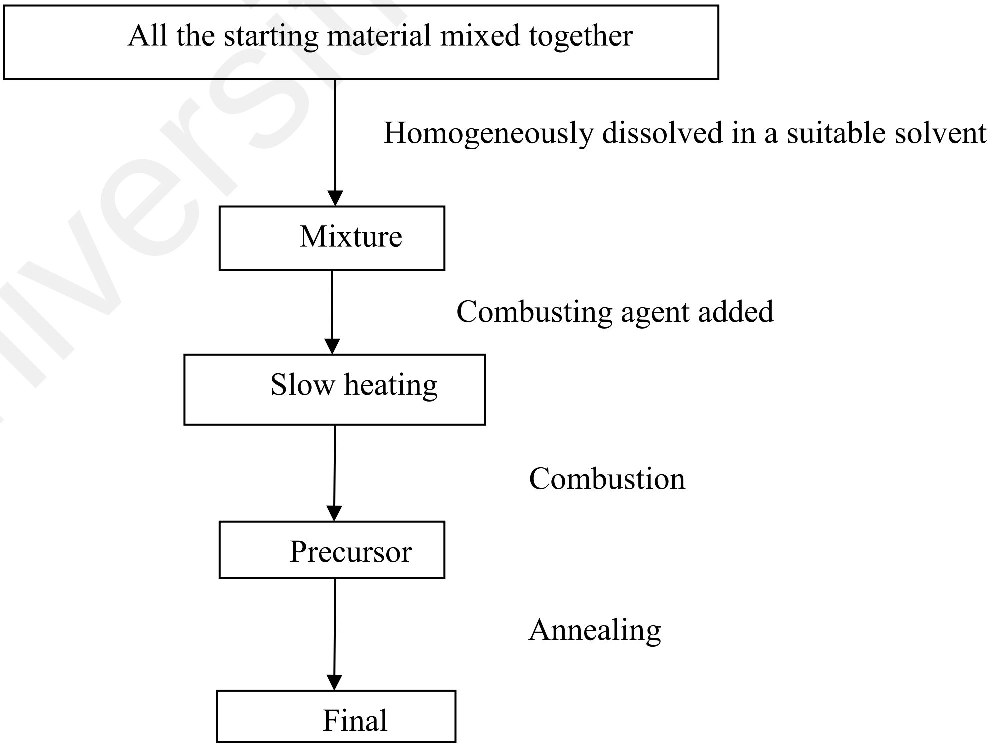

Figure 3.2: Self – propagating combustion method for $MgMn_{2-x}O_4$, $MgMn_{2-x}Sr_xO_4$ and $MgMn_{2-x}Ca_xO_4$.

3.2 Materials characterization and testing: Principle. Instrumentation and Measurements

The properties of the materials were characterized by Simultaneous Thermogravimetric Analyzer (TGA), X–ray diffraction (XRD), Field Emission Scanning Electron Microscope (FESEM), energy dispersive X-ray spectroscopy (EDX) , Raman spectroscopy, Transmission Electron Microscopy (TEM), Brunauer-Emmett-Teller (BET) and Electrochemical impedance spectroscopy (EIS).

3.2.1 Thermogravimetric Analyzer (TGA)

Thermogravimetric Analysis (TGA) and Differential Scanning Calorimetry (DSC) were performed in order to study the thermal characteristics of the materials and to determine the annealing temperature for the precursors. The TGA provides information of the weight loss at different stages in different range of temperature. From this temperature, we can identify the stable temperature for samples to be annealed. The thermal analysis of the precursor $MgMn_2O_4$, $MgMn_{2-x}Ca_xO_4$ and $MgMn_{2-x}Sr_xO_4$ samples were performed by using SETARAM SETSYS Evolution 1750 (TGA-DSC 1500) as shown in Figure 3.3.

Figure 3.3: Instrumentation of TGA/DSC (SETARAM SETSYS Evolution 1750 (TGA-DSC 1500)).

Universiti Malaya

The samples were weighted about 12-15 mg in an alumina crucible for measurement purposes. The standard TGA uses a pan balance where the references crucible are supported by a pair of thermocouple. They are placed carefully with the balance load. Then, the sample will heat at 10°C / min within a temperature range from 30°C to 1000°C. The furnace is heated and cooled based on the programmed thermal cycle setup. The differential thermocouple output (DSC signal) and balance output (TGA signal) are recorded, displayed on a PC monitor and data was collected. After data was analyzed, the precursor was annealed at the stable temperature to obtain final products.

3.2.2 X-ray Diffraction (XRD)

X-ray diffraction is a common method for the study of crystal structures and atomic spacing. It is a high-tech, nondestructive technique for analyzing a wide range of materials including fluids, metals, minerals, polymers, catalysts, plastics, pharmaceuticals, thin-film coatings, ceramics, solar cells, and semiconductors. The technique finds numerous industries applications, including microelectronics, power generation, aerospace, and many more (Bunaciu et al., 2015). XRD analysis can easily detect the presence of defects in a particular crystal, its resistance level to stress, its texture, its size and degree of crystallinity. X-ray diffraction is based on constructive interference of monochromatic X-rays and a crystalline sample. These X-rays are created by a cathode ray tube, filtered to generate monochromatic radiation, collimated to concentrate, and directed toward the sample (Banerjee, n.d.). The interaction of the incident rays with the sample produces constructive interference and a diffracted ray when conditions satisfy as a Bragg's Law ($n\lambda=2d \sin \theta$), n (order of diffraction), λ (wavelength of the rays), d (spacing between layer of atoms), θ (angle between the incident ray and the surface of crystal) as shown in Figure 3.4.

Universiti Malaya

This law relates the wavelength of electromagnetic radiation to the diffraction angle and the lattice spacing in a crystalline sample. These diffracted X-rays are then detected, processed and counted. The sample were scannned through range of 2θ angles, all possible diffraction directions of the lattice should be accomplished due to the random orientation of the powdered material. Conversion of the diffraction peaks to d-spacings allows identification of the mineral because each mineral has a set of unique d-spacings. Typically, this is achieved by comparison of d-spacings with standard reference patterns. There is three basic elements in X-ray diffractometers that consist of an X-ray tube, a sample holder, and an X-ray detector (Dutrow, 1912). The schematic diagram is shown in Figure 3.5. The phenomena X-rays are generated in a cathode ray tube by heating a filament to produce electrons, accelerating the electrons by applying a voltage, and impact of the electrons with the target material. When electrons have sufficient energy to displace inner shell electrons of the target material, characteristic X-ray spectra are produced.

Universiti Malaya

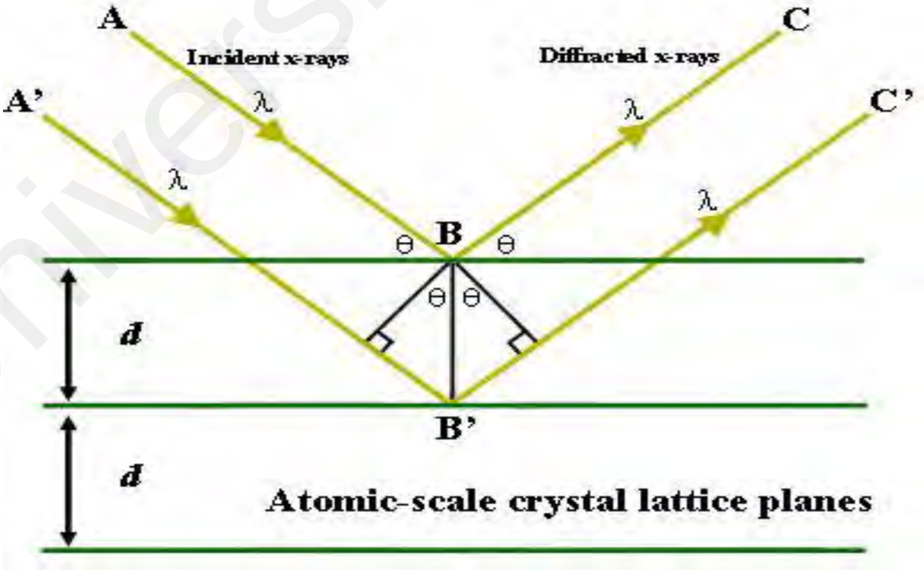

Figure 3.4: Bragg's Law Reflection ("Bragg's Law," 2009).

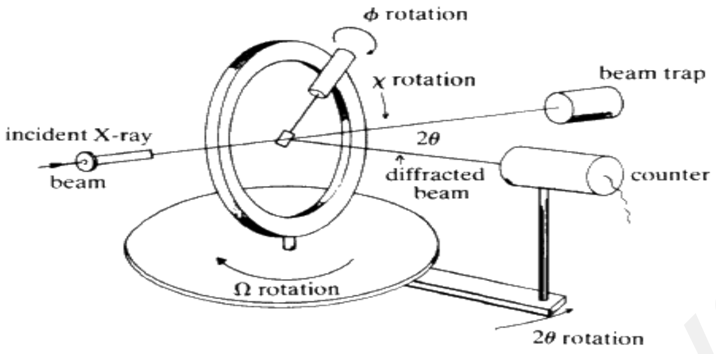

Figure 3.5: The angles between the incident ray, the detector and the sample (Barbour, 2017).

In this work, samples were prepared by using back loading method as shown in Figure 3.6. XRD was measured by using PANalytical X'pert Pro Powder Diffraction using Bragg-Brentano optical configuration with Cu Kα radiation at Universiti Teknologi Mara (UiTM) Shah Alam. The accelerating voltage and current applied was 45 kV and 40 mA respectively. The angle range is between 15°–90 ° and the time taken for each step was 5 seconds.

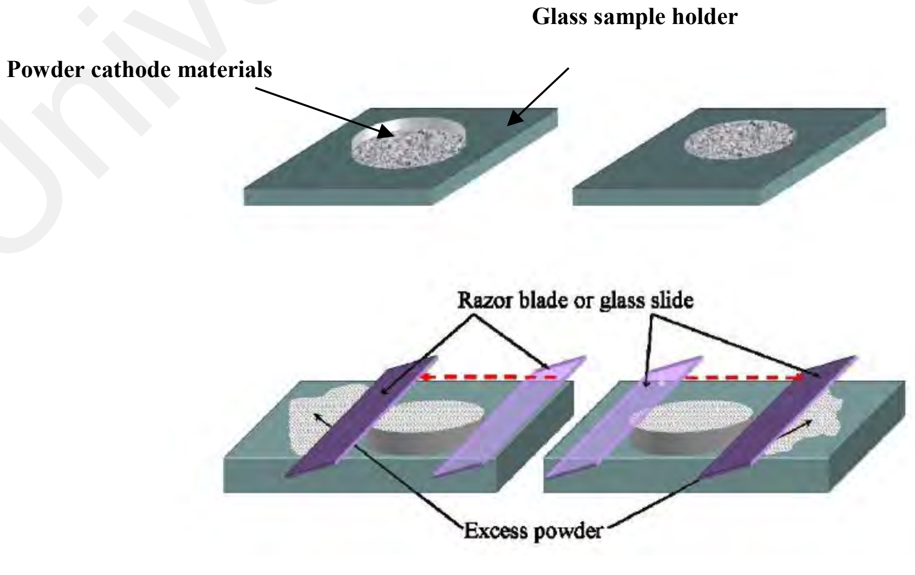

Figure 3.6: Back loading method (Carlo, 2013).

Universiti Malaya

3.2.3 Field Emission Scanning Electron Miscroscopy (FESEM)

Field emission scanning electron microscope (FESEM) used to investigate the morphological, structural properties and the crystallite size of the materials. There are two classes of emission source which are thermionic emitter and field emitter. Emitter type is the main difference between the Scanning Electron Microscope (SEM) and the Field Emission Scanning Electron Microscope (FESEM). Figure 3.7 shows the fundamental of FESEM with specific components.

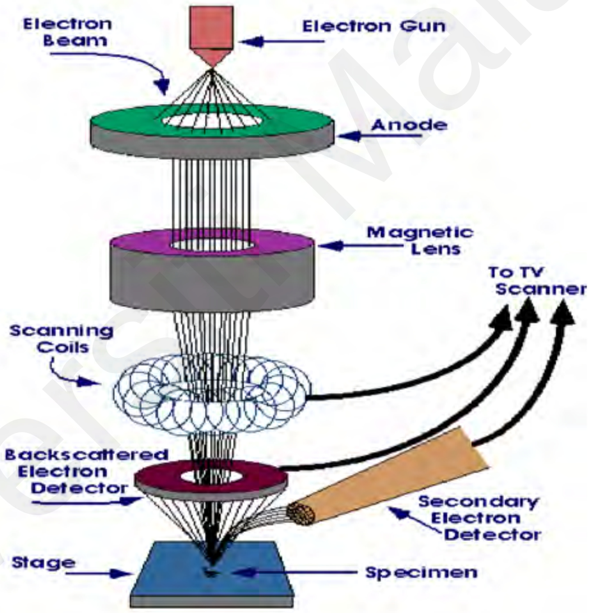

Figure 3.7: Fundamental of FESEM ("Scanning electron microscopy," 1968).

The sample was measured using Filed Emission Scanning Electron (JEOL JSM-7600F) with a resolution of 1.5 nm at 1 kV and 1 nm at 15 kV for secondary electron imaging mode. This instrument can go through magnification of from ~10 to over 300,000 at voltages 0.5 to 30 kV. The sample was placed on stub hold of the holder before go

University of Malaya

through vacuum chamber. Then, only small amount needed to be dispersed on the carbon paint in a specific FESEM holder.

Figure 3.8: Instrumentation of Field Emission Scanning Electron (JEOL JSM-7600F).

3.2.4 Energy Dispersive X-ray Spectroscopy

Energy Dispersive X-ray Spectroscopy (EDX) is defined as simple and powerful technique used to identify the elemental composition of material. The equipment is connected to the SEM to give elemental information to be gathered about the sample under investigation (Intertek, 2016). This is non-destructive technique and has a sensitivity of > 0.1% for elements heavier than C. EDX works by detecting X-rays that are produced by a sample placed in an electron beam as shown in Figure 3.9. The electron beam excites the atoms in the sample thus produce X-rays to discharge the excess energy. The energy of X-rays is one of characteristics of the atom forming peaks in the spectrum.

As the electron beam can be completely controlled, EDX spectra can be shown in a specific point/particle on the sample, giving an analysis of a few cubic microns of material. Alternatively, the beam can sweep over a selected area of the sample to identify

Universiti Malaya

the elements in that region. In addition, line profiles and X-ray maps can be acquired which depict the elemental distribution across the specimen. The sample preparation is quite similar to FESEM sample since EDX integrated with SEM (JEOL JSM-7600F). The accelerating voltage applied to the sample was 15 kV and 10000 magnification.

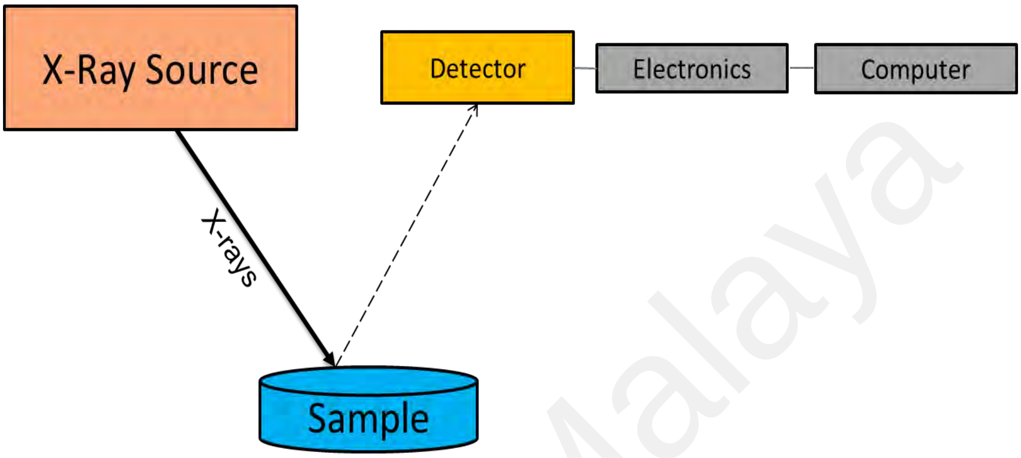

Figure 3.9: Schematic diagram of basic principle of Energy dispersive spectroscopy (EDX).

3.2.5 Brunner-Emmet-Teller theory (BET)

The Brunner-Emmett-Teller theory (BET) is a technique used to measure the surface area of solid or porous materials. It provides important information on their physical structure as the area of a material’s surface affects how that solid will interact with its environment. The properties such as dissolution rates, catalytic activity, moisture retention, and shelf life are often correlated to a material’s surface area (Wikipedia, 2014). The adsorption process is studied through graphs know as adsorption isotherm. Six type of adsorption isotherms can be classified as Type I, Type II, Type III, Type IV, Type V and Type VI as provided in Figure 3.10. It is the graph between the amounts of adsorbate adsorbed on the surface of adsorbent and pressure at constant temperature. Adsorption

Universiti Malaya

isotherms shown in Table 3.1 is based on the strength of the interaction between sample surface and adsorptive and the existence or absence of pores. The structure of porosity is also can be classified as micropores, mesopore and nonporous with a pore diameter size of >2 nm, 2 nm to 5 nm and ≥ 50 nm respectively. Different adsorption isotherms have been Freundlich, Langmuir and BET theory (Hutchinson & Schilt, 1999).

Universiti Malaya

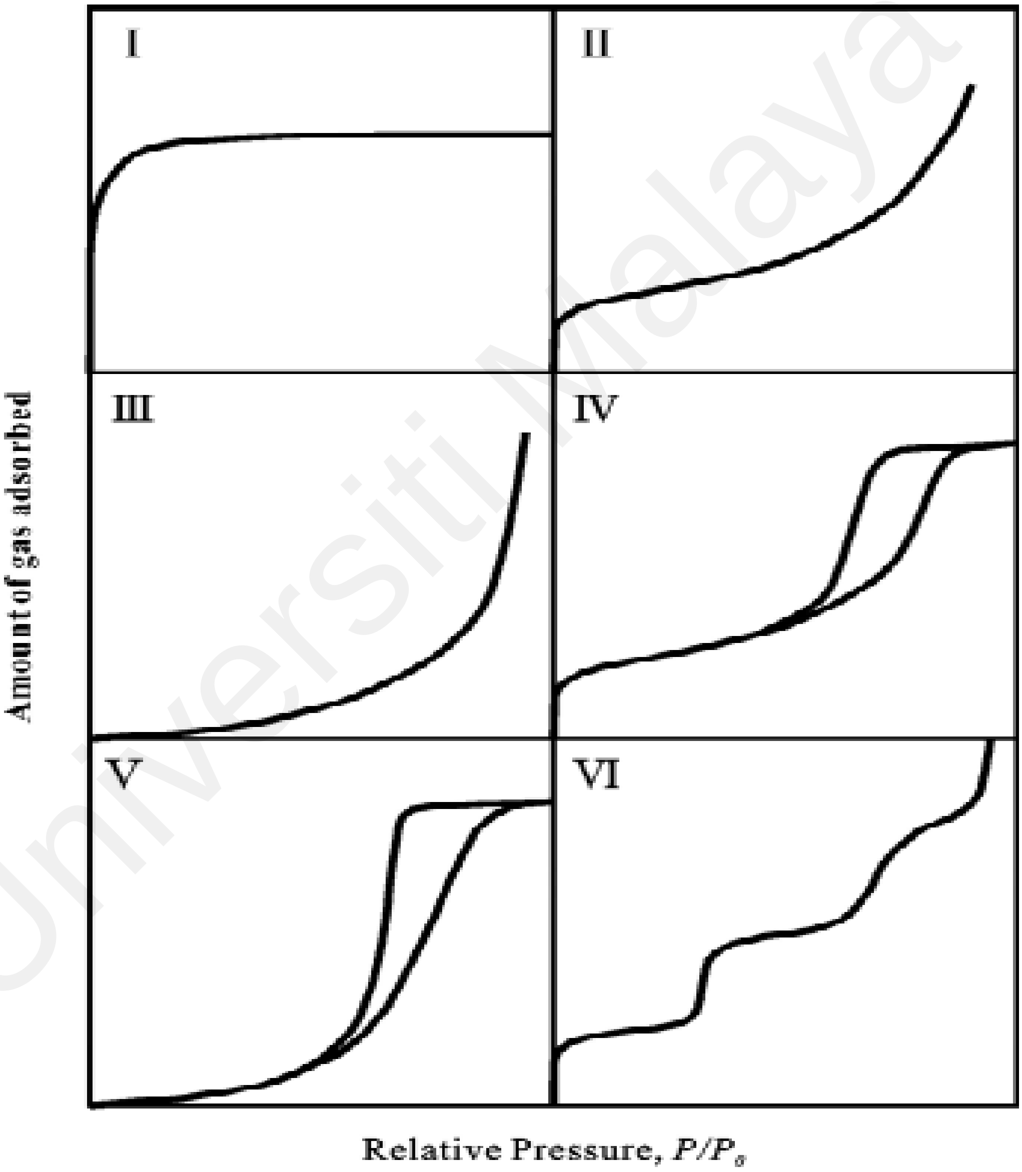

Figure 3.10: IUPAC classification of adsorption isotherms (BEL, 2013).

Table 3.1: Important features of BET measurements isotherm plot (BEL, 2013).

Type	Features		Sample – Adsortive sample
	Interaction between sample surface and adsorbate	Porosity	
I	Relatively strong	Micropores	Activated carbon - Nitrogen
II	Relatively strong	Nonporous	Oxide – Nitrogen
III	Weak	Nonporous	Carbon – Water vapour
IV	Relatively strong	Mesopore	Silica – Nitrogen
V	Weak	Mesopore	
		Micropore	Activated carbon – Water vapour
VI	Relatively strong Sample surface has even distribution of energy	Nonporous	Graphite - Krypton

Universiti Malaya

3.2.6 Raman spectroscopy

During the 1960s, researchers used Raman to clarify numerous of the basic principle of spectral features of the minerals and inorganic materials widely utilize in battery research today (Tarte, 1967). The use of Raman spectroscopy for analysis of battery materials has been around past years. It is a good fit for these materials because many of the characteristic vibrational and rotational modes happen within the low wavenumber region of the spectrum (Wieboldt & Hahn, n.d.). Several significant Raman applications in various fields dedicated to the characterization of a wide range of materials: inorganic solids, ceramics, semiconductor materials, protective coatings, polymers, and battery materials (Baddour-Hadjean & Pereira-Ramos, 2010b).

Advances in instrumentation have greatly increased the ease-use of Raman making it a much more useful technique. Latest area of application ensued such as the exploding interest in rechargeable lithium ion batteries. Many researchers are involved in the studies of materials specifically related to Li-ion batteries as well as next generation batteries. A Baddour-Hadjean et al. (2010) had published a review paper that focus on the application of in situ application of Raman spectroscopy as it relates to battery research (Baddour-Hadjean & Pereira-Ramos, 2010a).

Raman spectroscopy relies upon inelastic scattering of photons, known as Raman scattering. A source of monochromatic light comes from a laser in the visible, near infrared, or near ultraviolet range is used. The laser light interacts with molecular vibrations, phonons or other excitations in the system, resulting in the energy of the laser photons being shifted up or down. The shift in energy gives information about the vibrational modes in the system (Furtak, 1983).

Typically, a sample is illuminated with a laser beam. Electromagnetic radiation from the illuminated spot is collected with a lens and sent through a monochromator. Elastic

Universiti Malaya

scattered radiation at the wavelength corresponding to the laser line (Rayleigh scattering) is filtered out by either a notch filter, edge pass filter, or a band pass filter, while the rest of the collected light is dispersed onto a detector (Figure 3.11). The Raman presented in this work were recorded using a Bruker dispersive Raman spectroscope with laser of 532 nm a Raman shift range between 100 and 800 cm^{-1}.

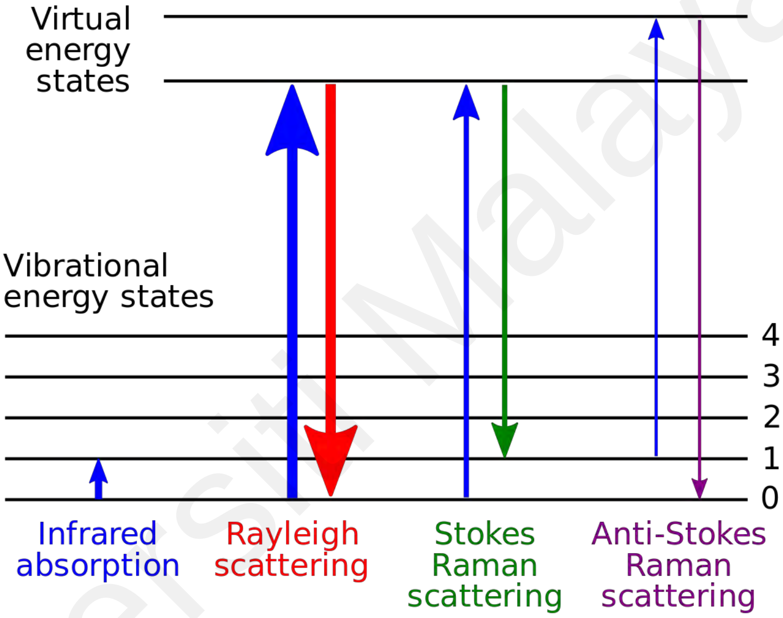

Figure 3.11: Energy level diagram in Raman signal ("Geos 306, Raman Spectroscopy," n.d.).

3.2.7 Transmission Electron Miscroscopy (TEM)

Transmission electron microscopy (TEM) is a microscopy technique where a beam of electrons is transmitted through an ultra thin specimen, interacting with the specimen as it passes through (Tecnai & Centre, n.d.). TEMs produce a topographical, morphological, compositional and crystalline information. The electrons interaction that pass through the specimen will formed an image. TEMs applications include in semiconductor analysis and production and the manufacturing of computer and silicon chips (anka, 2018).

Universiti Malaya

A TEM contains four parts which are electron source, electromagnetic lens system, sample holder, and imaging system shown in Figure 3.12. The electron source consists of a cathode and an anode. The cathode is a tungsten filament, which emits electrons when being heated. A negative cap confines the electrons into a loosely focused beam as in Figure 3.12. The beam is then accelerated towards the specimen by the positive anode. Electrons at the rim of the beam will fall onto the anode while the others at the center will pass through the small hole of the anode. The electron source mechanisms same as cathode ray tube. After leaving the electron source, the electron beam is tightly focused using electromagnetic lens and metal apertures. The system only allows electrons within a small energy range to pass through, so the electrons in the electron beam will have a well-defined energy. The sample holder is a platform equipped with a mechanical arm for holding the specimen and controlling its position. The imaging system consists of another electromagnetic lens system and a screen. The electromagnetic lens system contains two lens systems, one for refocusing the electrons after they pass through the specimen, and the other for enlarging the image and projecting it onto the screen. The screen has a phosphorescent plate, which glows when being hit by electrons. Image forms in a way similar to photography (Shiu-Sing T, 2020).

Universiti Malaya

TEMs work the same way except that they shine a beam of electrons through the specimen. However, in TEM, the transmission of electron beam is highly dependent on the properties of material being examined. Such properties include density, composition, etc. For example, porous material will allow more electrons to pass through while dense material will allow less. As a result, a specimen with a non-uniform density can be examined by this technique. The user can see whatever part transmitted onto a phosphor screen. In this studies, the sample used is about 0.25 mg which is just a small amount is needed and the samples was mixed in an solvent which is ethanol.

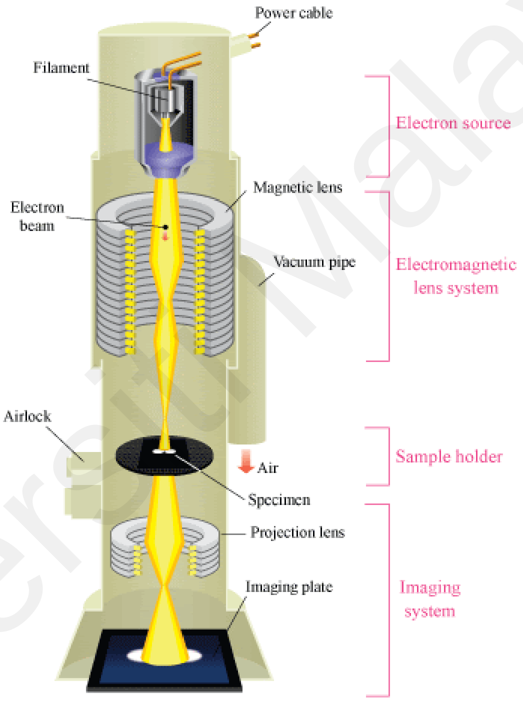

Figure 3.12: The schematic outline for TEM (Shiu-Sing T, 2020).

3.2.8 Electrochemical Impedance Spectroscopy (EIS)

Electrochemical Impedance Spectroscopy (EIS) is an electrochemical technique uses in variety range of applications and over 20,000 publications in a different fields include science, biosensors, battery development, fuel cell development, physical electrochemistry and coating/paint characterization (Gamry Instruments, 2018). During EIS experiments, a small amplitude ac signal is applied to the system being studied. EIS

University Malaya

is a non-destructive method for the evaluation of a wide range of materials, including coatings, anodized films, corrosion inhibitors, batteries and fuel cells.

Impedance spectroscopy is measured using HIOKI 3531-01 LCR bridge with a frequency range of 50 Hz to 500 kHz. The software can control the measurement calculation of the real and imaginary impedance. From Cole-Cole plot with the horizontal and vertical axes having the same scale, bulk resistance, R_b can be obtained. The electrical conductivity, σ of the sample can be calculated from the equation

$$\sigma = \frac{t}{RbA} \tag{3.1}$$

Where *t* represents the sample thickness and *A* is the contact area. Other functions of impedance spectroscopy are complex admittance *A(ω)* , complex dielectric constant or complex permittivity *ε(ω)* and complex dielectric modulus *M(ω)*. The basic general admittance can be denoted as , $A(\omega) = A_r + jA_i$ .Whenever R_b was difficult to obtain from complex impedance data, the impedance data was converted into admittance data by plotting the imaginary admittance A_i versus the real admittance A_r, the $1/R_b$ may be easier to be obtained. The complex admittance can be calculated using equation.

$$A(\omega) = \frac{1}{Z\ (\omega)}$$

$$= \frac{1}{Zr+jZi}$$

$$= \frac{1}{Zr+jZi} x \frac{Zr-jZi}{Zr-jZi}$$

$$= \frac{Zr}{Zr2+Zi2} - \frac{jZi}{Zr2+Zi2} \tag{3.2}$$

Universiti Malaya

3.2.9 Electrochemical studies

Electrochemical studies of the materials was performed by measuring the linear sweep voltammetry (LSV), Cyclic Voltammetry (CV), Charge discharge behavior and cycling stability. In linear sweep voltammetry (LSV), the three-electrode setup consists of a working electrode(WE), counter electrode(CE), and a reference electrode (RE) deliver a potential to a solution and monitor its change in current. The electrode potential is varied at voltage range of -5 V to 5 V at a constant scan rate of 5 mVs^{-1} throughout the scan and the resulting current and electrochemical stable potential window is measured.

Cyclic voltammetry (CV), one of the more commonly used electroanalytical techniques, is a good methods development tool. Its main advantage in electroanalysis is its ability to characterize an electrochemical system. From CV, the redox reactions process can be determined include oxidation and reduction reactions which can be reversible reactions. The scientist use electrochemistry to studies the loss of electrons (oxidation) or gain of electrons (reduction) that a material undergoes during the electrical stimulation. The cyclic voltammogram are characterized by cathodic peak potential, anodic peak potential, anodic peak current and cathodic peak current. In this work, magnesium metal is used for both RE and CE and the cathode materials as a WE. The electrolyte used is 1.0 M of magnesium trifluoromethanesulfonate $Mg(CF_3SO_3)_2$ in 1:1 ratio of ethylene carbonate (EC) and 1,2-Dimethoxyethane (DME). LSV and CV were performed using WonaTech equipment with pontentiostat/Galvanostat (WPG100e). The cell voltage range used was 0.5 V to 3 V at a scanning rate of 1 mVs^{-1}.

3.3 Preparation of cathode

The cathode preparation are illustrated in Figure 3.13. Three materials knows as Super P carbon, PTFE and active materials (our product) was first mix together by grinding in a mortar. Then, a black paste was formed and the paste was press onto stainless steel mesh

Universiti Malaya

grid act as current collector and put one drop of acetone that act as a solvent onto the mesh. After a cathode material was successfully paste on the grid, the product will be dry in an oven for 24 hour at 100 °C. Further electrochemical studies such as LSV, CV and CD was performed in order to check the electrochemical properties of cathode materials.

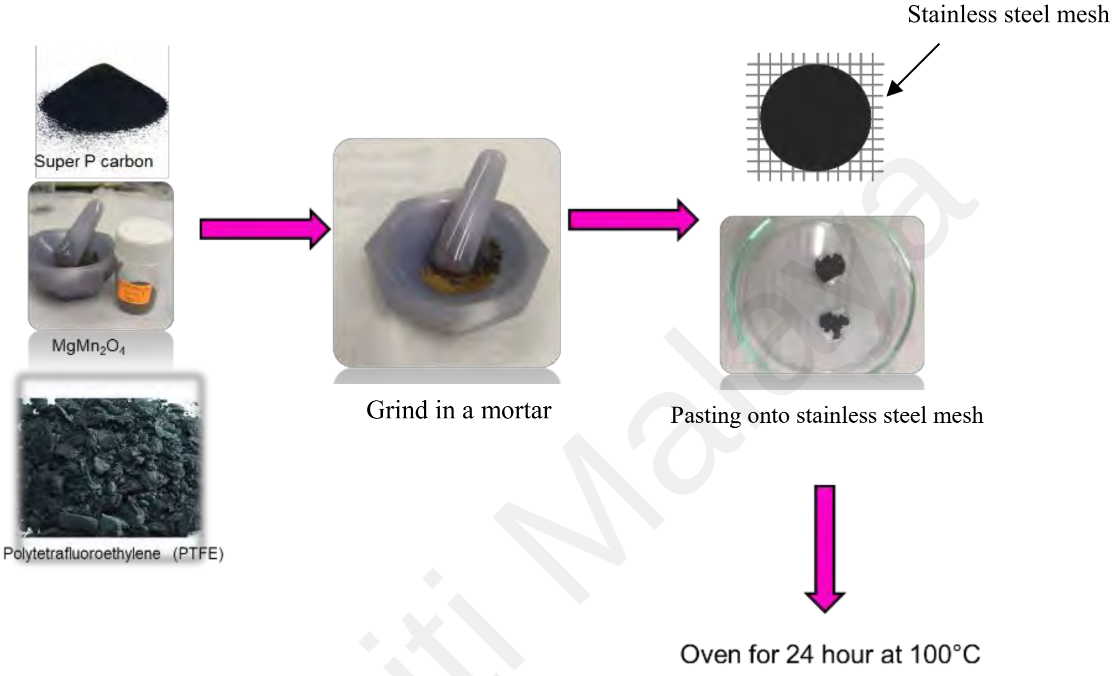

Figure 3.13: Cathode materials preparation.

3.4 Fabrication of Mg cells

The cells were assembled by using magnesium metal that act as anode, the separator, which is Polypropylene (PP), and the prepared cathode materials. The separator were soaked in 1 M of $Mg(CF_3SO_3)_2$ electrolyte which is the prepared liquid electrolyte for a few minutes. These materials are stacking started with prepared cathode materials at the bottom followed by the PP separator with a drop of electrolyte and the magnesium metal on the top of that as shown in Figure 3.14. The galvanostatic charge discharge profile was tested by using Neware battery tester, which was conducted in open air. The parameters was setup with a charge discharge current of 0.1 mA and the voltage range of 0.5 V to 2.5 V.

Universiti Malaya

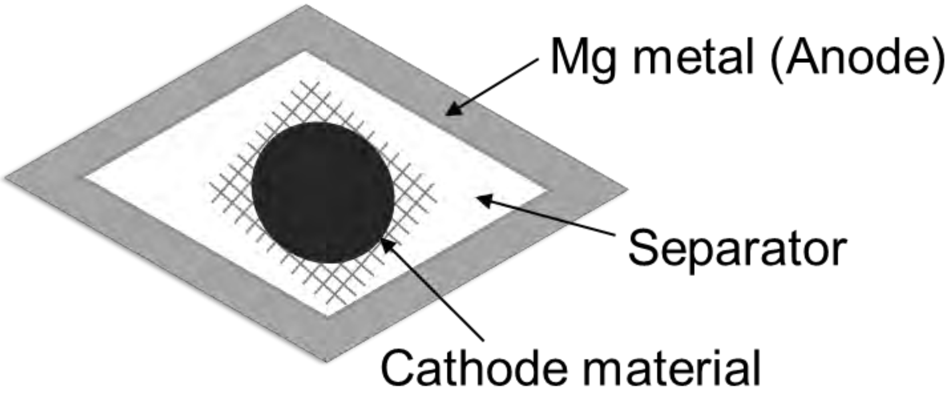

Figure 3.14: Schematic diagram of battery fabrication.

Universiti Malaya

CHAPTER 4: THERMAL STUDIES

4.1 Introduction

In this work, thermogravimetric Analysis (TGA) and the Differential Scanning Calorimetry (DSC) techniques were used to study thermal stability of the cathode materials and annealing temperature of the precursor. In this chapter, the thermal analysis has been conducted for sample $MgMn_2O_4$, $MgMn_{2-x}Sr_xO_4$ and $MgMn_{2-x}Ca_xO_4$. The synthesized product from self-propagating combustion method was thermally analyses from temperature ranging from 30°C to 1000°C at heating rate of 10°C/min using SETARAM SETSYS Evolution 1750. The effect of Calcium (Ca) and Strontium (Sr) doping on the thermal properties of $MgMn_2O_4$ based cathode materials also will be presented in this chapter.

4.1.1 TGA and DSC measurements of $MgMn_2O_4$

Figure 4.1 shows the TGA/DSC curve representing the different four stages of decompositions for undoped cathode materials that represent as $MgMn_2O_4$. The initial weight loss of 21.5% is attributed to water dehydration from the sample at temperature range of 30°C to 190°C. This corresponds to the endothermic peak in DSC trace at 90°C and 123°C. From the TG curve at temperature range between 250°C to 350°C, the weight loss is about 19.5%. From DSC trace, it can be observed that there is an endothermic at 268°C means there is any remaining weight loss there. Stage three within temperature range of 350°C to 650°C shows a weight loss around 3.28%. According to Rahman et al. (2015) the peak at 250°C and 650°C represents the formation MgO and Mn_2O_3 (Rahman et al., 2015).

In the fourth stage, the TG curve shows a plateau from 700°C-1000°C. This plateau indicating the stabilization of the sample was occurred. The samples is quite stable and there is no mass changes in this region. The DC trace also is much shallower within this

Universiti Malaya

temperature. It can be concluded that from TG/DSC curve, these materials have approximately stable, which are within the temperature range of 700°C-1000°C. Therefore, the samples were chosen to be annealed at temperatures of 700°C and 800°C. The explanation of each region has been summarized in Table 4.1.

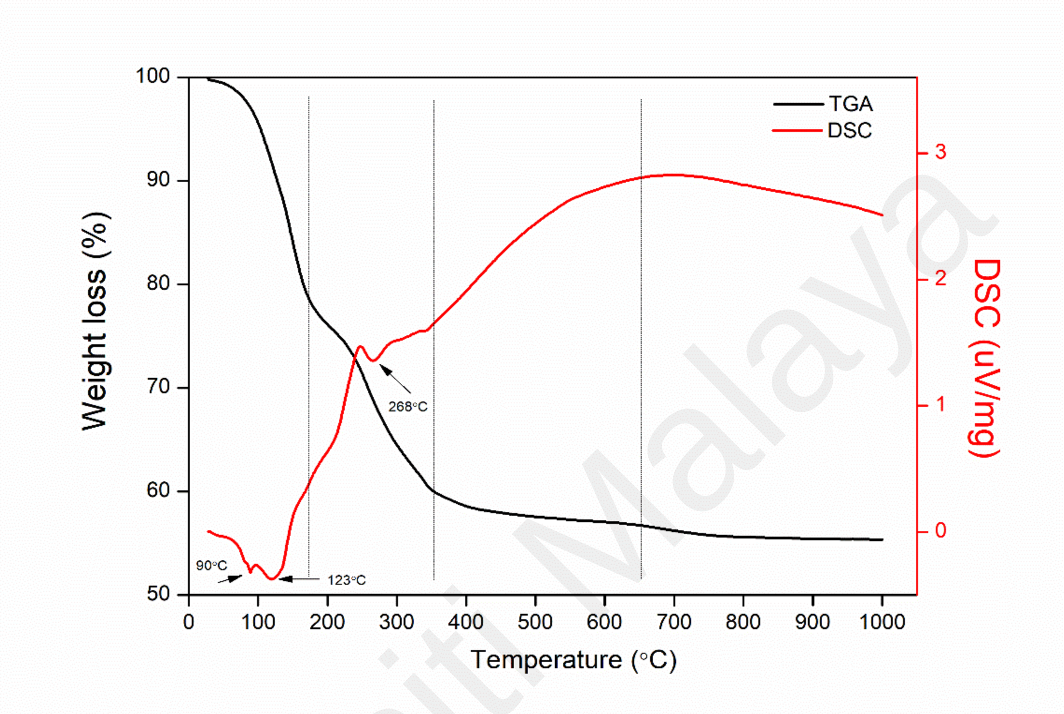

Figure 4.1: TGA and DSC curves of $MgMn_2O_4$ precursor.

Universiti Malaya

Table 4.1: Decomposition processes in $MgMn_2O_4$ precursor.

TGA / DSC Curve			
Temperature range of weight loss (°C)			
Stage I	Stage II	Stage III	Stage IV
30°C - 190°C Endothermic band (90°C and 123°C)	190°C - 350°C Endothermic band (268°C)	350°C to 650°C No exothermic or endothermic band	650°C to 1000°C Flat region (stable)

Table 4.1, continued,

Loss of water molecules	Formation of MgO at (250°C) (Rahman et al., 2015)	Formation of Mn_2O_3 at (650°C) (Rahman et al., 2015)	The samples was annealed at 700°C and 800°C for 24 hour

4.1.2 TGA and DSC measurements of $MgMn_{2-x}Sr_xO_4$

$MgMn_{2-x}Sr_xO_4$ (x=0.2) have been selected to perform thermal analysis among others. The TG/DSC curves of Sr doped $MgMn_2O_4$ cathode material were shown in Figure 4.2 .There are three stages of decomposition for sample $MgMn_{1.8}Sr_{0.2}O_4$ where the first stage is in the range of 100°C to 300°C indicating weight loss about 23% represents the loss and evaporation of the water molecules. For Sr doped samples, there is no endothermic band or exothermic band shows from 30°C-300°C, which attributed to the loss of water molecule left in the precursor. The second weight loss determined is 18% at temperature range of 310°C-680°C indicating this weight loss is due to decomposition of the citric acid used in the precursor. From DC curve, it can be observed there are two exothermic curve at 351°C and 572°C attributed the loss of citric acid.

The TG/DC curves at the last stages is seem to be quite stable from 700°C to 1000°C. Therefore, based on this stable range peak, the samples was be chosen to be annealed at temperature 700°C and 800°C for 24 hours and will further characterized under structural and morphological studies. The study shows that annealing at higher temperatures at 24 hours is the best duration which resulted in increased particle size, differentiated surface composition thus improved electrochemical performance (Younesi et al., 2014). The explanation of each region has been simplified as in Table 4.2.

Universiti Malaya

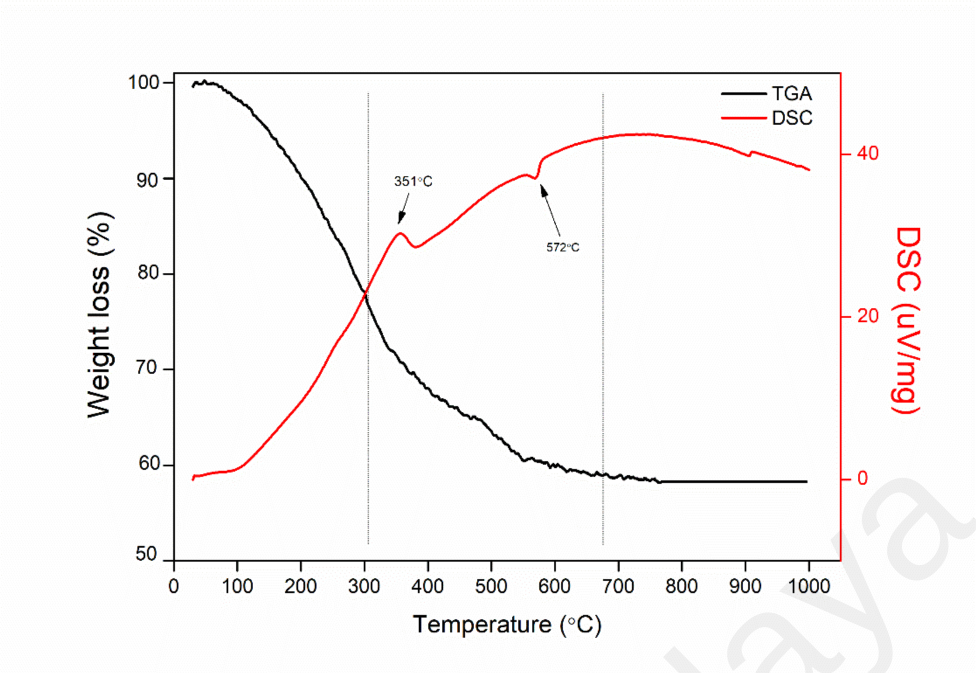

Figure 4.2: TGA and DSC curves of $MgMn_{2-x}Sr_xO_4$ precursor.

Table 4.2: Decomposition processes in $MgMn_{2-x}Sr_xO_4$ precursor.

TGA/DSC Curve		
Temperature range of weight loss (°C)		
Stage I	Stage II	Stage III
100°C to 300°C	300°C - 700°C Exothermic band (351°C and 572°C)	700°C to 1000°C Flat region (stable)
loss and evaporation of the water molecules	Decomposition of the citric acid	The samples was annealed at 700°C and 800°C for 24 hour

Universiti Malaya

4.1.3 TGA and DSC measurements of $MgMn_{2-x}Ca_xO_4$

$MgMn_{2-x}Ca_xO_4$ (x=0.2) have been selected to performed thermal analysis among others. The TG/DSC curves of Ca doped $MgMn_2O_4$ cathode material were shown in Figure 4.3. There are three stages of decomposition involve in this doped cathode materials. In the first stage, it can be observed that there is one endothermic peak from DC trace at 111°C in the range of 30°C to 130°C indicating small weight loss about 7.09% represents the loss and evaporation of the water molecules. The TG trace in the stage II indicates a high weight loss, which is 29.5% between temperature range 130°C and 253°C. In this stage II, there is a sharp exothermic peak at 245°C, which attributed to the decomposition of citric acid left in the precursor. From TG trace for stage III, the weight loss determined is 7.94% at temperature range of 253°C-666°C indicating this weight loss is due to decomposition of the starting materials. The DSC trace also depicts an endothermic band at 263°C attributed to the decomposition of citric acid.

The TG/DSC curve at the last stage is seem to be quite stable from 666°C to 1000°C. So based on this observation, the samples were chosen to be annealed at temperature 700°C and 800°C based on the TGA results obtained for 24 hours and will further be characterized for structural and morphological studies. The explanation of this four stages has been simplified as in Table 4.3.

Universiti Malaya

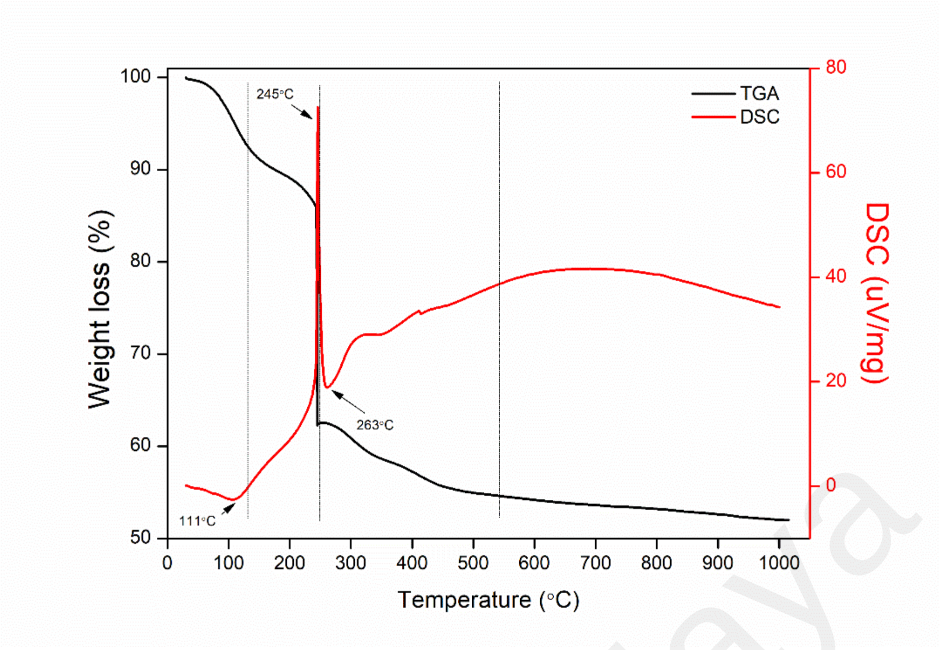

Figure 4.3: TGA and DSC curves of $MgMn_{2-x}Ca_xO_4$ precursor.

Table 4.3: Decomposition processes in $MgMn_{2-x}Ca_xO_4$ precursor

TGA / DSC Curve			
Temperature range of weight loss (°C)			
Stage I	Stage II	Stage III	Stage IV
30°C to 130°C Endothermic peak (111°C)	130°C to 253°C Exothermic peak (245°C)	253°C - 666°C Endothermic band (263°C)	666°C to 1000°C Flat region (stable)
loss and evaporation of the water molecules	decomposition of citric acid	decomposition of starting materials	The samples was annealed at 700°C and 800°C for 24 hour

Universiti Malaya

CHAPTER 5: STRUCTURAL AND MORPHOLOGICAL STUDIES

5.1 X-Ray diffraction Analysis (XRD)

Several studies have been reported on the specific interest of $MgMn_2O_4$ spinel in structural properties, the degree of inversion and electronic properties. Analysis of XRD diffraction has been tested for a structural properties with $MgMn_2O_4$, $MgMn_{2-x}Sr_xO_4$ and $MgMn_{2-x}Ca_xO_4$. All samples annealed at 700°C and 800°C for 24 hours using a furnace.

5.1.1 XRD of $MgMn_2O_4$

Figure 5.1(a) and (b) show X-ray diffractogram of $MgMn_2O_4$ at 700°C and 800°C respectively. The XRD patterns of $MgMn_2O_4$ at temperature 700°C and 800°C corresponds to the tetragonal spinel-structure in which Mg^{2+} and $Mn^{3+}/^{4+}$ ions occupy tetrahedral and octahedral sites (Sinha & Munichandraiah, 2008) with space group and ICDD database of I41/amd and 01-072-1336. It can be clearly seen that all the fingerprints are easily observed in all XRD patterns. The entire diffraction pattern for both temperatures shows high crystallinity with sharp peaks and high intensities. As shown in both figures, it can be clearly observed fingerprints namely (101),(200),(103),(211),(202),(220),(303),(215),(116) and (323) at 2θ = 18°, 29°, 32°, 36°, 37°, 44°, 56°, 61°,64°, 66° respectively which belongs to $MgMn_2O_4$ cathode materials. The intensity of the peak at a range of 2θ=70°-90° are very low as compared to other observed peaks. Therefore, these peaks can be ignored.

Obviously, the intensity between these two temperatures is slightly different. This can be explained for intensity of all the diffraction peaks at 700°C show lower intensity compared to temperature 800°C. When the materials was annealed at higher temperature, 800°C, it can be observed that the two peaks become more intense as planes (101) and (211). The structural and the XRD patterns were unchanged even though when heating at these two temperatures.

Universiti Malaya

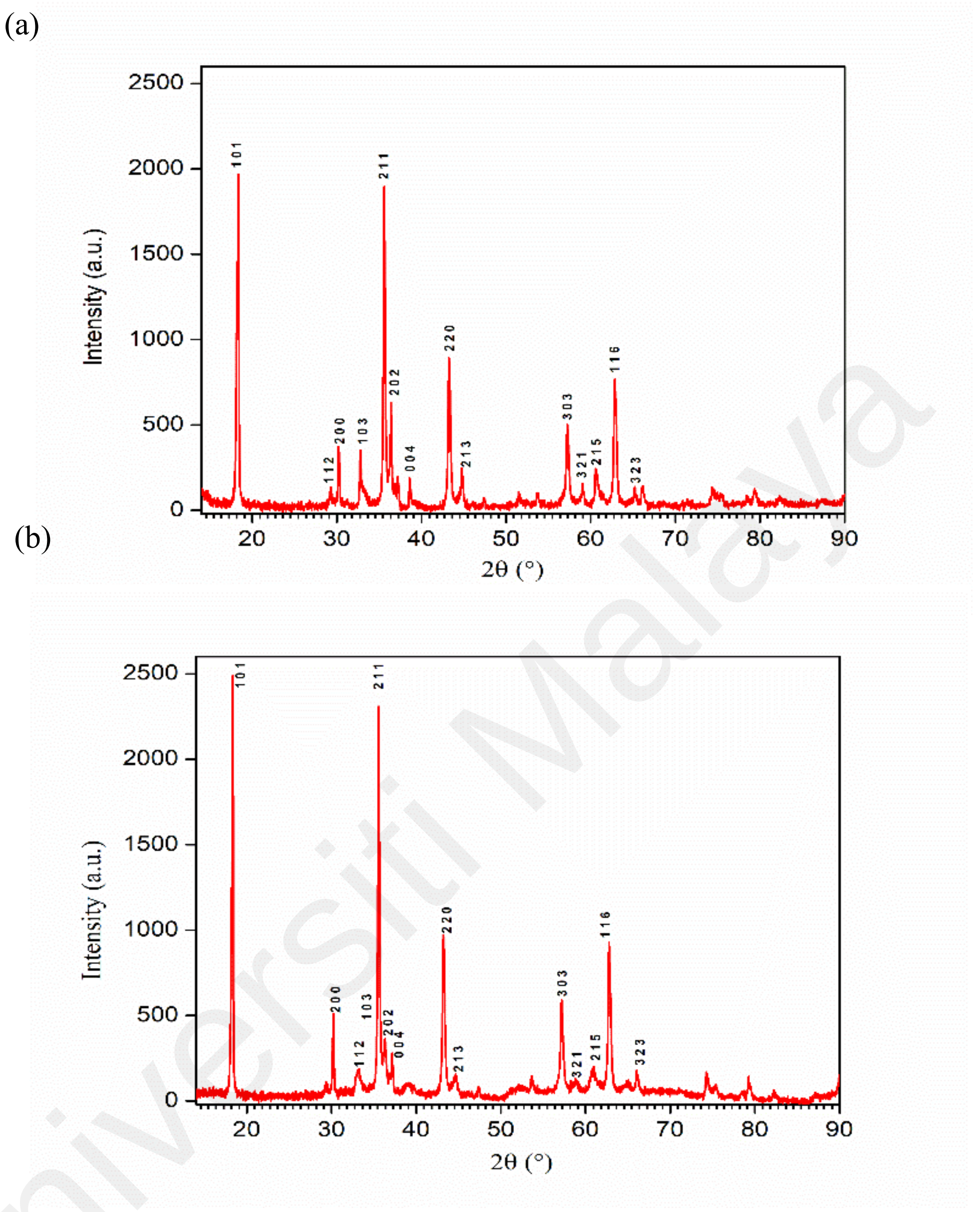

Figure 5.1: XRD patterns for $MgMn_2O_4$ at temperature (a) 700°C (b) 800°C.

5.1.2 XRD of $MgMn_{2-x}Ca_xO_4$

The XRD patterns for $MgMn_{2-x}Ca_xO_4$ (x=0.1, 0.2, 0.3, 0.4, 0.5) materials annealed at 700°C and 800°C for 24h is depicted in Figure 5.2 and Figure 5.4. For Ca doped compounds, the diffraction peaks could be indexed in 01-089-3684 with a cubic pattern and a space group of Im-3m. The diffraction peaks of these Ca doped samples are broader

Universiti Malaya

with increases of Ca amounts composition as compared to the undoped sample. This might be due to the poor crystallinity and smaller particle size. Moreover, it is clear that the presence of new peaks of Ca doped samples are appeared when calcium composition increases and the appearance of these peaks are more obvious as the amount of calcium increases as shown in Figure 5.3.

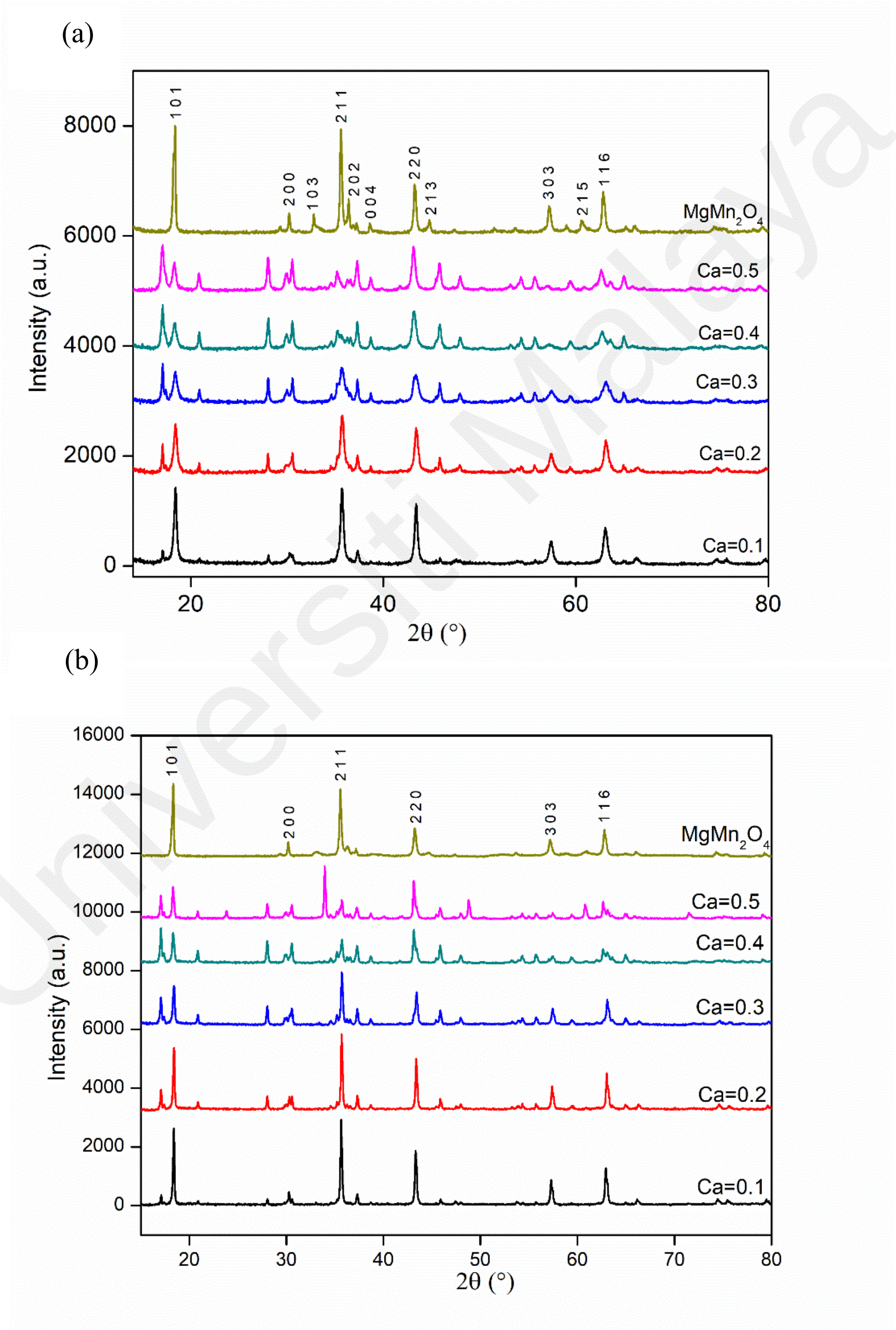

Universiti Malaya

Figure 5.2: XRD for $MgMn_2O_4$ and Ca doped, $MgMn_{2-x}Ca_xO_4$ (x=0.1,0.2,0.3,0.4,0.5) at temperature (a) 700°C and (b) 800°C.

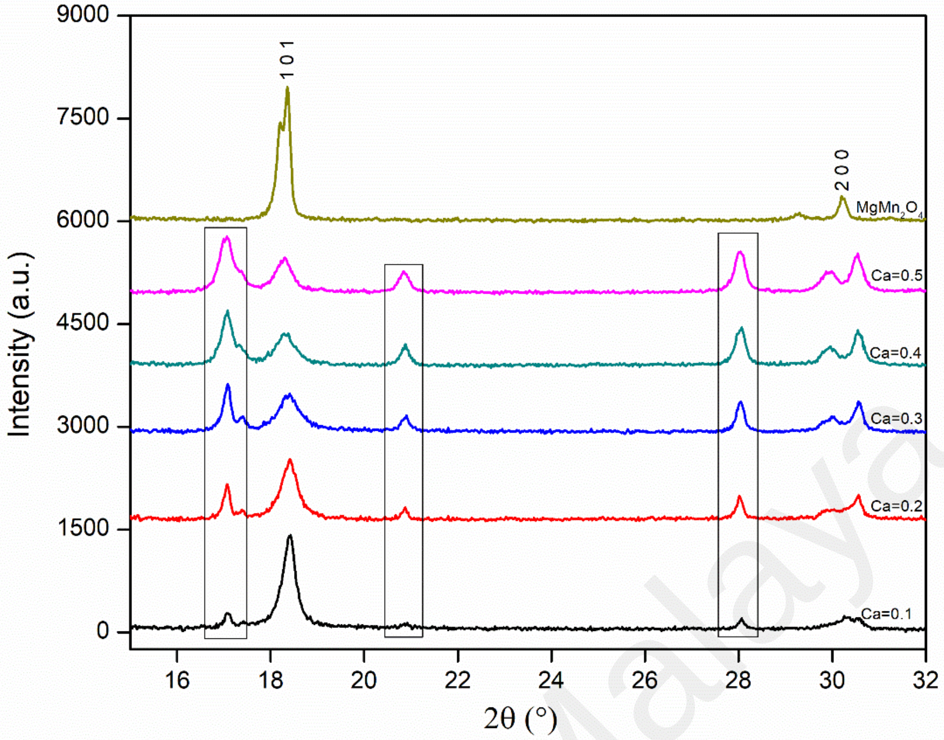

Figure 5.3: XRD patterns for undoped $MgMn_2O_4$ and Ca doped $MgMn_2O_4$ at 2θ = 17°, 21° and 28° at 700°C.

Universiti Malaya

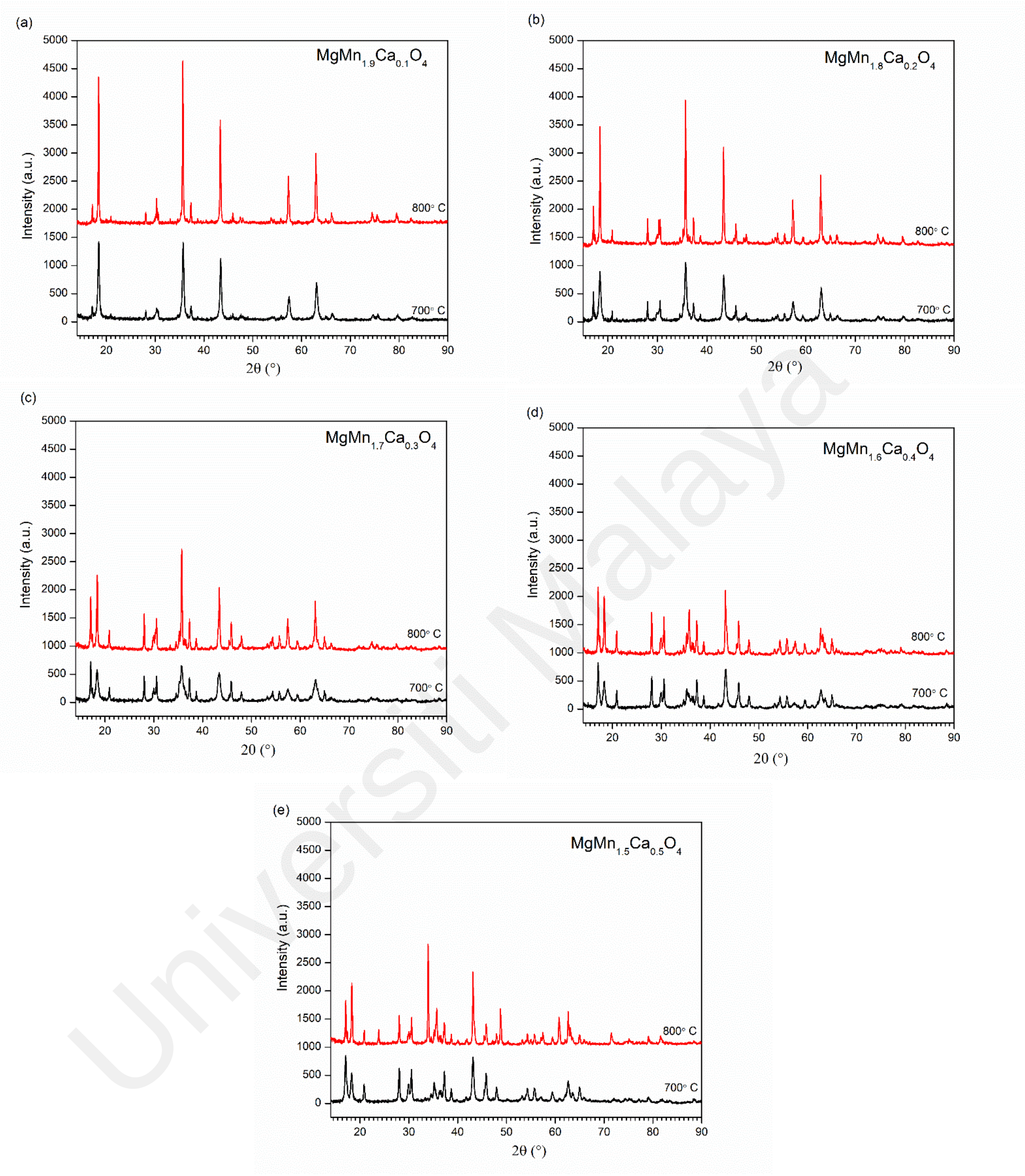

Figure 5.4: XRD patterns of $MgMn_{2-x}Ca_xO_4$ (x=0.1,0.2,0.3,0.4,0.5) at temperatures 700°C and 800°C (a) Ca=0.1 (b) Ca=0.2 (c) Ca=0.3 (d) Ca=0.4 (e) Ca=0.5.

Universiti Malaya

5.1.3 XRD of $MgMn_{2-x}Sr_xO_4$

The XRD patterns for $MgMn_{2-x}Sr_xO_4$ (x=0.1, 0.2, 0.3, 0.4, 0.5) materials annealed at 700°C and 800°C for 24h is depicted in Figure 5.5 and Figure 5.6. For Sr doped compounds, the diffraction peaks could be indexed in 01-089-4047 with a cubic pattern and a space group of Im-3m. For Sr doped sample annealed at 700°C, it can be observed that a peak at (110) was appeared whereas for the sample annealed 800°C the same fingerprint as undoped sample was obtained. This implies that the Sr is interstitially doped in $MgMn_2O_4$ structure with a crystal system of cubic and a space group of Im-3m corresponding to the reference code 01-089-4047. It is expected that the interstitial doping of strontium into the $MgMn_2O_4$ structure could stabilize the manganese site, which can improve the performance and cycle ability of the Mg ion cells when this sample been used as cathode.

The peak of Sr doped at $2\theta = 18°$ was obviously decreased as Sr compositions increase up to x=0.5. It is also can be observed the intensity of XRD diffraction peaks at 800°C was higher than that of 700°C.

Universiti Malaya

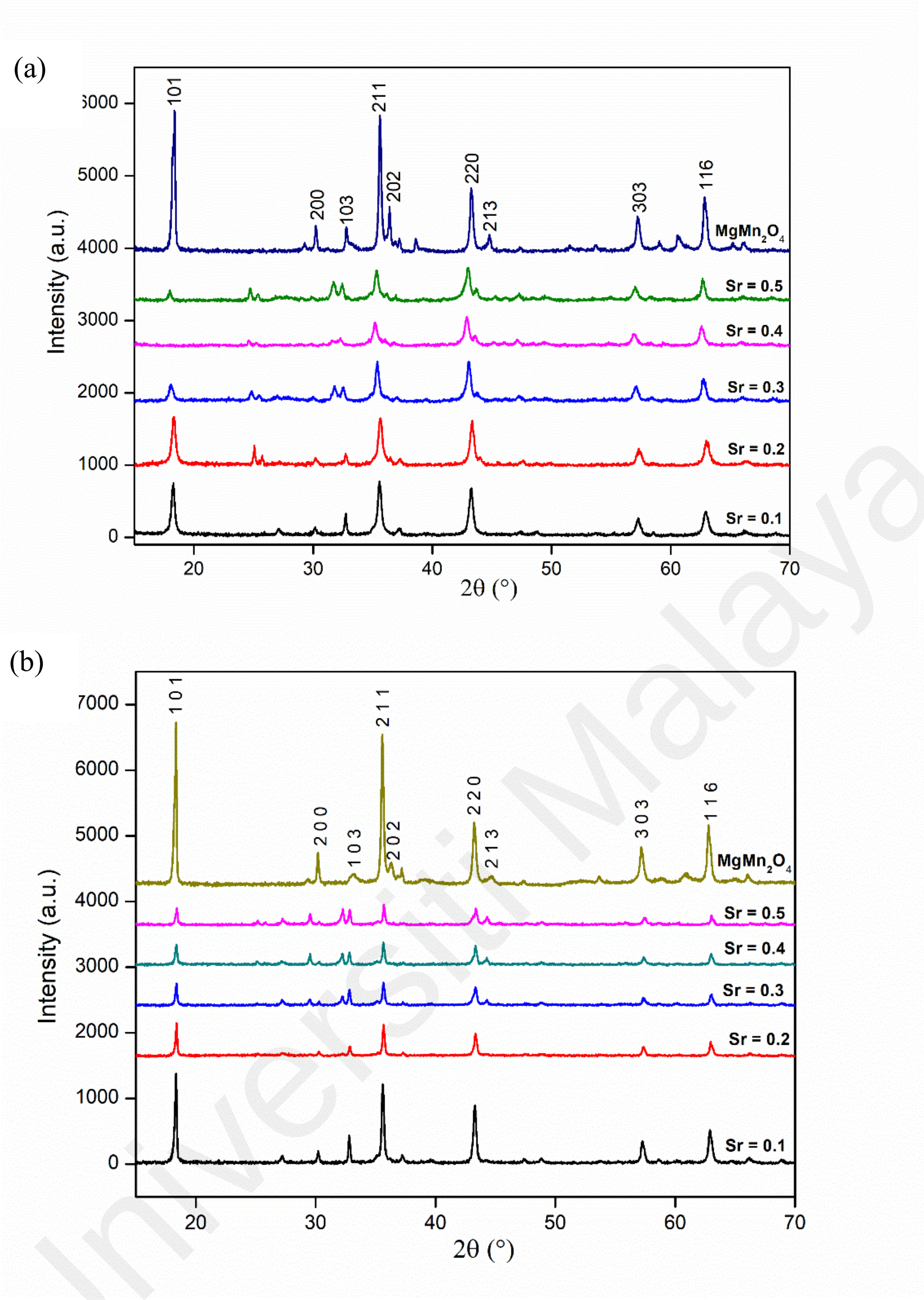

Universiti Malaya

Figure 5.5: XRD for $MgMn_2O_4$ and Sr doped, $MgMn_{2-x}Sr_xO_4$ (x=0.1,0.2,0.3,0.4,0.5) at temperature (a) 700°C and (b) 800°C.

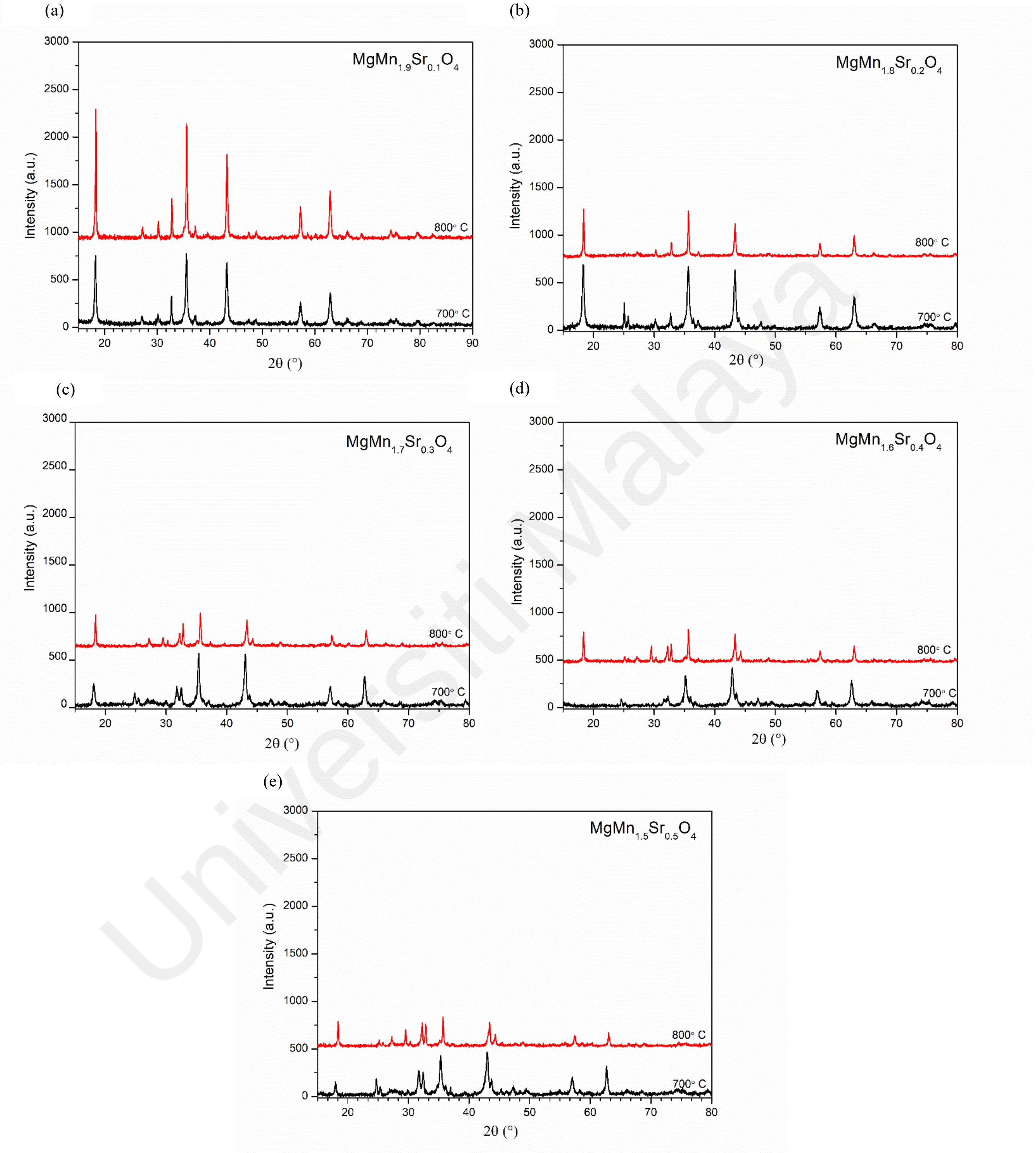

Universiti Malaya

Figure 5.6: XRD patterns of $MgMn_{2-x}Sr_xO_4$ (x=0.1,0.2,0.3,0.4,0.5) at temperatures 700°C and 800°C (a) Sr=0.1 (b) Sr=0.2 (c) Sr=0.3 (d) Sr=0.4 (e) Sr=0.5.

5.2 Field Emission Scanning Electron Microscope (FESEM)

The FESEM images of $MgMn_2O_4$ based cathode materials are shown in Figure 5.7. The sample was annealed within two different temperatures, which are at 700°C and 800°C. The formation of dense aggregates of polyhedral shape nanoparticles with the range of particle size between 100 nm–150 nm can be observed from $MgMn_2O_4$ annealed at 700°C and 800°C respectively. It can be seen that as temperature increases, the particle size also increases as shown Figure 5.7(a) and (b).

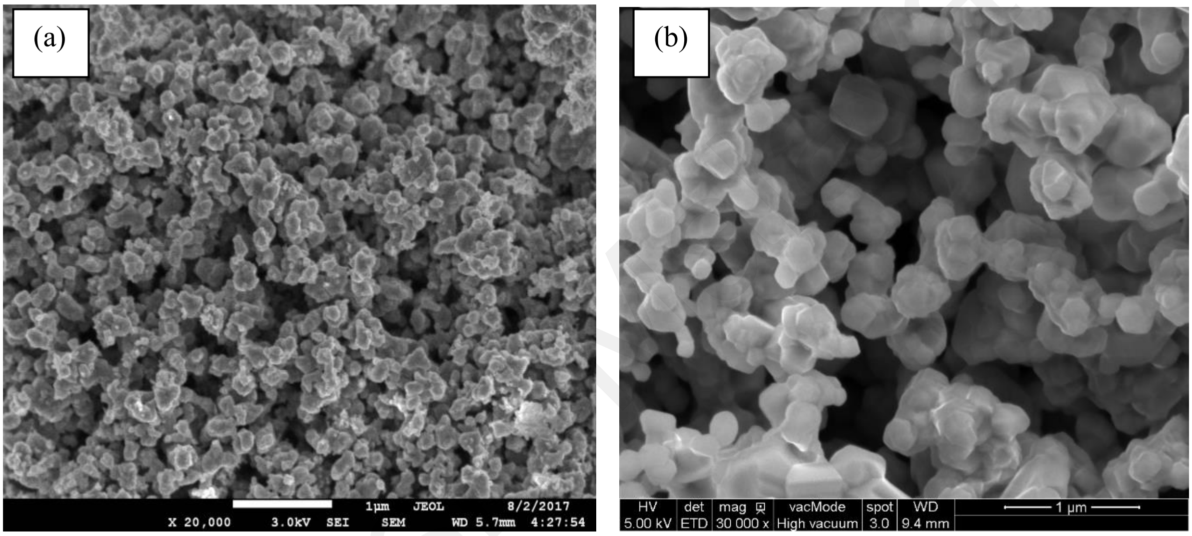

Figure 5.7: FESEM images of $MgMn_2O_4$ at (a) 700°C and (b) 800°C.

FESEM images of $MgMn_{2-x}Ca_xO_4$ (x=0.1, 0.2, 0.3, 0.4, 0.5) cathode materials samples annealed at 700°C and 800°C are shown in Figure 5.8 and Figure 5.9 respectively. As seen in these figures of all compositions, the morphology of $MgMn_{2-x}Ca_xO_4$ samples shown the sponge-like framework or porous formation of interconnected pores. This may be attributed to the effect of doping calcium into $MgMn_2O_4$, which helps to reduce the capacity fading during the cyclability and improve the cycling stability of Mg-ion cells. At temperatures 700°C and 800°C, the porosity becomes larger as Ca content increases and the highest porosity is can be found in the sample x=0.2. It was reported that structures of cathode materials having high porosity crystallinity played a vital role in improving the ions intercalation processes and shows better electrochemical properties (Sufri & Kamarulzaman, 2018).

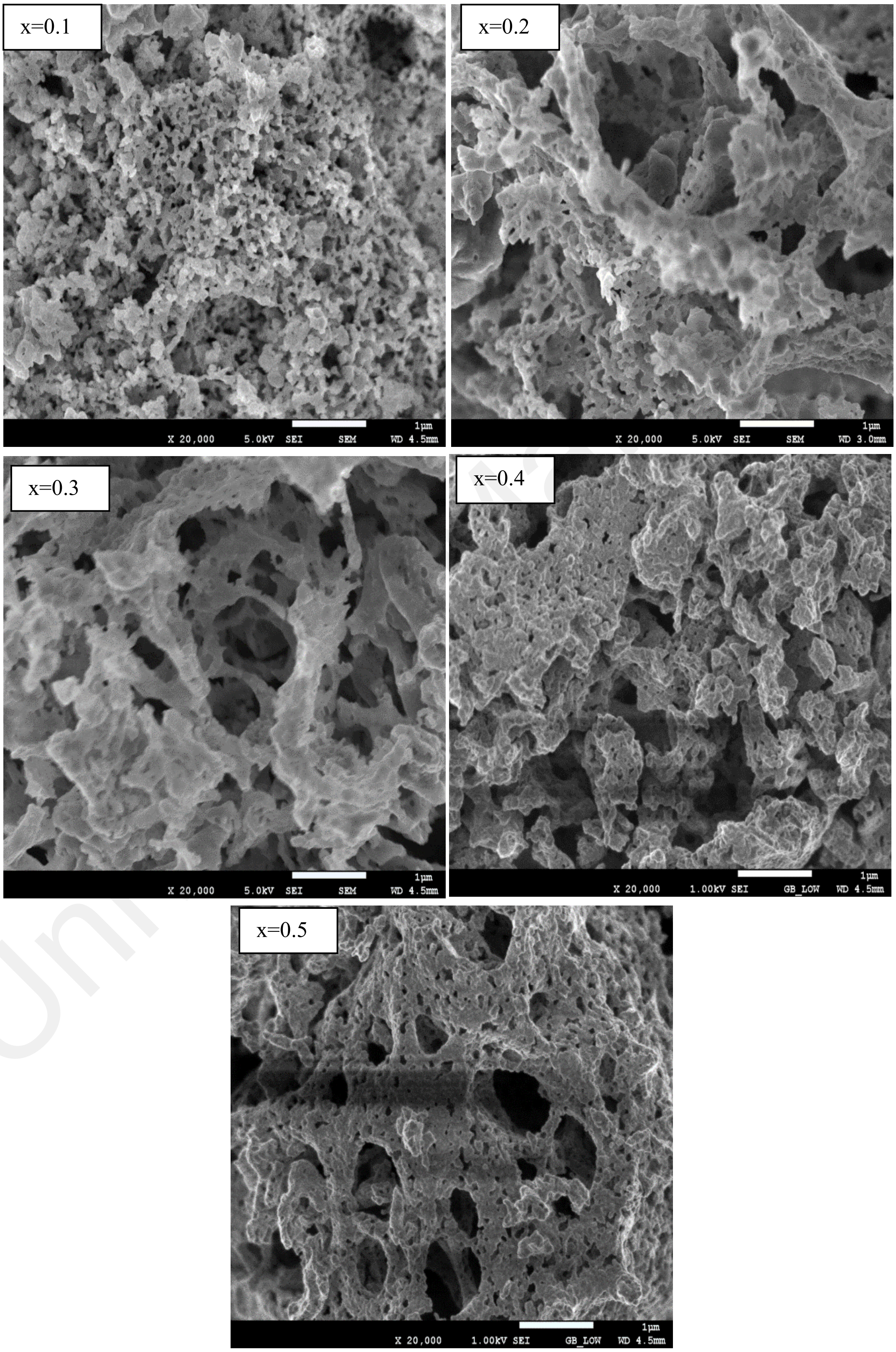

Figure 5.8: FESEM images of $MgMn_{2-x}Ca_xO_4$ (x=0.1,0.2,0.3,0.4,0.5) at 700°C.

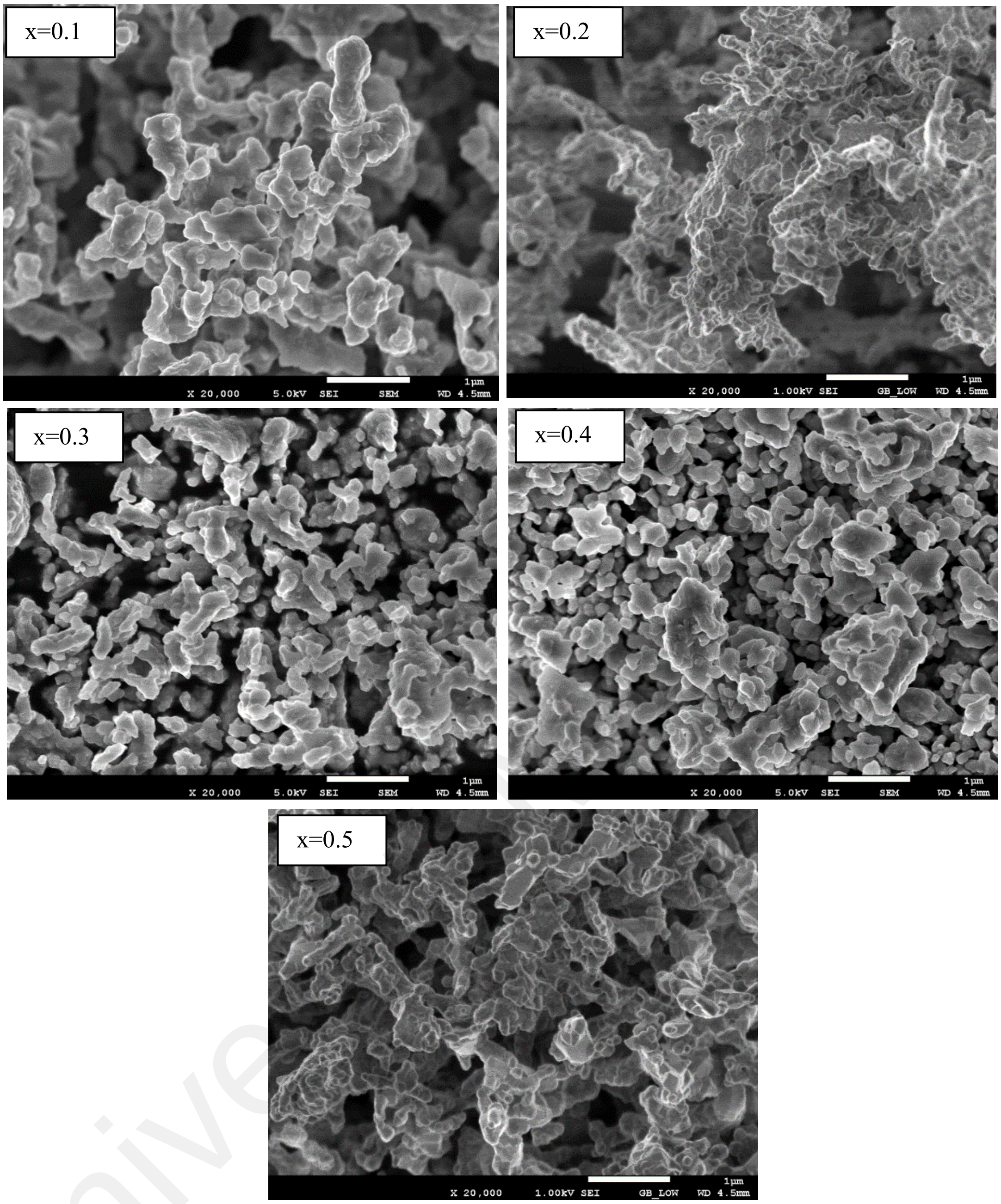

Figure 5.9: FESEM images of $MgMn_{2-x}Ca_xO_4$ at (x=0.1,0.2,0.3,0.4,0.5) at 800°C.

Figure 5.10 and Figure 5.11 show FESEM images for $MgMn_{2-x}Sr_xO_4$ (x=0.1, 0.2, 0.3, 0.4 and 0.5) annealed at temperatures 700°C and 800°C respectively. On the other hand, the morphology of Sr doped sample at 700°C and 800°C shows the sponge-like framework or porous formation of interconnected pores. The porous formation of the samples could be attributed to the doping effect of Sr in $MgMn_2O_4$. As displayed in Figure

5.10(b) and Figure 5.11(b) the image of $MgMn_{1.8}Sr_{0.2}O_4$ (x=0.2) at 700°C and 800°C depicts a higher porosity with multiple interconnected pores and smaller particle size compared to the other compositions of both temperatures. The porous formation and smaller particle size is expected to facilitate in ion intercalation and de-intercalation during the charge - discharge processes, thus give a better cycling performance of the magnesium cells which will be discussed in the battery performance section. The relationship between porosity and surface area of the particle was determined by BET measurements which will be discussed in Section 5.5.

Universiti Malaya

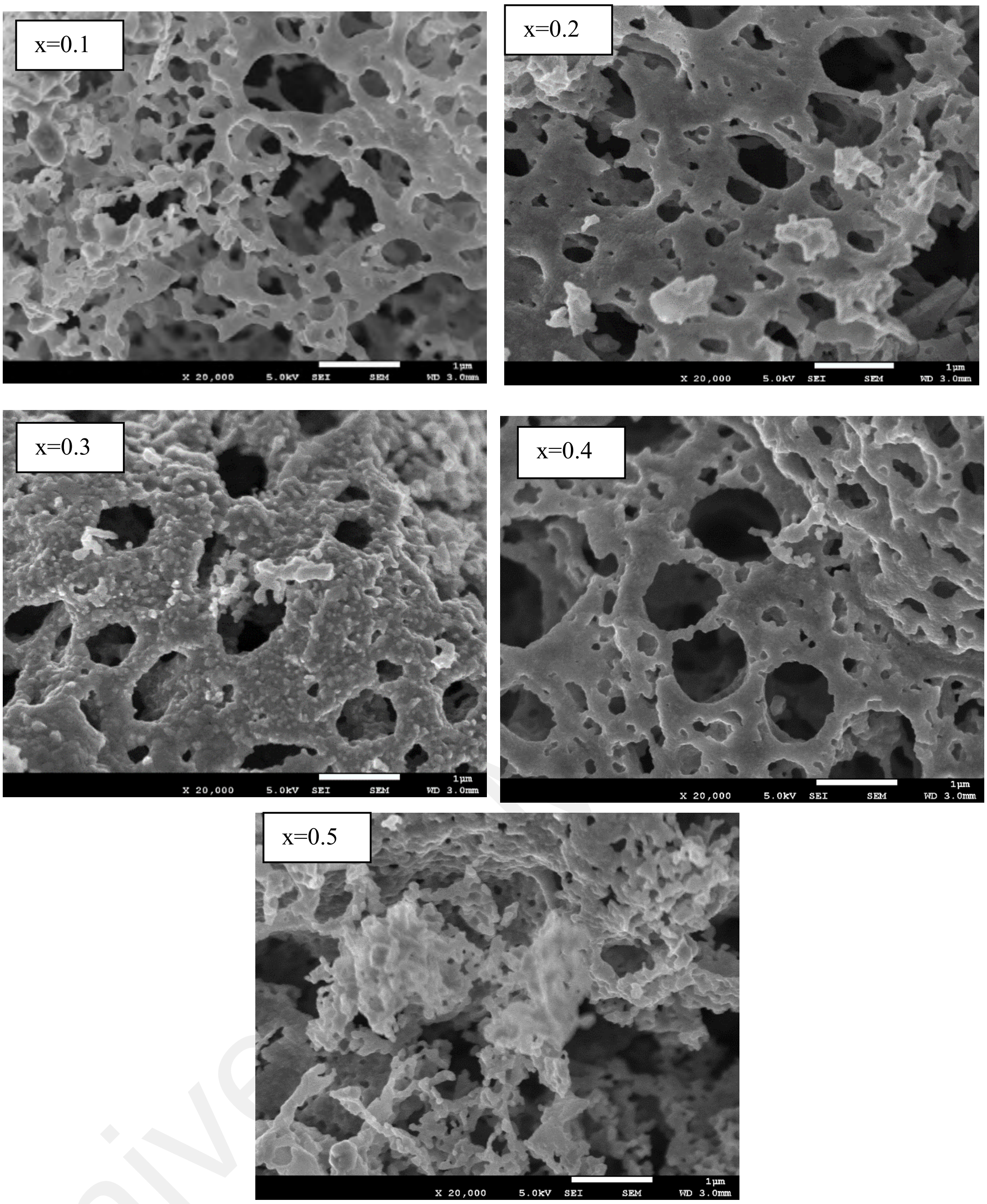

Figure 5.10: FESEM images of $MgMn_{2-x}Sr_xO_4$ (x=0.1,0.2,0.3,0.4,0.5) at 700°C.

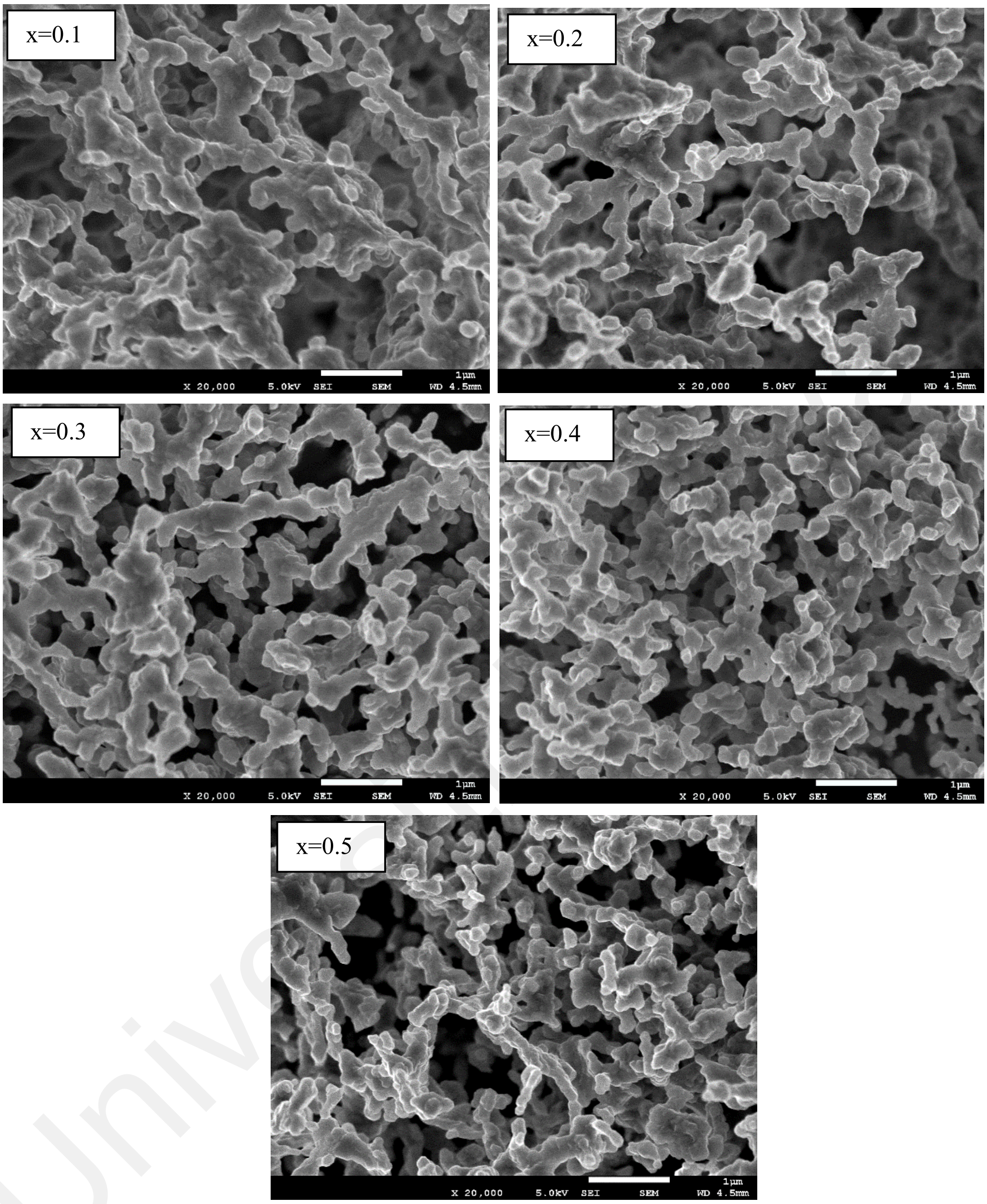

Figure 5.11: FESEM images of $MgMn_{2-x}Sr_xO_4$ (x=0.1,0.2,0.3,0.4,0.5) at 800°C.

5.3 Energy dispersive x-ray (EDX) and EDS mapping

Figure 5.12(a), (b) and (c) shows the EDX spectrum of $MgMn_2O_4$, $MgMn_{1.8}Ca_{0.2}O_4$ and $MgMn_{1.8}Sr_{0.2}O_4$ samples respectively. The presence of Ca and Sr elements is visibly detected in $MgMn_{1.8}Sr_{0.2}O_4$ and $MgMn_{1.8}Ca_{0.2}O_4$ samples as shown in the EDX spectrum, Figure 5.12(b) and (c). This implies that both doping has been successfully done through the self-propagating combustion synthesis.

Universiti Malaya

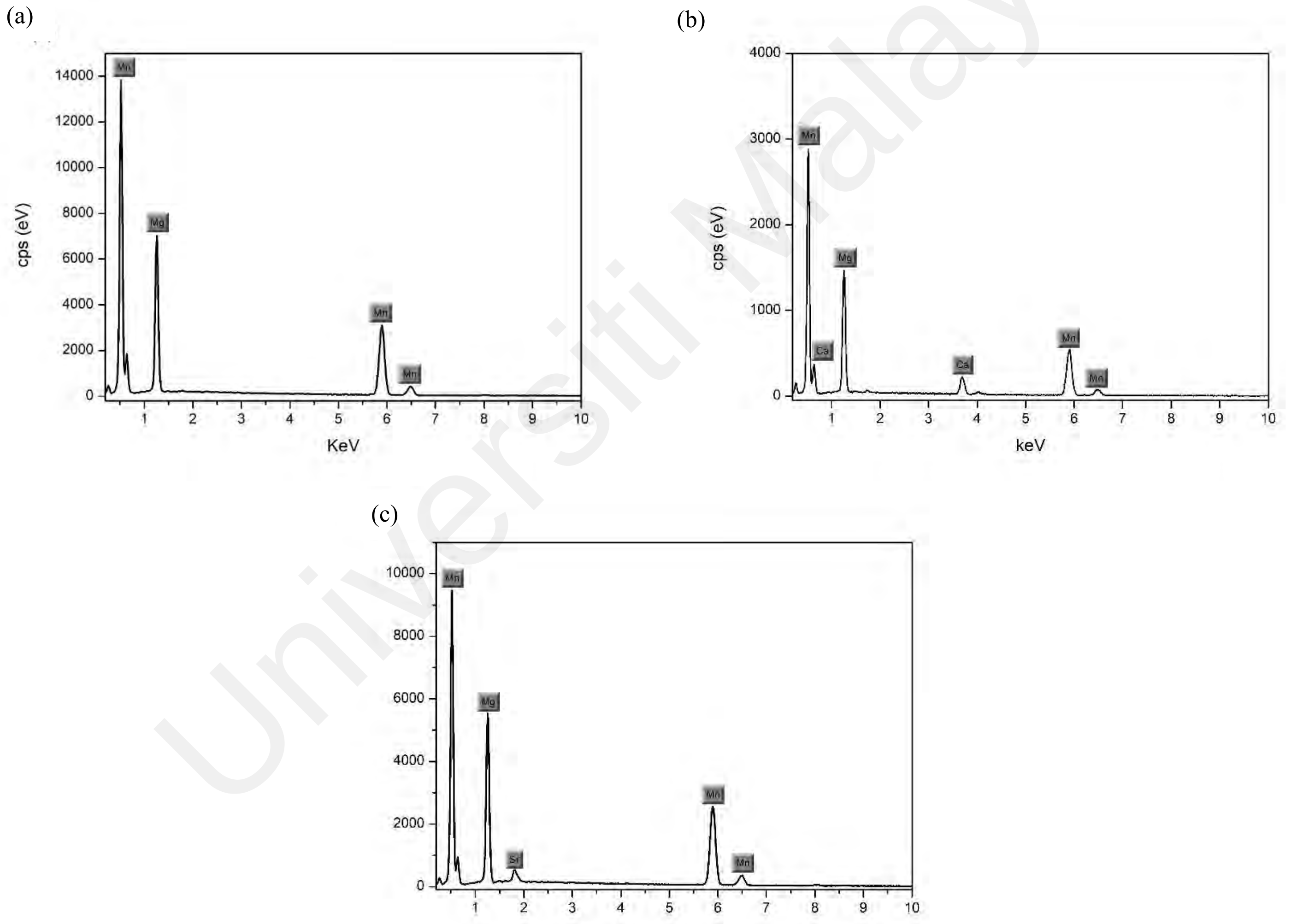

Figure 5.12: EDX spectrum of (a) $MgMn_2O_4$ (b) $MgMn_{1.8}Ca_{0.2}O_4$ and (c) $MgMn_{1.8}Sr_{0.2}O_4$.

The atomic percentages obtained from FESEM-EDX are compared with the calculated values as summarized in Table 5.1. It is observed that the atomic percentages of each element in the samples are approximately the same as the calculated values. Atomic ratios of the elements are related to the weight percentage of the element that composed in the samples in term of elements concentrations. The calculation has been done based on the stoichiometry value, where the amount of oxygen has been neglected considering the oxygen atoms had been reacted to the surrounding. Therefore, the presence of both Sr and Ca are confirmed and proved inside the magnesium manganese oxide samples. To confirm the distribution of each element in undoped and doped samples, EDS mapping has been performed as shown in Figure 5.13. The red distribution refers to Magnesium (Mg) atom while green distribution in the figure prefers to Manganese (Mn) element. The blue, grey and white distributions belong to O, Sr and Ca atoms respectively. The obtained results clearly verify the elementally homogeneous distribution of Sr and Ca within the $MgMn_2O_4$ samples.

Universiti Malaya

Table 5.1: Atomic percentage versus calculated percentage (%) of $MgMn_2O_4$, $MgMn_{1.8}Ca_{0.2}O_4$ and $MgMn_{1.8}Sr_{0.2}O_4$.

Element	Atomic percentage (%)	Calculated percentage (%)
$MgMn_2O_4$		
Mg	36.00	33.33
Mn	64.00	66.66
Total	100	100
$MgMn_{1.8}Ca_{0.2}O_4$		
Mg	22.88	25.40
Mn	66.97	65.62
Ca	10.14	8.98
Total	100	100
$MgMn_{1.8}Sr_{0.2}O_4$		
Mg	36.62	33.33
Mn	58.22	60.00
Sr	5.160	6.67
Total	100	100

Universiti Malaya

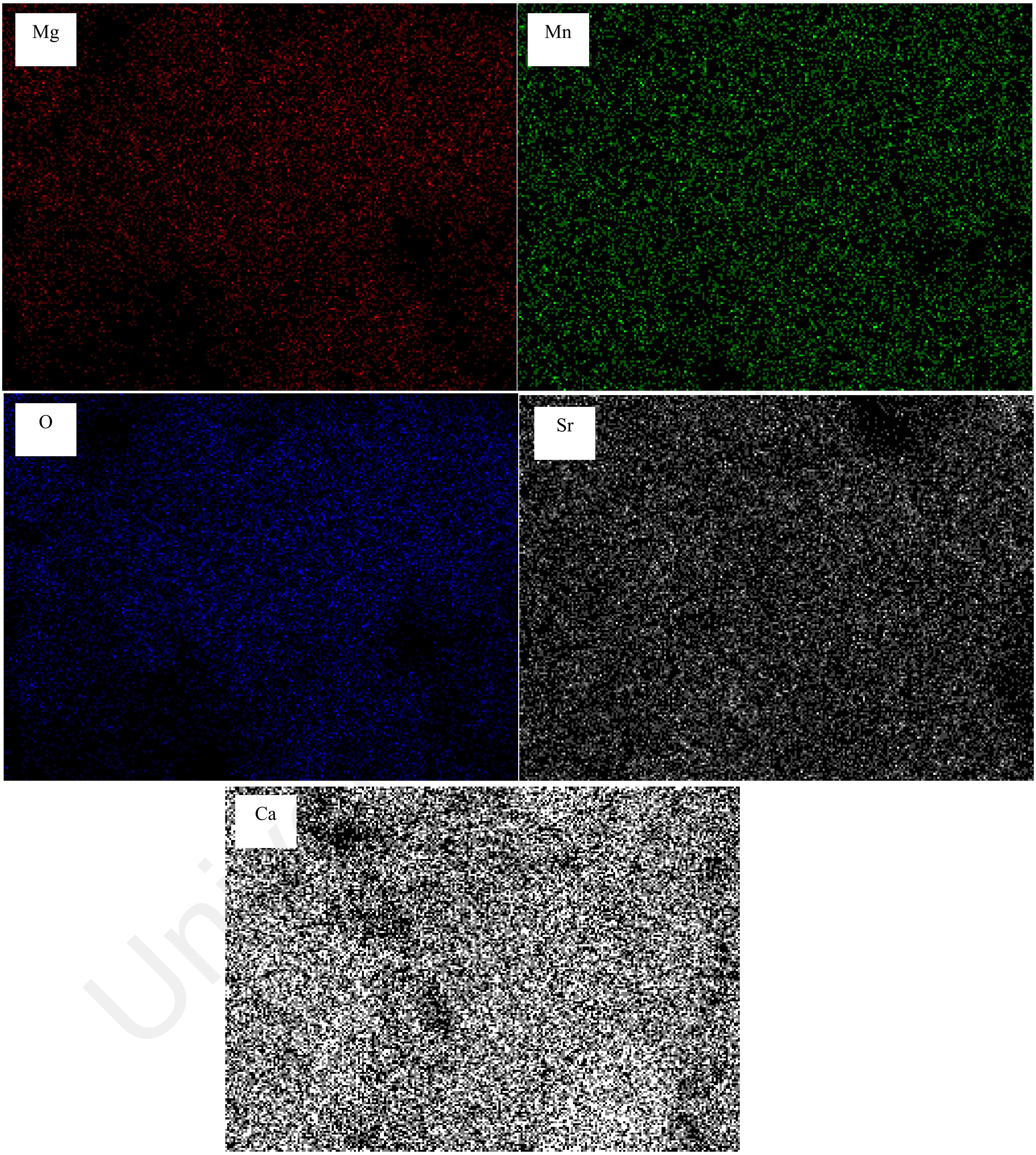

Figure 5.13: EDS mapping of Mg, Mn, O, Ca and Sr elements.

5.4 TEM Analysis

The morphology studies for this work are still not clear if only depends on the FESEM results alone since the obtained FESEM micrographs display almost the same properties. Therefore, the TEM analysis was done to investigate the detailed morphology of the samples for a better understanding on the structure and the particle behavior. The TEM images of selected $MgMn_2O_4$ and optimized $MgMn_{1.8}Sr_{0.2}O_4$ and $MgMn_{1.8}Ca_{0.2}O_4$ are display in Figure 5.14. The images show the homogenous nature which were found to be polycrystalline in nature. The particle size from the TEM images were found to be 342 nm for $MgMn_2O_4$. Figure 5.14(b) depicts a particle size of 263.4 nm for $MgMn_{1.8}Sr_{0.2}O_4$ while $MgMn_{1.8}Ca_{0.2}O_4$ at 700°C (x=0.2) and $MgMn_{1.6}Ca_{0.4}O_4$ (x=0.4) at 800°C depicts a size of 27.64 nm and 72.6 nm respectively. It can be seen the cubic shapes from Figure 5.14(b), (c) and (d). This work is consistent with the XRD results, in which a structural phase of $MgMn_2O_4$ transformed from a tetragonal to a cubic structure in the doped sample. Since cubic is the most stable structure, so this result proved that the transformation of the structural could be a factor that affect the performance of the Mg cell.

Universiti Malaya

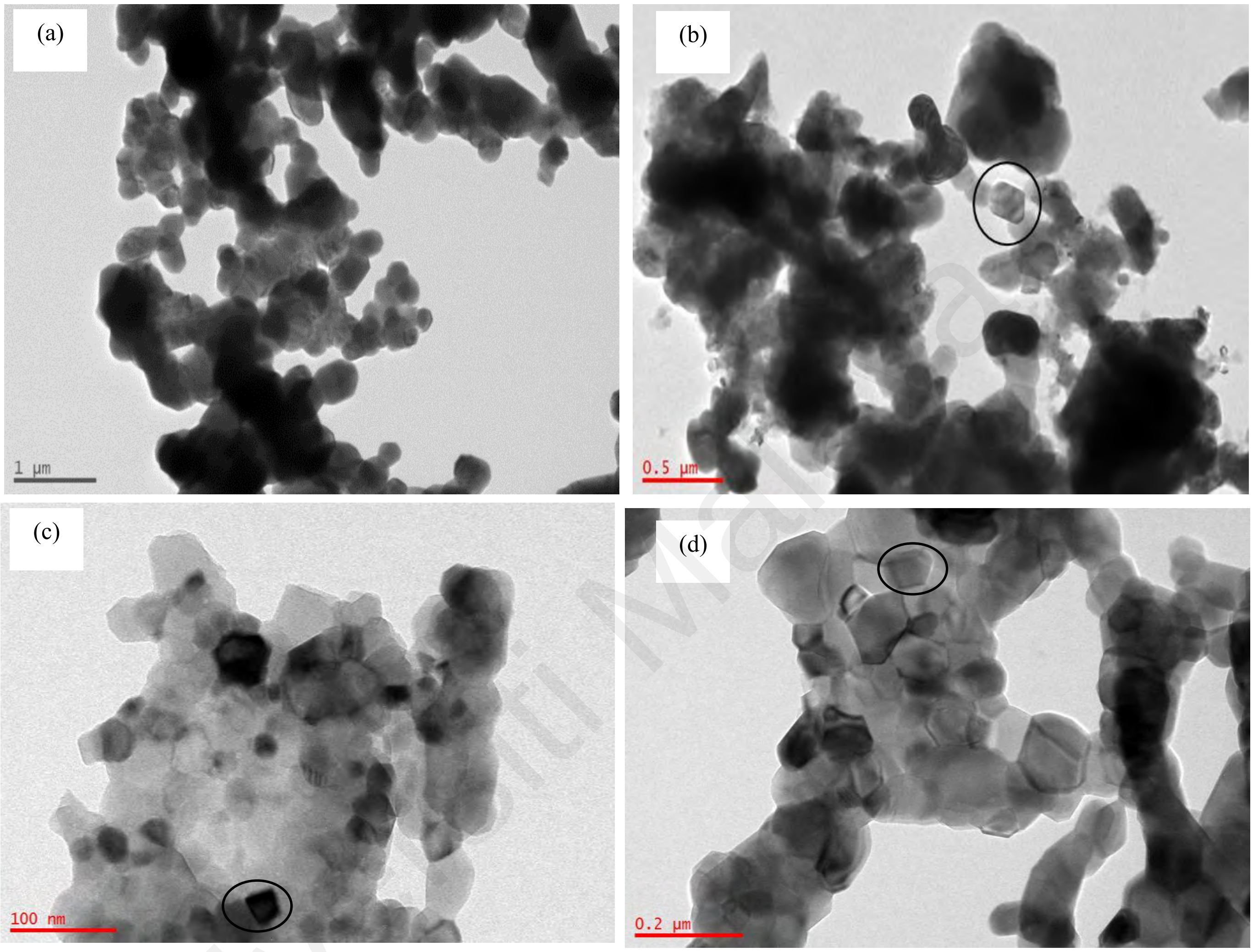

Figure 5.14: TEM images for samples (a) $MgMn_2O_4$ at 800°C (b) $MgMn_{1.8}Sr_{0.2}O_4$ at 800°C (c) $MgMn_{1.8}Ca_{0.2}O_4$ at 700°C and (d) $MgMn_{1.6}Ca0._4O_4$ at 800°C.

Universiti Malaya

5.5 BET Measurements

In order to further study about the porosity of the undoped and optimized Ca and Sr doped $MgMn_2O_4$, Brunner-Emmett-Teller theory (BET) measurements were carried out.

5.5.1 N_2 Adsorption / desorption isotherm of optimized cathode materials at temperature 700°C and 800°C

Based on the classification standard of International of Pure and Applied Chemistry (IUPAC), the adsorption isotherm can be classified as type II for the $MgMn_2O_4$, $MgMn_{1.8}Sr_{0.2}O_4$ and $MgMn_{1.8}Ca_{0.2}O_4$ at temperature 700°C and 800°C as shown in Figure 5.15 and Figure 5.16 respectively. This means they are macroporous. Table 5.2 shows the specific surface area (S_{BET}), the total pore volume, and average diameter for the undoped sample and optimized Sr and Ca samples were calculated using BET method at temperature 700°C and 800°C.

It can be observed that at temperature 700°C, the S_{BET} of the undoped sample, $MgMn_2O_4$ is 2.5504 $m^2\ g^{-1}$ while for optimized Sr and Ca doped samples are 8.5967 $m^2\ g^{-1}$ and 10.1907 $m^2\ g^{-1}$ respectively. For temperature 800°C, S_{BET} of the undoped sample, $MgMn_2O_4$ is 2.9999 $m^2\ g^{-1}$ while for optimized Sr and Ca doped samples are 4.5929 $m^2\ g^{-1}$ and 10.4214 $m^2\ g^{-1}$ respectively. This shows that both Sr and Ca doped samples at both temperatures have a larger specific surface area than undoped $MgMn_2O_4$ sample. This result can be related to FESEM and TEM images where the smallest particle size gives larger surface area. The doping $MgMn_2O_4$ with Ca and Sr dopant also affected the aspect of the porosity of the materials. The larger porosity can deliver the good ions movements, ions intercalations, and give better electrochemical properties of the cathode materials, thus it is expected a better performance of Mg ion cell.

Universiti Malaya

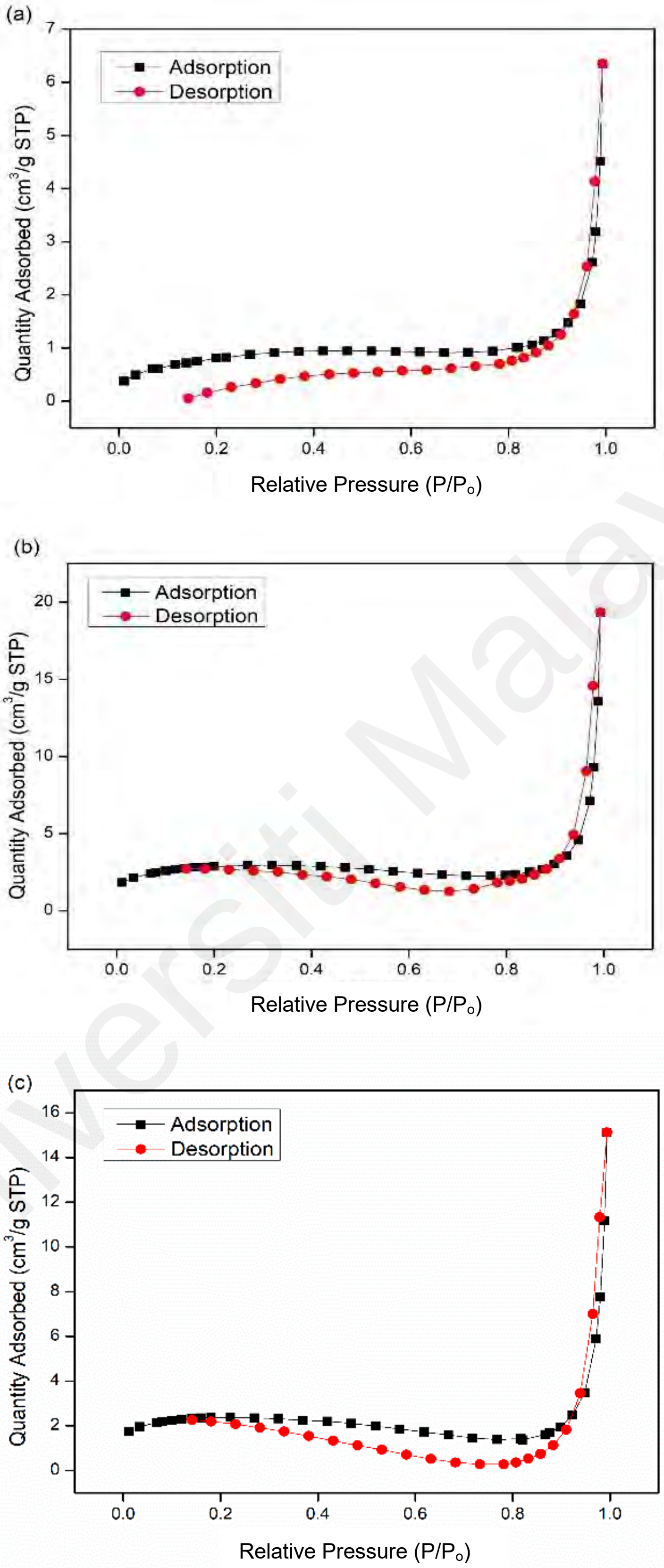

Universiti Malaya

Figure 5.15: N_2 adsorption – desorption isotherms of (a) $MgMn_2O_4$ (b) $MgMn_{1.8}Sr_{0.2}O_4$ and (c) $MgMn_{1.8}Ca_{0.2}O_4$ at temperature 700°C.

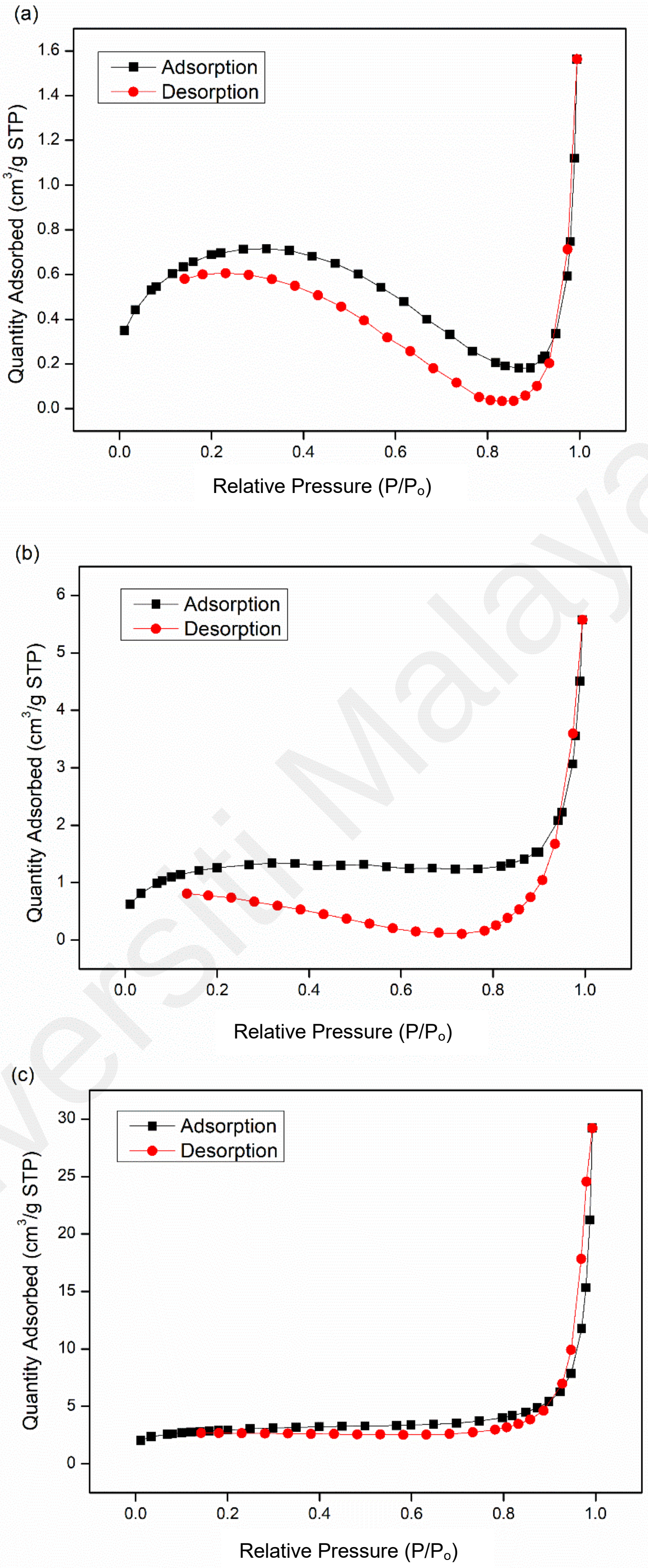

Universiti Malaya

Figure 5.16: N_2 adsorption – desorption isotherms of (a) $MgMn_2O_4$ (b) $MgMn_{1.8}Sr_{0.2}O_4$ and (c) $MgMn_{1.6}Ca_{0.4}O_4$ at temperature 800°C.

Table 5.2: BET surface area , pore size and pore volume of $MgMn_2O_4$, $MgMn_{1.8}Sr_{0.2}O_4$, $MgMn_{1.8}Ca_{0.2}O_4$ and $MgMn_{1.6}Ca_{0.4}O_4$ at temperature 700°C and 800°C.

Cathode materials	Specific surface area, S_{BET} (m^2 g^{-1})	Pore Volume (cm^3 g^{-1})	Pore size (Å)
$MgMn_2O_4$ - 700	2.5504	0.009815	13.08702
Sr0.2 - 700	8.5967	0.023395	108.8540
Ca0.2 - 700	10.1907	0.029899	11.73596
$MgMn_2O_4$ - 800	2.9999	0.002417	3.79096
Sr0.2 - 800	4.5929	0.008617	75.04630
Ca0.4 - 800	10.4214	0.045183	173.4242

Universiti Malaya

5.6 Raman Spectroscopy

In this work, Raman experiments had been performed in room temperature (RT) to characterize the Raman spectra of optimized $MgMn_2O_4$, $MgMn_{2-x}Sr_xO_4$ and $MgMn_{2-x}Ca_xO_4$. Manganese oxides compounds have been reported in the previous studies which consist of three major vibrational features regions (Julien & Massot, 2003; Julien, 2006). These regions include vibrational modes at 200-450 cm^{-1}, 450-540 cm^{-1} and 550-740cm^{-1} which corresponds to spectral domains where skeletal vibrations, deformation modes of a metal-oxygen chain of Mn-O-Mn in the octahedral lattice of MnO_2 and stretching modes of Mn-O bonds in MnO_6 octahedra respectively.

Figure 5.17 depicts the overall Raman spectra for $MgMn_2O_4$, $MgMn_{2-x}Sr_xO_4$ (x=0.2) and $MgMn_{2-x}Ca_xO_4$ (x=0.2 and x=0.4) at 700°C and 800°C in the region between 200 cm^{-1} and 1000 cm^{-1}. All the spectra show common characteristics: a strong peak around 630–660 cm^{-1}, a group of peaks between 200 and 470 cm^{-1}, and a less intense peak at around 530–600 cm^{-1}. In this work, peak at around 650 cm^{-1} is the most intense peak for $MgMn_2O_4$, $MgMn_{2-x}Sr_xO_4$ and $MgMn_{2-x}Ca_xO_4$ samples for both temperatures. At temperature 700°C and 800°C, the most intense peak of $MgMn_2O_4$ shifted from 655 cm^{-1} to 635 cm^{-1} and 646 cm^{-1} to 652 cm^{-1} in $MgMn_{1.8}Sr_{0.2}O_4$ respectively. For optimized Ca-doped samples, the peak was shifted to the high frequency at 700°C and 800°C, which are 662 cm^{-1} and 665 cm^{-1} respectively. These results can be explained by the relative intensity of the peak that decrease with decrease of tetragonal distortion as given by c/a lattice constant (Malavasi et al., 2002). It is consistent with XRD results in the previous section. This distortion is the evidence that interstitial both Sr and Ca doping into $MgMn_2O_4$ was successfully done.

Universiti Malaya

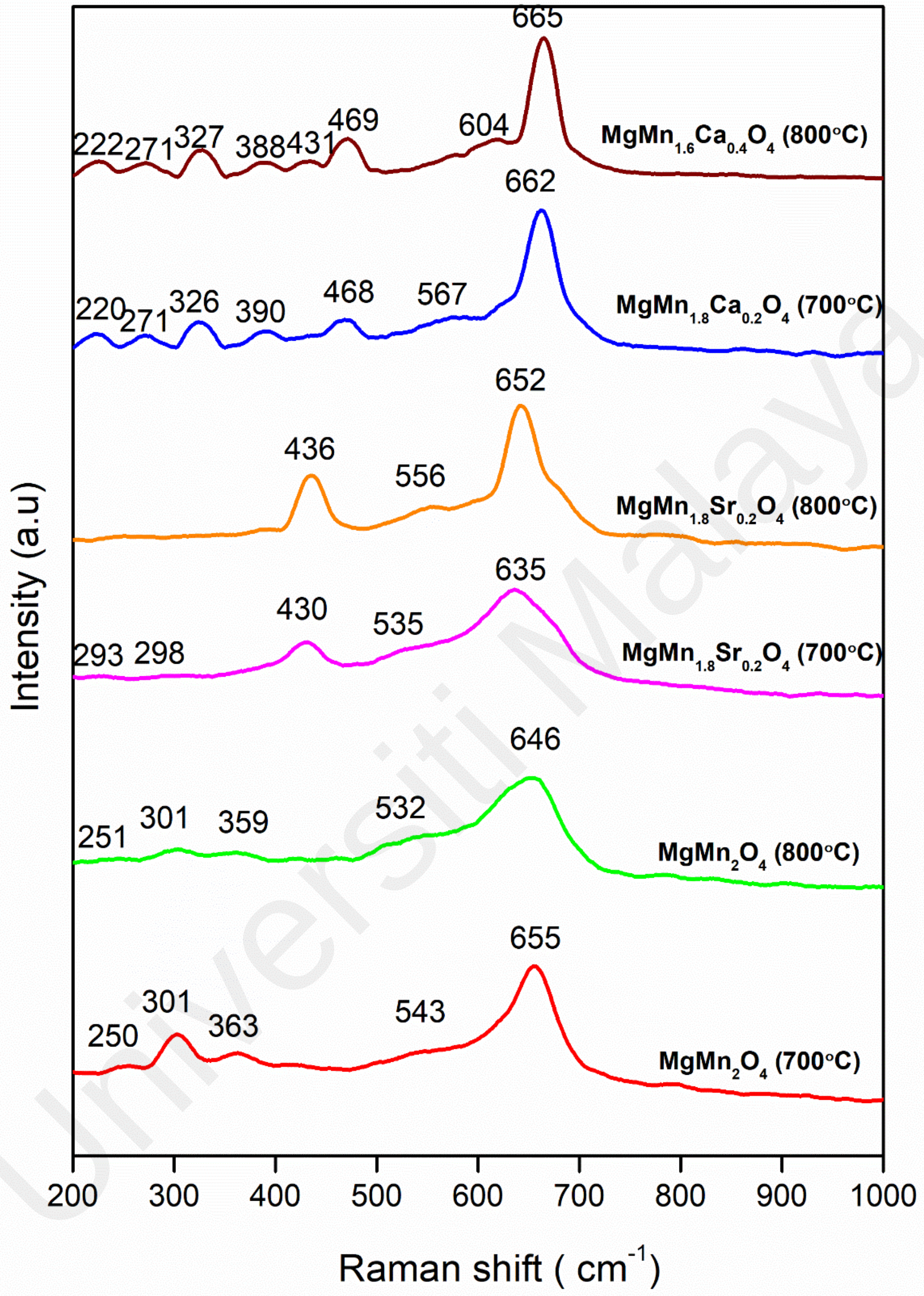

Universiti Malaya

Figure 5.17: Raman spectra for optimized $MgMn_2O_4$, $MgMn_{1.8}Sr_{0.2}O_4$, $MgMn_{1.8}Ca_{0.2}O_4$ and $MgMn_{1.6}Ca_{0.4}O_4$ at temperature 700°C and 800°C.

A very broad peak and very low intensity are centered in a range of 530 to 600 cm^{-1} show in Figure 5.18(a) and (b) for $MgMn_2O_4$ optimized $MgMn_{2-x}Sr_xO_4$ and $MgMn_{2-x}Ca_xO_4$ samples at temperatures 700°C and 800°C. This range of a peak has similar features for Raman scattering for cubic $LiMn_2O_4$ that related to Li–O motion at around 500 cm^{-1} as reported by Prabaharan et al. (2004) (Prabaharan et al., 2004). In this study, it can be proved that the shift of the peaks can be related to Mn-O bonds in MnO_6 octahedra in $MgMn_2O_4$ materials. Figure 5.18(a) and (b) show there is a frequency peak at around 400 cm^{-1} present in Ca and Sr doped samples at both temperatures. The frequency of $MgMn_{1.8}Sr_{0.2}O_4$ and $MgMn_{1.8}Ca_{0.2}O_4$ at temperature 700°C was 431 cm^{-1} and 468 cm^{-1} respectively as shown in Figure 5.18(a). There is one peak for $MgMn_{1.8}Sr_{0.2}O_4$ which is 436 cm^{-1} and two peaks for $MgMn_{1.6}Ca_{0.4}O_4$ are 431 cm^{-1} and 469 cm^{-1} at 800°C which refer to the cation disorder due to Ca and Sr doping as shown in Figure 5.18(b).

The second broadening peak was found in the undoped sample, $MgMn_2O_4$, that is located at 363 and 359 cm^{-1} for 700°C and 800°C, respectively. It also can be noticed that the peak at 800°C is broader and high intense than at 700°C. The broadening peak can be related to the cation–anion, Mn-O bond lengths and polyhedral distortion occurring in this sample (Michalska et al., 2018). The peak between 300 cm^{-1} and 360 cm^{-1} also can be observed in $MgMn_{2-x}Ca_xO_4$ with different temperatures but was disappeared in Sr-doped samples at 800°C. These observations might be due to the interstitial Sr and Ca doping towards Mn ions, which located at tetrahedral sites thus influenced structure changes from tetragonal to cubic structure.

At very low frequency regions, there was a group of peak present for undoped and doped samples within range 220 cm^{-1} to 290 cm^{-1}. The intensity of optimized Ca doped samples for both temperatures are increases as compared to undoped sample. Figure 5.18

Universiti Malaya

(a) displays that the frequency peak within this region for Sr doped cathode materials is broader. At temperature 700°C, the peak for undoped sample was shifted from 250 cm^{-1} to 293 cm^{-1} for Sr doped and to 271 cm^{-1} for Ca doped and at temperature 800°C, the peak spectra shifted from 251 cm^{-1} to 271 cm^{-1} for Ca doped samples. From a previous study, Lorenzo et al. (2002) reported that a new peak centered around 270 cm^{-1} is due to appreciable inversion degree has been detected at RT for $MgMn_2O_4$ then suggested that this kind of mode can be related to the presence of a non-null inversion degree (Malavasi, Ghigna, et al., 2002).

Universiti Malaya

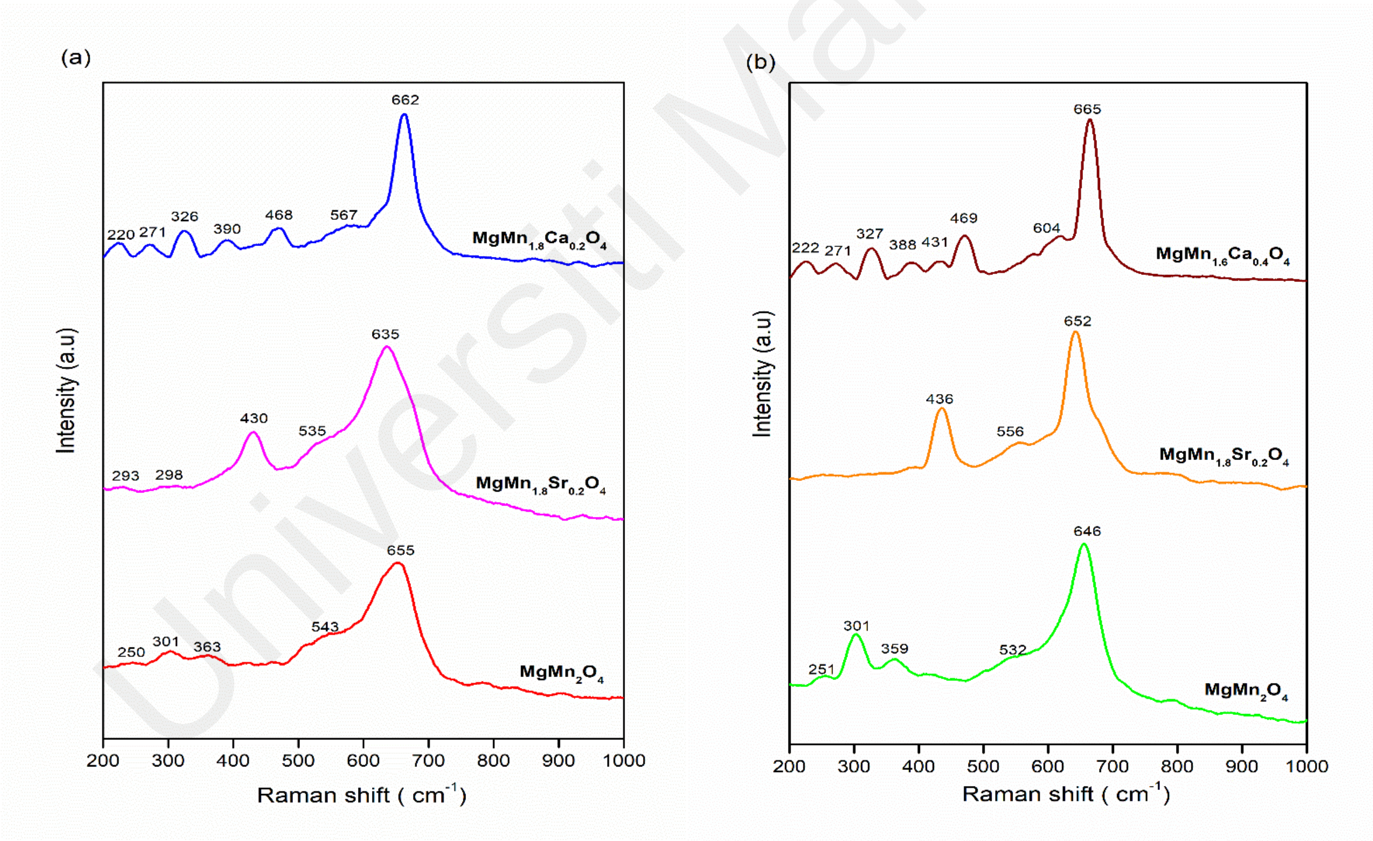

Figure 5.18: Raman spectra for $MgMn_2O_4$, $MgMn_{1.8}Sr_{0.2}O_4$, $MgMn_{1.8}Ca_{0.2}O_4$ and $MgMn_{1.6}Ca_{0.4}O_4$ at (a) 700°C (b) 800°C.

CHAPTER 6: ELECTROCHEMICAL STUDIES

6.1 Electrochemical studies

The electrochemical studies were carried out using the Linear sweep voltammetry (LSV) and Cyclic voltammetry (CV) in order to check the electrochemical potential window anodic stability limits of the above current collectors and understand the redox reaction potentials of the cathode materials during cycling respectively. LSV was performed using magnesium metal as the counter and reference electrodes, cathode materials as the working electrode.

The type of electrolytes used in electrochemical testing is very important as it may influence the voltage stability, capacities and cycling stability. In this project, the electrolyte used based on 1M Magnesium trifluorometahnesulfonate ($Mg(CF_3SO_3)_2$). The LSV and CV of $MgMn_2O_4$ and all compositions of $MgMn_{2-x}Sr_xO4$ and $MgMn_{2-x}Ca_xO_4$ annealed at 700°C and 800°C are shown in Figures 6.1 to Figures 6.9. The LSV studies were conducted at a voltage range of -5 V to 5 V for all samples at speed 5 mV s^{-1}.

6.1.1 LSV of $MgMn_2O_4$ at 700°C and 800°C

Figure 6.1(a) and (b) shows linear sweep voltammetry of undoped samples, $MgMn_2O_4$ at temperatures 700°C and 800°C. The electrochemical potential window of undoped samples is observed within range -2.81V to 2.72 V and -2.50 V to 3.09 V at 700°C and 800°C respectively as in Figure 6.1(a) and (b) in $Mg(CF_3SO_3)_2$ electrolyte. High oxidation voltage was obtained from $MgMn_2O_4$ at 800°C as in Figure 6.1(b) which higher temperature will increase the oxidation voltage thus improving the stability of the samples. Hence, temperature influenced the stability of the samples where high temperature will produce a high electrochemical potential window. The cut-off voltage produces at 700°C and 800°C was 2.72 V and 3.09 V respectively.

Universiti Malaya

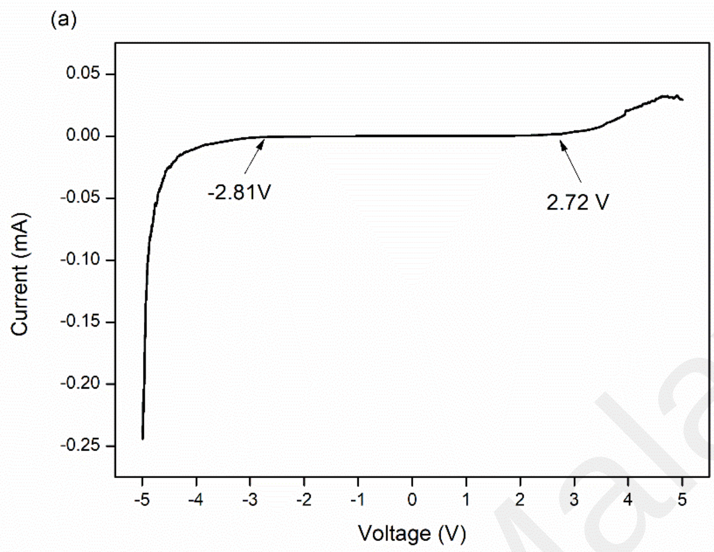

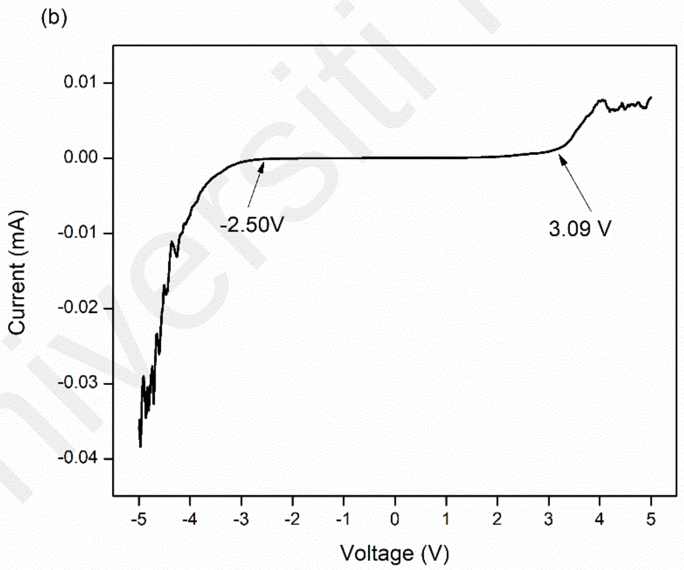

Figure 6.1: Linear sweep voltametry (LSV) of $MgMn_2O_4$ at temperature (a) 700°C (b) 800°C.

Universiti Malaya

6.1.2 LSV of $MgMn_{2-x}Ca_xO_4$ at 700°C and 800°C

Figure 6.2, 6.3 and 6.4 show linear sweep voltammetry of $MgMn_{2-x}Ca_xO_4$ for all compositions (x=0.1, 0.2, 0.3, 0.4 and 0.5) at temperatures of 700°C and 800°C. The result of Ca-doped samples at 700°C as in Figure 6.3, all the compositions are electrochemically stable within range -0.5 V to 3.2 V.

Several authors have reported that the working electrode (platinum (Pt), stainless steel (SS) , copper (Cu), Aluminium (Al)) used for the measurement will affect the results of the stability of the cells (Lv et al., 2013). Tyler et al. (2014) were reported that the oxidation onset potential for Pt, SS, Al was similar at around 3.2 V vs. Mg where the oxidation onset was always highly dependent on the electrode material (Carter et al., 2014). In this study, the current collector used was stainless steel (SS) mesh and the results shown that the stability voltage can be up to 3.2 V. As shown in Figure 6.3, the Ca-doped with composition x=0.2 at temperature 700°C exhibit the highest voltage stability compared to undoped sample and other Ca compositions which is 3.15 V. For magnesium battery, although the voltage stability can achieve higher voltage but in terms of current, it only can produce a minimal current which is up to 0.03 mA for undoped and doped samples as shown in Figure 6.3 and Figure 6.4. According to Saha et al. (2014), this minimal anodic/oxidation current is due to the electrolyte oxidation/decomposition observed in the positive scan until potential of ~2.2 V (Saha et al., 2014).

From the Ca-doped results at 800°C as in Figure 6.4, all the compositions are electrochemically stable within range -0.45 V to 3.4 V. Ca-doped samples with composition x=0.4 at 800°C exhibited the most stable potential window within range of -3.12 V to 3.37 V.

Universiti Malaya

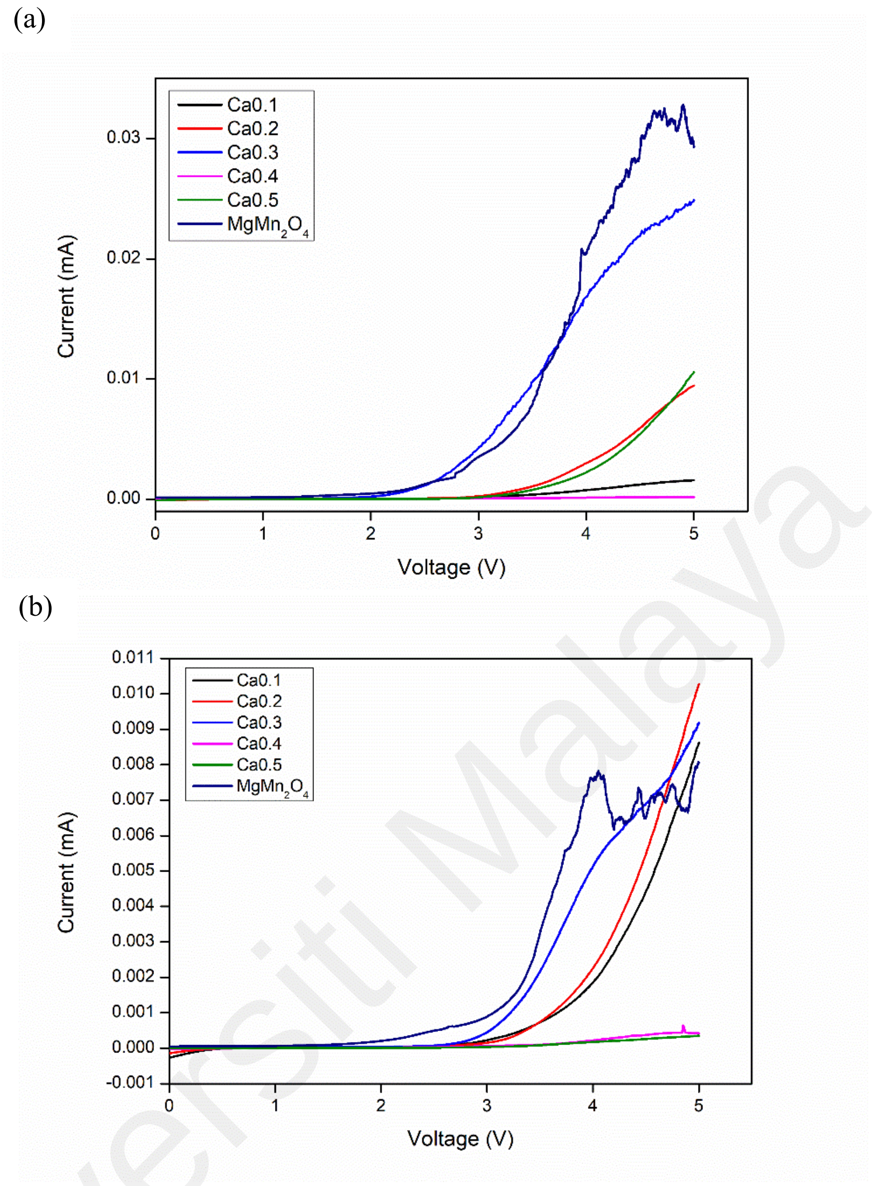

Figure 6.2: Linear sweep voltammetry (LSV) of undoped and all compositions of Ca doped samples at temperature (a) 700°C and (b) 800°C.

It can be summarized for Ca doped samples for both temperatures, x=0.2 at 700°C exhibited higher oxidation voltage which is 3.15 V while at 800°C, x=0.4 delivered higher oxidation voltage but from overall results, the samples at temperature 800°C produce very high stability as compared to 700°C. The optimized Ca doped samples were further explored to perform cyclic voltammetry and battery performance profiles.

Universiti Malaya

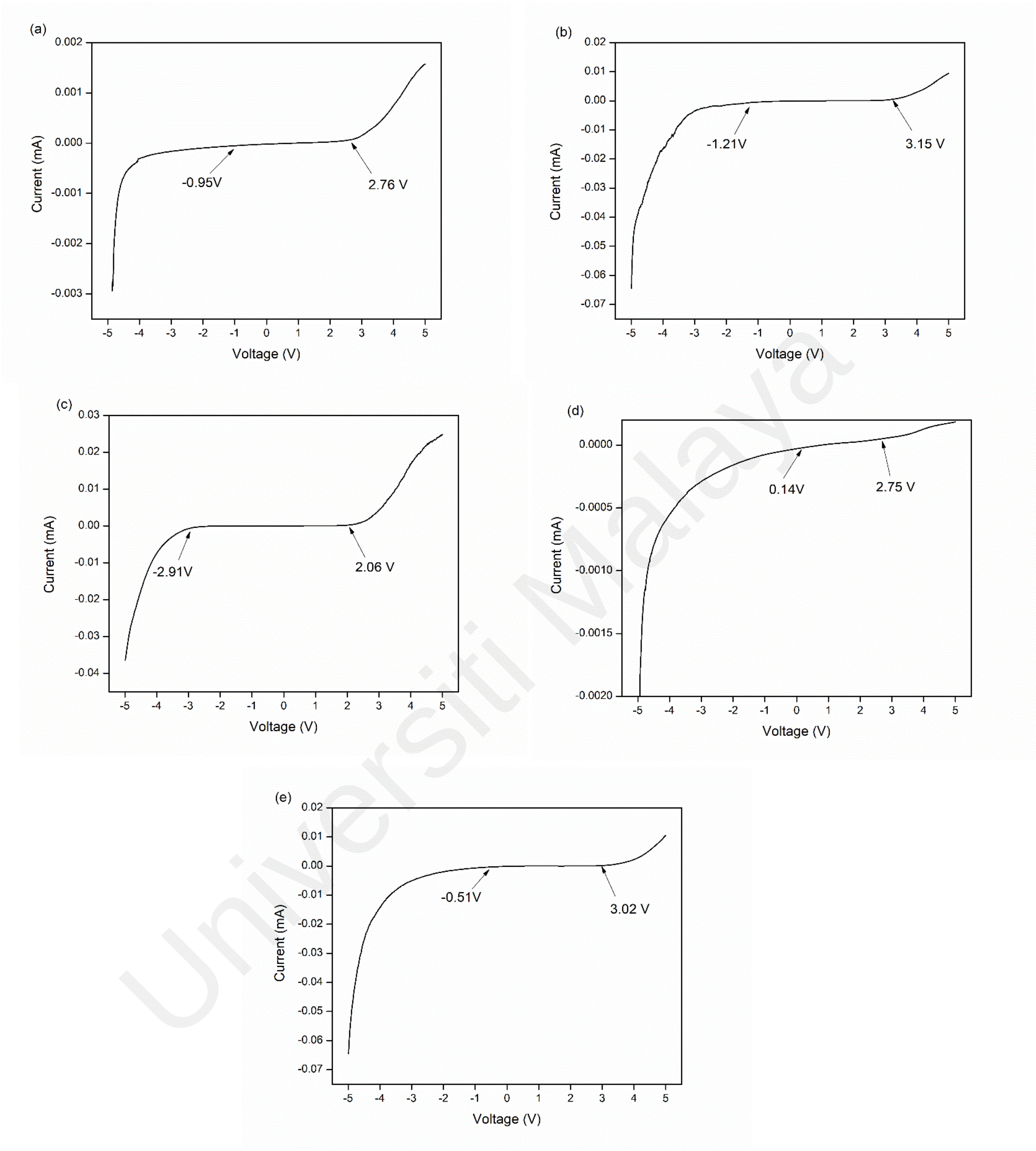

Universiti Malaya

Figure 6.3: Linear sweep voltammetry (LSV) of $MgMn_{2-x}Ca_xO_4$ at 700°C (a) x=0.1 (b) x=0.2 (c) x=0.3 (d) x=0.4 (e) x=0.5.

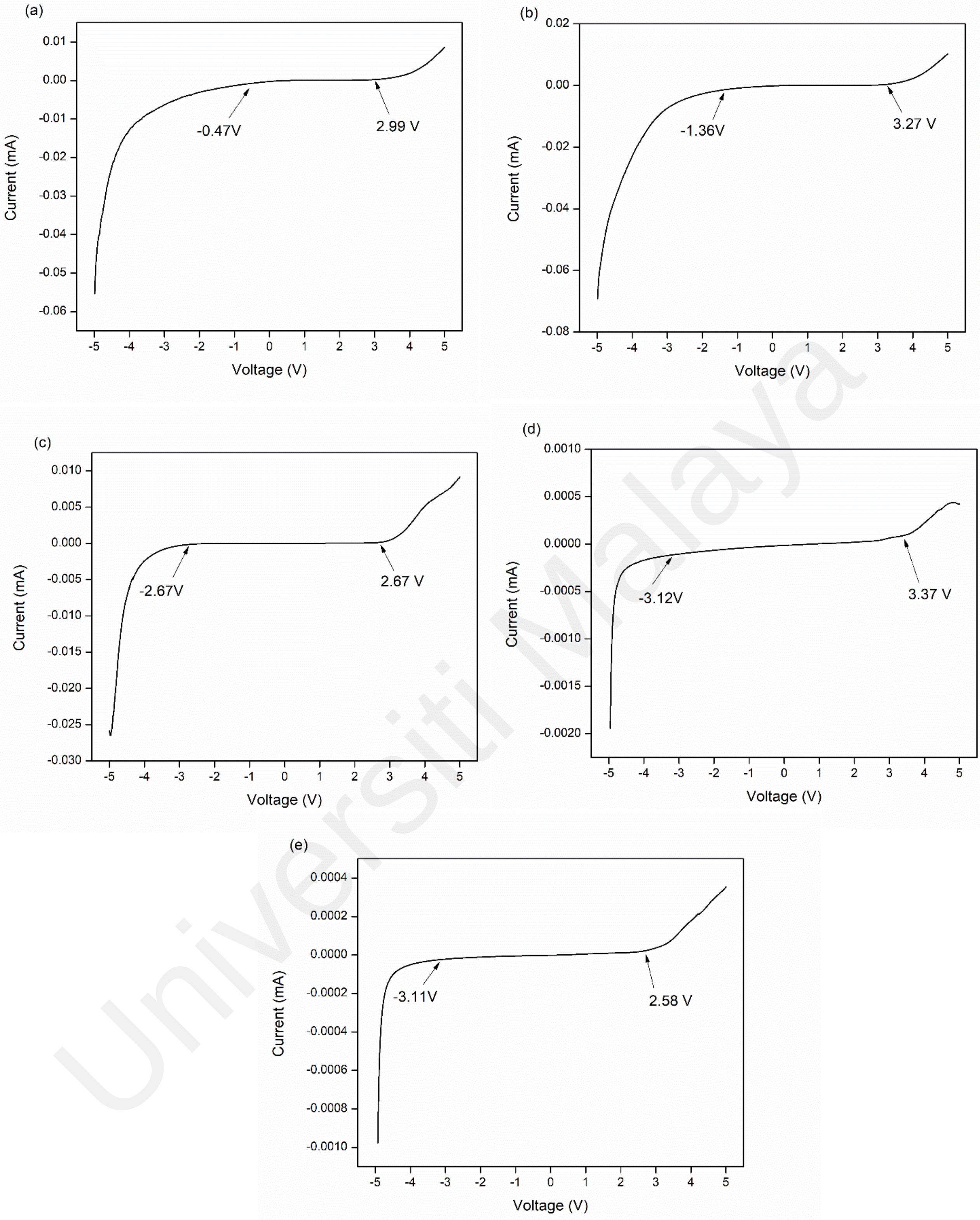

Universiti Malaya

Figure 6.4: Linear sweep voltammetry (LSV) of $MgMn_{2-x}Ca_xO_4$ at 800°C (a) x=0.1 (b) x=0.2 (c) x=0.3 (d) x=0.4 (e) x=0.5.

6.1.3 LSV of $MgMn_{2-x}Sr_xO_4$ at 700°C and 800°C

Figures 6.5, 6.6 and 6.7 show linear sweep voltammetry of $MgMn_{2-x}Sr_xO_4$ for all compositions (x = 0.1, 0.2, 0.3, 0.4 and 0.5) at temperatures of 700°C and 800°C. For the Sr-doped samples, at temperature 700°C, all the compositions are electrochemically stable within range -0.45 V to 3.15 V. Among all the compositions, sample with x=0.2 is selected to be the optimized Sr doped samples that produced a high electrochemical potential window at temperatures 700°C and 800°C. At 700°C, $MgMn_{1.8}Sr_{0.2}O_4$ was stable from -3.43 V to 2.72 V which the potential voltage difference was 6.15 while the other compositions show low voltage differences, about 3.5. On the other hand, at 800°C, the electrochemical potential window stability of the sample is within the range of -3.75 V to 3.20 V where it depicts a higher potential difference of 6.95 compared to undoped and other compositions. The stability of all the doped and undoped samples at both temperatures can obviously be displayed in Figure 6.5(a) and (b).

The anodic current was observed at the range of 0.004 mA to 0.03 mA for all samples at both temperatures but the highest anodic current belongs to the sample at composition x=0.2 at temperature 800°C which is 0.03 mA. For all compositions of Sr doped samples offered the higher oxidation voltage which is above 3.0 V are observed. This can be concluded that the samples at temperature 800°C possess a higher potential and high current peak as compared to 700°C. As been observed from the graph, the increase in the voltage will also increase the peak current. From the entire LSV graph, the potential range is chosen within that stable range in order to conduct cyclic voltammetry and charge-discharge profile.

Universiti Malaya

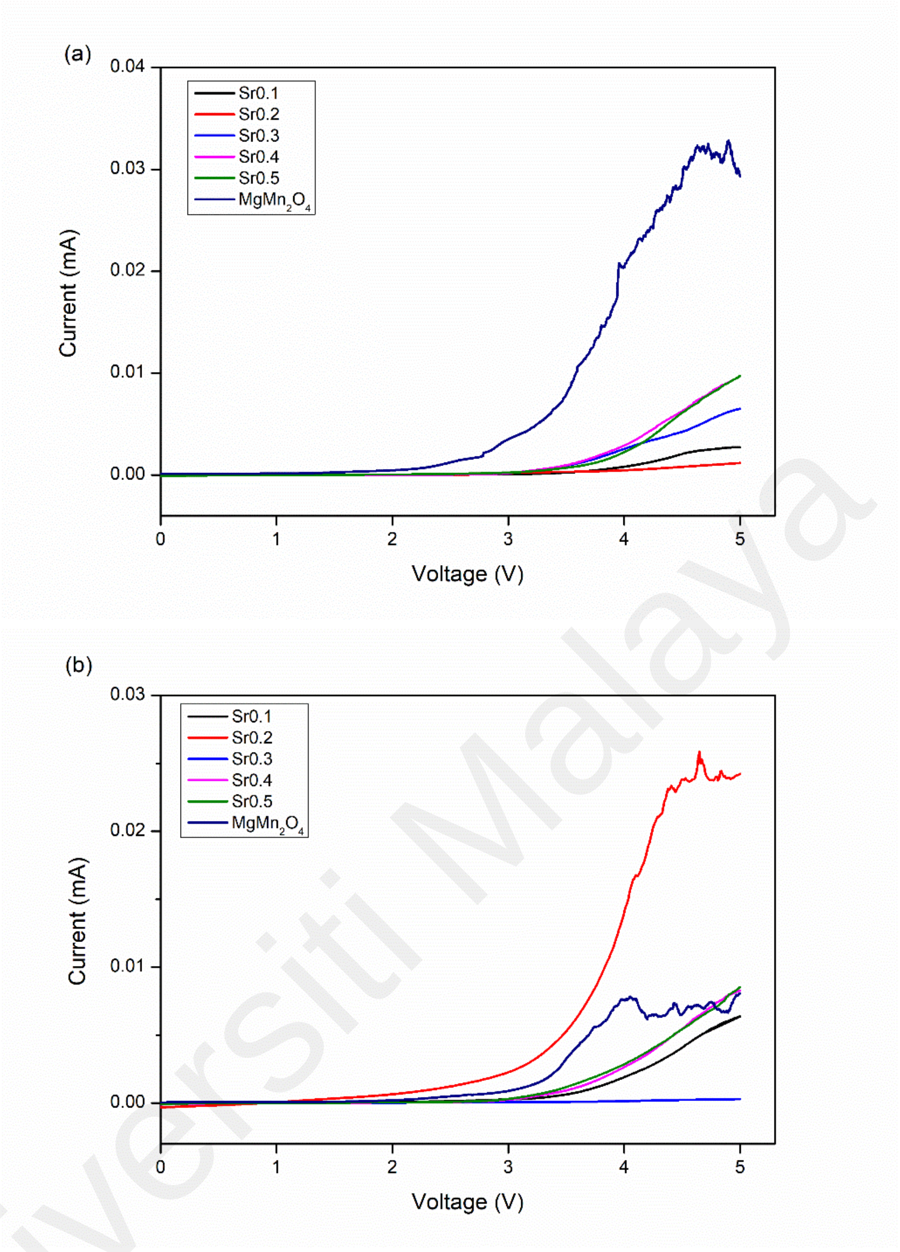

Figure 6.5: Linear sweep voltammetry (LSV) of undoped and all compositions of Sr doped samples at temperature (a) 700°C and (b) 800°C.

Universiti Malaya

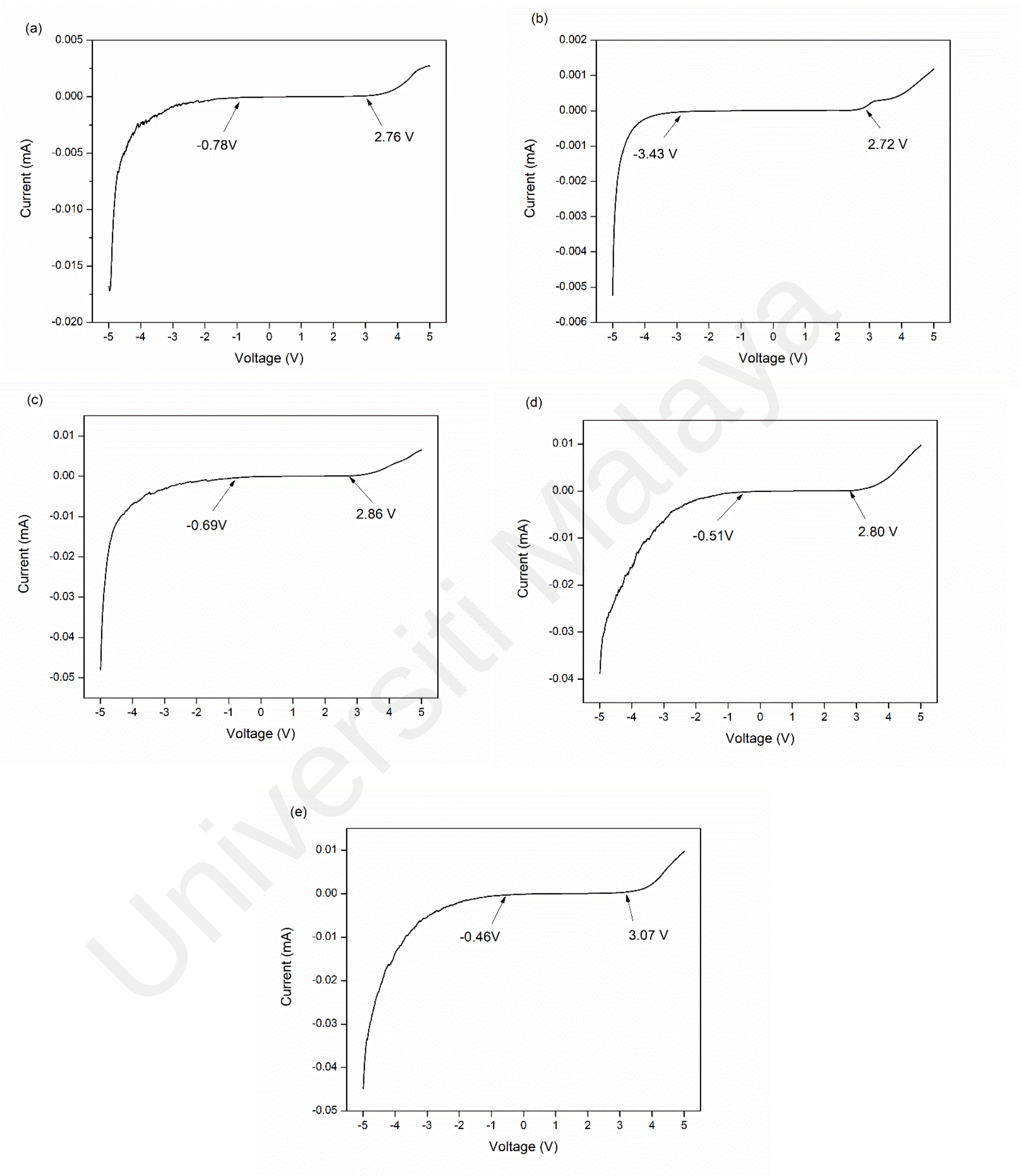

Universiti Malaya

Figure 6.6: Linear sweep voltammetry (LSV) of MgMn$_{2-x}$Sr$_x$O$_4$ at 700°C (a) x=0.1 (b) x=0.2 (c) x=0.3 (d) x=0.4 (e) x=0.5.

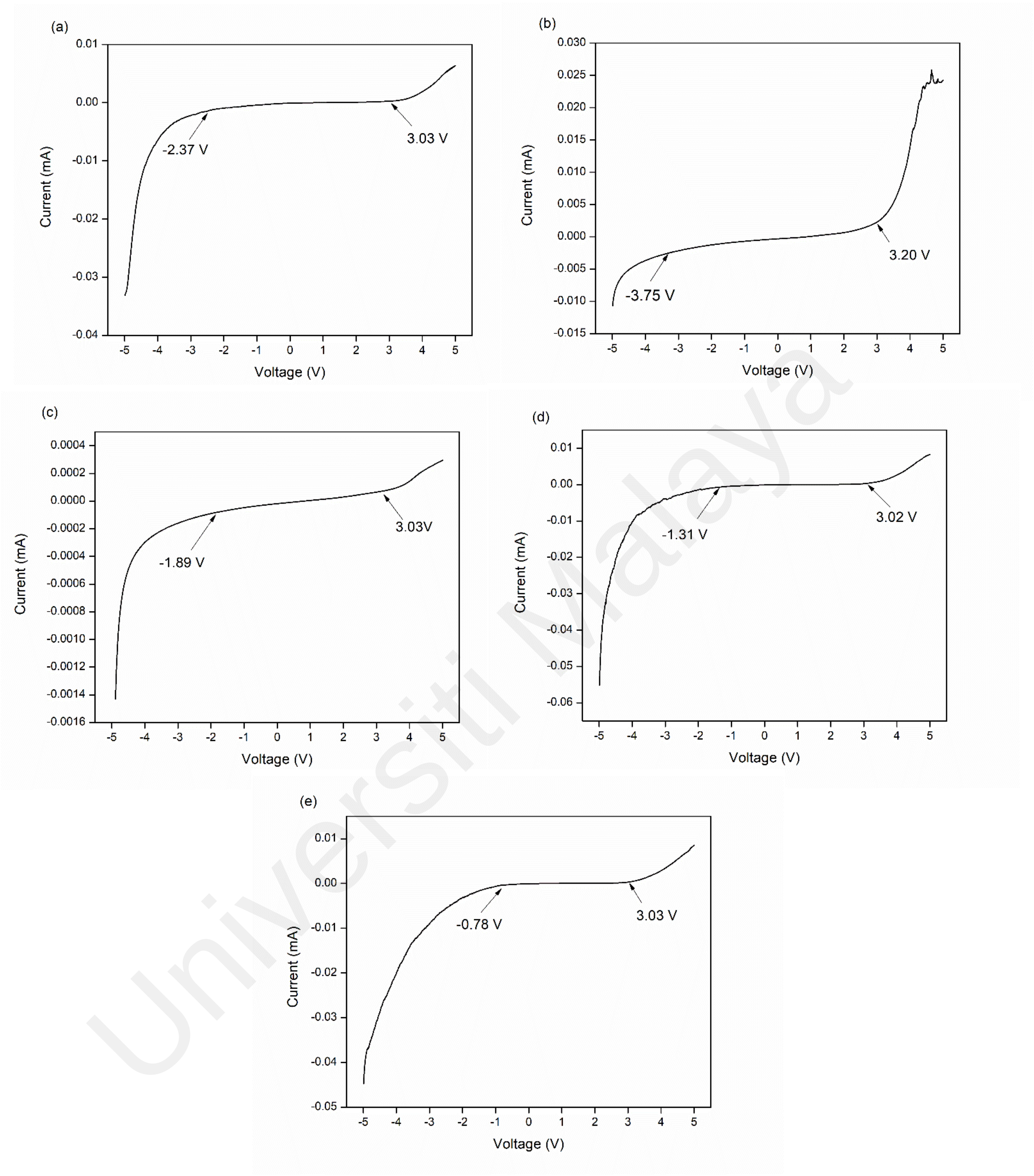

Universiti Malaya

Figure 6.7: Linear sweep voltammetry (LSV) of $MgMn_{2-x}Sr_xO_4$ at 800°C (a) x=0.1 (b) x=0.2 (c) x=0.3 (d) x=0.4 (e) x=0.5.

6.2 Cyclic Voltammetry

Cyclic voltammetry (CV) was carried out to study the kinetics characteristics of the insertion/deinsertion of Mg^{2+} ions. In this study, redox reactions, which includes oxidation and reduction reactions that occurred during the process will be discussed correspond to insertion/deinsertion of Mg^{2+} behavior into/from the $MgMn_2O_4$, $MgMn_{2-x}Ca_xO_4$ and $MgMn_{2-x}Sr_xO_4$ cathode samples. Three-electrode cells had been used where the magnesium metal act as the counter electrode and reference electrode while the working electrode was the prepared cathode materials along with 1M Magnesium trifluoromethanesulfonate ($Mg(CF_3SO_3)_2$) electrolyte.

Universiti Malaya

6.2.1 CV of $MgMn_2O_4$, $MgMn_{2-x}Ca_xO_4$, $MgMn_{2-x}Sr_xO_4$ at 700°C

Figure 6.8 shows the CV curves of $MgMn_2O_4$, optimized $MgMn_{2-x}Ca_xO_4$ and $MgMn_{2-x}Sr_xO_4$ at 700°C in $Mg(CF_3SO_3)_2$ electrolyte at scan rate 1.0 mV s^{-1} within a potential range of 0.5 V to 2.5 V for $MgMn_2O_4$, $MgMn_{2-x}Ca_xO_4$ while for $MgMn_{2-x}Sr_xO_4$ within a potential range of 0.5 V to 3.0 V. The CV for all of the samples is repeated within 3 cycles.

As displayed in Figure 6.8(a), which refers to the $MgMn_2O_4$ sample, it can be observed that there is a small oxidation peak at around 1.74 V, which appears obviously during the third cycle, which indicates poor oxidation process due to its low potential. The current produce from this sample is a low current, which is only up to 0.002 mA. The cyclic voltammogram of the cell containing $MgMn_{1.8}Ca_{0.2}O_4$ sample is shown in Figure 6.8(b) at 700°C. From the observation, the CV includes one broadened oxidation peak at 1.52 V and two reduction peaks at 0.91 V and 1.59 V versus Mg/Mg^{2+}. The reduction peak can be correlated to Mg insertion while the oxidation peak is claimed to be Mg deinsertion . The proposed chemical reaction during the oxidation and reduction process for Ca doped is shown in equation 6.1 below. During the oxidation reaction, the electron will act as donor and form magnesium ions where during reduction process the equations attributed to the deintercalation process of magnesium ion in tetrahedral sites of $MgMn_2O_4$ that gain electrons.

Ca dopant:

Anode: $Mg \rightarrow Mg^{2+} + 2e$

Cathode: $Mg^{2+} + 2e + Mn_{2-x}Ca_xO_4 \rightarrow MgMn_{2-x}Ca_xO_4$

Overall : $Mg + Mn_{2-x}Ca_xO_4 \rightarrow MgMn_{2-x}Ca_xO_4$ (6.1)

Sr dopant:

Anode : $Mg \rightarrow Mg^{2+} + 2e$

Cathode: $Mg^{2+} + 2e + Mn_{2-x}Sr_xO_4 \rightarrow MgMn_{2-x}Sr_xO_4$

Overall: $Mg + Mn_{2-x}Sr_xO_4 \rightarrow MgMn_{2-x}Sr_xO_4$ (6.2)

Figure 6.8(c) displayed the CV curves for Sr doped , $MgMn_{1.8}Sr_{0.2}O_4$ at 700°C. For Sr doped, the potential can be conducted up to high voltage which is 3.0 V based on LSV result previously. For $MgMn_{1.8}Sr_{0.2}O_4$, there is a pair of oxidation/reduction peaks observed at 2.0 V and 1.29 V respectively and the current can be up to 0.01 mA. The peak separations (ΔE_p) of undoped and doped the samples were tabulated in Table 6.1. The peak separations at temperature 700°C of $MgMn_2O_4$, $MgMn_{1.8}Ca_{0.2}O_4$ and $MgMn_{1.8}Sr_{0.2}O_4$ are 1740 mV, 610 mV and 710 mV respectively. The peak separations of both doped samples is low as compared to undoped sample. From the previous studies, Kanevskii et al. (2005) stated that less peak separations value indicates that they have more reversible behavior (Kanevskii & Dubasova, 2005).

Universiti Malaya

Both of doped samples, $MgMn_{1.8}Ca_{0.2}O_4$ and $MgMn_{1.8}Sr_{0.2}O_4$ show more reversible and stable upon cycling compared to undoped sample due to the less peak separations. The peak current of the doped samples shown higher value than undoped sample, which can yield up to 0.01 mA. Therefore, at temperature 700°C, Ca and Sr doped samples possess better electrochemically stability and properties as compared to undoped samples and thus give better results on battery performances that will be discussed in charge discharge profile section.

Table 6.1: Oxidation and reduction peaks of cyclic voltammetry for $MgMn_2O_4$, $MgMn_{1.8}Ca_{0.2}O_4$ and $MgMn_{1.8}Sr_{0.2}O_4$ at temperature 700 °C.

Samples	ΔE vs Mg/Mg^{2+} oxidation peak (V)	ΔE vs Mg/Mg^{2+} reduction peak (V)	ΔEp (mV)
$MgMn_2O_4$	1.74	-	1740
$MgMn_{1.8}Ca_{0.2}O_4$	1.52	0.91 , 1.59	610,-70
$MgMn_{1.8}Sr_{0.2}O_4$	2.0	1.29	710

Universiti Malaya

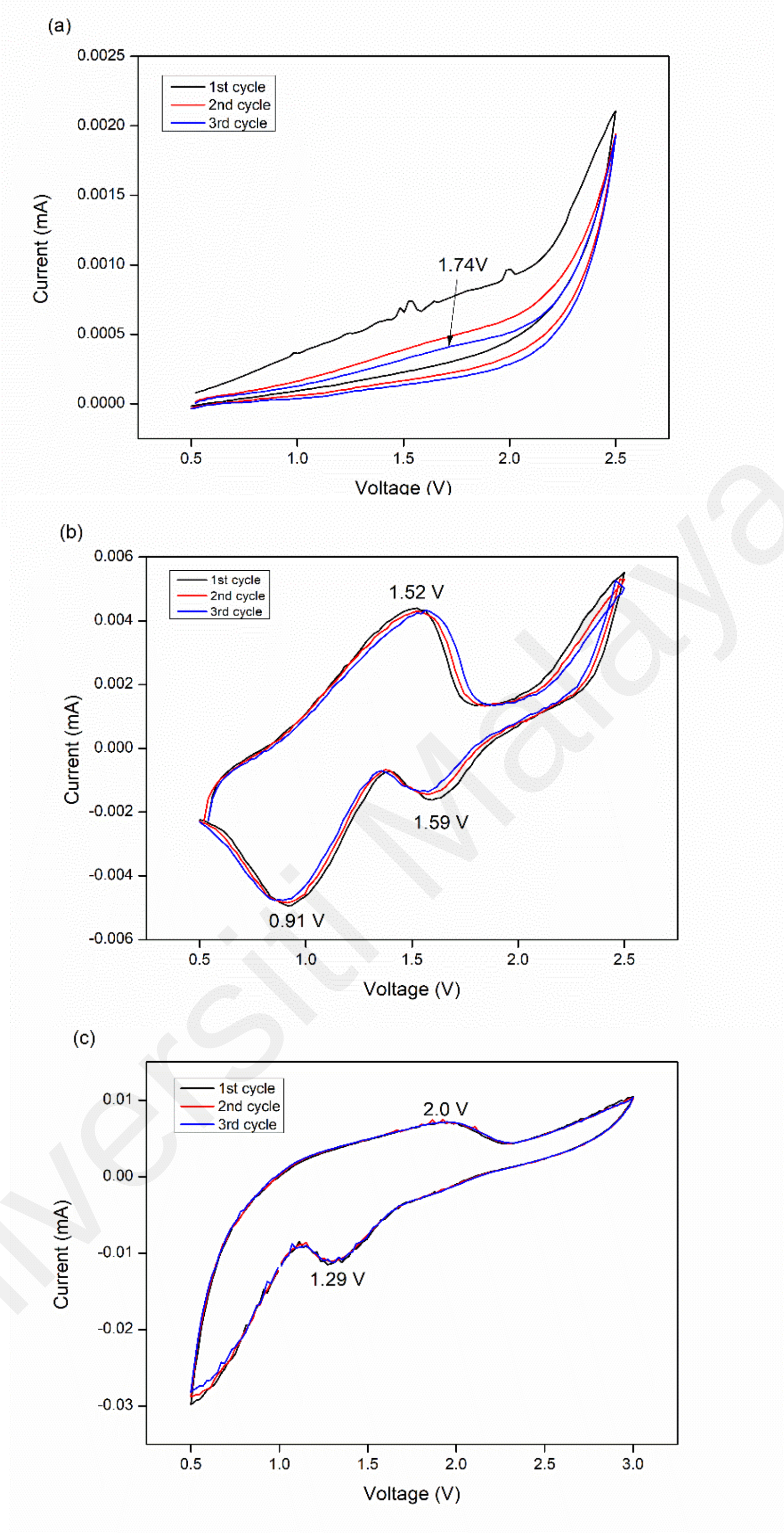

Universiti Malaya

Figure 6.8: Cyclic voltammetry of (a) $MgMn_2O_4$, (b) $MgMn_{1.8}Ca_{0.2}O_4$ and (c) $MgMn_{1.8}Sr_{0.2}O_4$ at temperature 700°C.

6.2.2 CV of $MgMn_2O_4$, $MgMn_{2-x}Ca_xO_4$, $MgMn_{2-x}Sr_xO_4$ at 800°C

Figure 6.9 shows the CV curves of $MgMn_2O_4$, optimized $MgMn_{2-x}Ca_xO_4$ and $MgMn_{2-x}Sr_xO_4$ at 800°C in $Mg(CF_3SO_3)_2$ electrolyte at scan rate 1.0 mVs^{-1} within a potential range of 0.5 V to 2.5 V for $MgMn_2O_4$, $MgMn_{2-x}Ca_xO_4$ while for $MgMn_{2-x}Sr_xO_4$ within a potential range of 0.5 V to 3.0 V. The CV for all of the samples at 800°C was also repeated within 3 cycles.

Figure 6.9(a) displays the cyclic voltammogram of undoped sample, $MgMn_2O_4$ at 800°C. It can be observed that there are two pairs of broadened anodic peak that are 1.32 V and 2.24 V while for a cathodic peak at 1.01 V and 1.65 V as in Table 6.2. The first peak during oxidation / reduction process is attributed to the removal of magnesium ions from tetrahedral site where Mg-Mg ions interactions occurs, whereas the second peak is due to removal of ions again tetrahedral sites where Mg-Mg interaction does not occur (Kiani et al., 2011).

The CV curves of the optimized Ca-doped sample at x=0.4 are shown in Figure 6.9 (b). From the observation, the CV curve contain two pair of oxidation/reduction peak where the first peak during oxidation are at 1.38 V for anodic and 0.99 V for cathodic whereas for reduction, the anodic and cathodic peak arise at potential 2.38 V and 1.63 V respectively as summarized in Table 6.2. The reduction/oxidation couples are resulted from the donor and acceptor of electrons associated the Mg^{2+} insertion/deinsertion into/from the lattice of $MgMn_2O_4$ that can be explained in the equation 6.1.

Figure 6.9(c) shows the CV curves of optimized Sr doped cathode materials at composition x=0.2 at 800°C. There are two oxidation peaks which are 1.44 V and 1.32 V and one reduction peak at 1.49 V stated in Table 6.2. The CV pattern of the Sr-doped are reversible and electrochemically stable up to three cycle. The peak current observed could be up to 0.015 mA, which is higher than undoped samples. Therefore, at

Universiti Malaya

temperature 800°C, the oxidation peak both Sr and Ca doped appeared at higher voltage and high current at the same time. This prove that these two dopants influenced in Mg ion insertion/deinsertion process towards $MgMn_2O_4$ due to its good electrical properties expected comes from these dopants. The effects of these dopants towards battery performances was explained in the battery performance studies on the next chapter.

Table 6.2: Oxidation and reduction peaks of cyclic voltammetry for $MgMn_2O_4$, $MgMn_{1.6}Ca_{0.4}O_4$ and $MgMn_{1.8}Sr_{0.2}O_4$ at temperature 800 °C.

Samples	ΔE_1 vs Mg/Mg^{2+} oxidation peak (V)	ΔE_2 vs Mg/Mg^{2+} oxidation peak (V)	ΔE_1 vs Mg/Mg^{2+} reduction peak (V)	ΔE_2 vs Mg/Mg^{2+} reduction peak (V)	ΔEp_1 (mV)	ΔEp_2 (mV)
$MgMn_2O_4$	1.32	2.24	1.01	1.65	310	590
$MgMn_{1.6}Ca_{0.4}O_4$	1.38	2.38	0.99	1.63	390	750
$MgMn_{1.8}Sr_{0.2}O_4$	1.44	1.32	1.49	-	-50	1490

.

Universiti Malaya

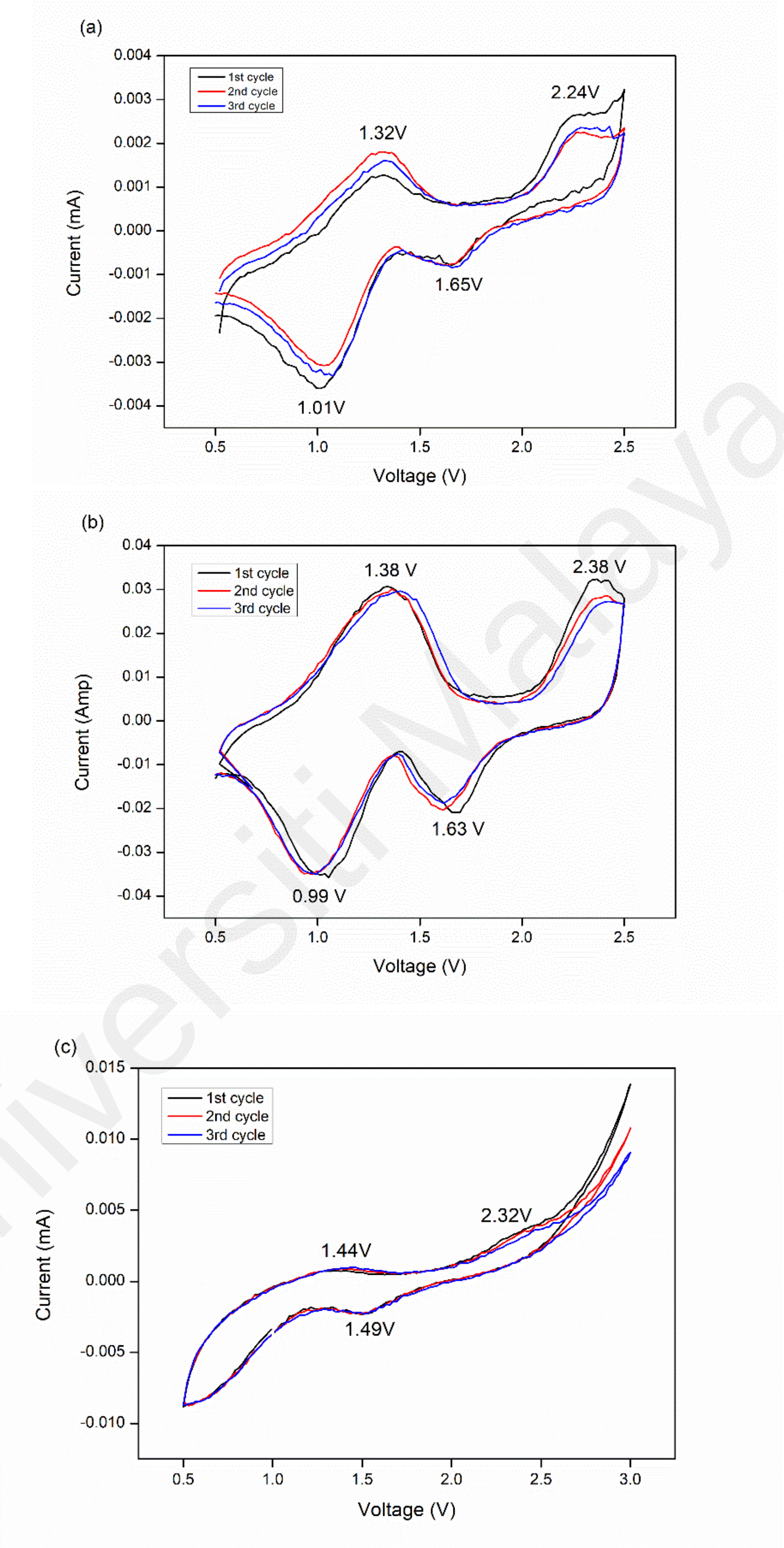

Figure 6.9: Cyclic voltammetry of (a) $MgMn_2O_4$, (b) $MgMn_{1.6}Ca_{0.4}O_4$ and (c) $MgMn_{1.8}Sr_{0.2}O_4$ at temperature 800°C.

Universiti Malaya

CHAPTER 7: CHARACTERIZATION OF MAGNESIUM ION BATTERIES

7.1 Charge Discharge profile

Galvanostatic charge and discharge measurements are used to study the performance of magnesium ion batteries that fabricated using the prepared cathode materials. Charge discharge profile of $MgMn_2O_4$, optimized $MgMn_{2-x}Ca_xO_4$ and $MgMn_{2-x}Sr_xO_4$ samples at 700°C and 800°C are performed with electrolyte containing $Mg(CF_3SO_3)_2$. The configuration of the cells consist of the magnesium metal that acts as anode, Polypropylene (PP) as a separator followed by a drop of 1M $Mg(CF_3SO_3)_2$ electrolyte and $MgMn_2O_4$ and doped $MgMn_2O_4$ as a cathode. The measurements were conducted at a constant potential within 0.5 V to 2.5 V at current 0.05 mA for all cells.

7.1.1 Charge - discharge curves of $MgMn_2O_4$, $MgMn_{1.8}Ca_{0.2}O_4$, $MgMn_{1.8}Sr_{0.2}O_4$ at 700°C

Charge discharge cycling of cells $MgMn_2O_4$, $MgMn_{1.8}Ca_{0.2}O_4$ and $MgMn_{1.8}Sr_{0.2}O_4$ at 700°C was performed at a constant current of 0.05 mA and potential of 0.5 V to 2.5 V by a galvanostatic method as appeared in Figure 7.1. Open circuit voltage (OCV) was carried out on the cells to check the battery electrical potential capability and stability of the fabricated samples before applying to charge discharge testing. The cells were tested up to 10 cycles. The discharge capacity of 38 mAh g^{-1} during first cycle was observed from $MgMn_2O_4$ sample at 700°C as in Figure 7.1(a). As the cycle increases, the capacity of the sample was dropped to 23 mAh g^{-1} in 10th cycle. This capacity fade is due to the slow migration of magnesium ions with increasing the number of cycles (Spotnitz, 2003).

Figure 7.1(b) shows the charge discharge curves of $MgMn_{1.8}Ca_{0.2}O_4$ at 700°C. The initial discharge capacity observed was at 60 mAh g^{-1} and slowly decreases upon cycling up to 10 cycles. Although the discharge capacity is gradually decreased with the repetition

Universiti Malaya

of cycle, the reversibility of Ca doped sample is high and more stable at temperature 700°C due to fast kinetic properties of the capacitive process (Lu Wang et al., 2018). The porosity of the cathode materials that discussed in FESEM previously also was influenced in the reversible reactions in capacities studies that involved intercalation and deintercalation process of Mg^{2+} ions. The smaller particles with higher specific surface areas will make the Mg intercalation reaction faster than bigger particles (Taleghani et al., 2017). This result is consistent with FESEM result.

Charge discharge for Sr doped samples in 10 cycles at 700°C is shown in Figure 7.1(c). The decrease of capacity was observed at 4th cycle, which decreases from 40 mAh g^{-1} at first cycle to 30 mAh g^{-1}. This result is corresponds to instability thermodynamics of Mg metals in electrolytes which passive film can be formed at the interphase. Mg passive film tends to block the transportation of Mg^{2+} ions with limited the area of accessible sites for Mg deposition (X. Sun et al., 2016; Connell et al., 2016).

Other researchers also reported the works of the doping with other elements towards $MgMn_2O_4$. Banu et al. (2019) reported the comparison between two dopants such as Nickel (Ni) and Cobalt (Co) towards $MgMn_2O_4$. They obtained a specific capacity of 46 mAh g^{-1} and 24 mAh g^{-1} for Ni and Co respectively during first cycle at a current density of 30mA g^{-1} (Banu et al., 2019). Titanium (Ti) doped $MgMn_2O_4$ was reported by Zainol et al. (2018). They found that the capacity of the dopant sample was 52 mAh g^{-1} at first cycle but is reducing for the following cycle. They claimed that the reduction of capacity of Ti–doped sample might be due to the poor crystallinity of $MgMn_{1.9}Ti_{0.1}O_4$ and the presence of dense passivating surface blocking layer on the electrode surface due to the deposition of the reduction products owing to the reaction of pure Mg metal. Besides, the surface films effectively block the electrodes, as the mobility of the Mg^{2+} ions through the impervious passivating films is extremely low (Zainol et al., 2018).

Universiti Malaya

It can be summarized that, for all samples at temperature 700°C, Ca and Sr dopant still delivered high capacity than the undoped samples. So this means that the interstitial doping onto $MgMn_2O_4$ plays an important role in order to improve the battery performances. In the present works at temperature 700°C, it shows that these dopants can produce high capacity at the first cycle.

Universiti Malaya

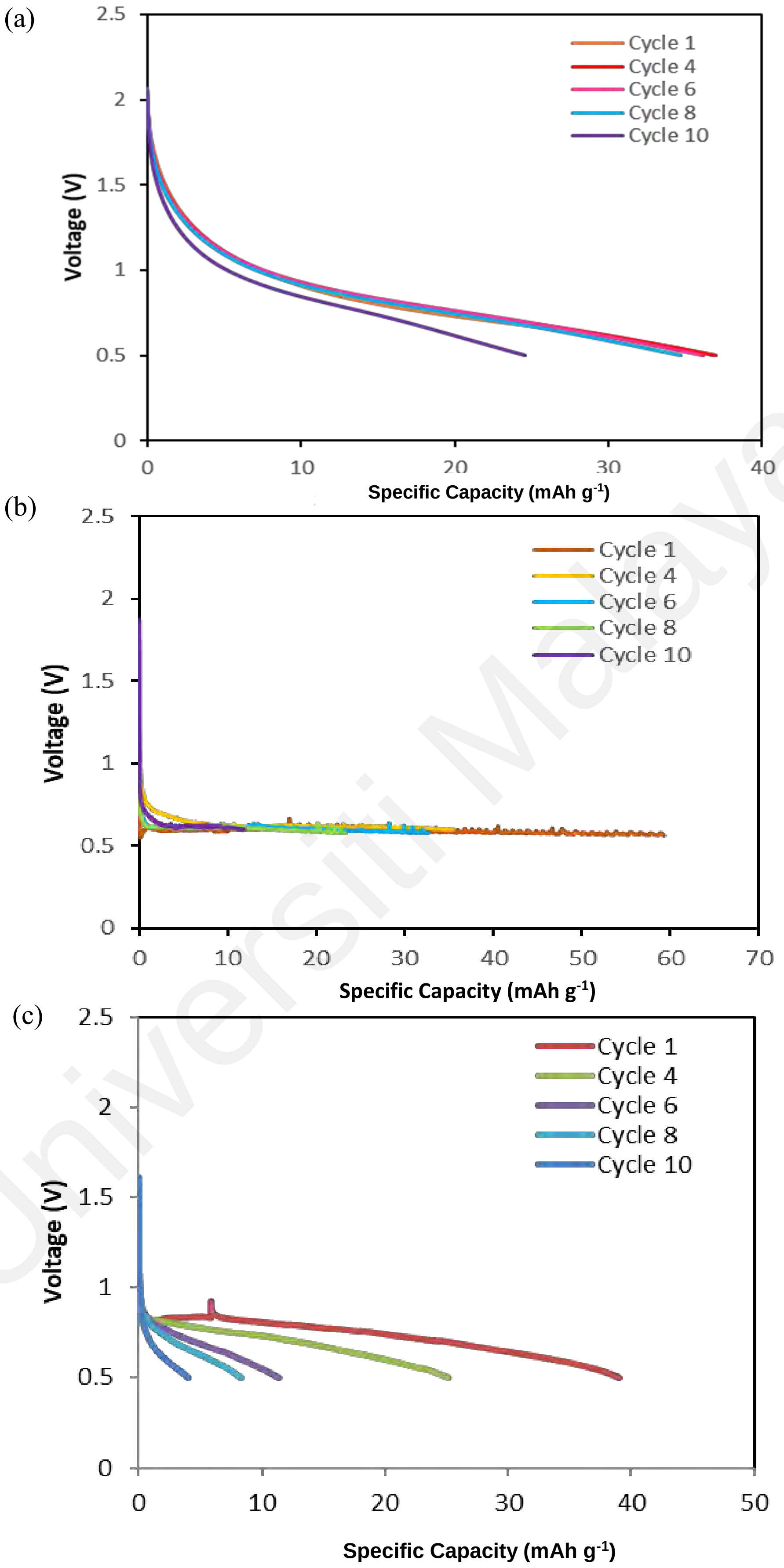

Figure 7.1: Galvanostatic charge-discharge curves of (a) $MgMn_2O_4$, (b) $MgMn_{1.8}Ca_{0.2}O_4$ and (c) $MgMn_{1.8}Sr_{0.2}O_4$ at temperature 700°C in 1M Mg $(CF_3SO_3)_2$ electrolyte.

Universiti Malaya

7.1.2 Charge – discharge curves of $MgMn_2O_4$, $MgMn_{1.6}Ca_{0.4}O_4$, $MgMn_{1.8}Sr_{0.2}O_4$ at 800°C

Charge discharge cycling of the cells using $MgMn_2O_4$, $MgMn_{1.6}Ca_{0.4}O_4$ and $MgMn_{1.8}Sr_{0.2}O_4$ at 800°C as cathode was performed at a constant current of 0.05 mA and potential of 0.5 V to 2.5 V by a galvanostatic method as shown in Figure 7.2. Figure 7.2 (a) shows discharge curves of undoped sample, $MgMn_2O_4$ up to 10 cycles. The discharge capacity decreased as increase the cycling which the first discharge capacity determined to be 49 mAh $g^{-1\cdot}$After 10th cycle , the capacity was dropped to 21 mAh g^{-1}.

Figure 7.2(b) shows the discharge curve of the best composition of Ca doped sample, $MgMn_{1.6}Ca_{0.4}O_4$ at temperature of 800°C. The samples delivered a high capacity at first cycle, which is 138 mAh g^{-1}. This result proved that Ca dopant element towards $MgMn_2O_4$ can achieve high specific capacity during the intercalated and deintercelated process. This observation can be related to the structure of the samples itself which also can influence the battery performances. From previous research, Jin et al. (2016) claimed that for Nickel (Ni) dopant onto $MgMn_2O_4$ has shown less dependence on the surface structures (Jin et al., 2016). The operating temperature is a key parameter controlling the cation distribution in terms of kinetics thermodynamics. Therefore, the dopants samples at high temperature which is 800°C affect the results of battery performance which can give more electrochemically reversible cycling stability than the samples at temperature 700°C.

The discharge curves of Sr doped cathode materials, $MgMn_{1.8}Sr_{0.2}O_4$ is shown in Figure 7.2(c). The discharge capacity of Sr doped samples is two times higher than undoped samples, which is 160 mAh g^{-1} at the first cycle followed by 120 mAh g^{-1} at 4th cycle. This result could be attributed to the Sr doped samples at 800°C having high porosity structure as discussed in FESEM and BET results, thus this means that the

Universiti Malaya

existence of easy transportation channels on the surface of this doped cathode material sample help the reversible intercalation and de-intercalation process of Mg^{2+} ions. Upon the cycling, the discharge capacity was dropped to lower capacity at 10th cycle which is 45 mAh g^{-1}.

It can be concluded that, for all samples at temperature 800°C, Ca and Sr dopant also delivered high capacity than the undoped samples. From the results observed, it can be concluded that the capacities from the samples at 800°C, is higher than 700°C. This implies that the temperature is important parameter which can help in the ion transportations during cycling process in order to achieve good battery performances. In the present works at temperature 800°C, it shows that both dopants can give high capacity at the first cycle.

Universiti Malaya

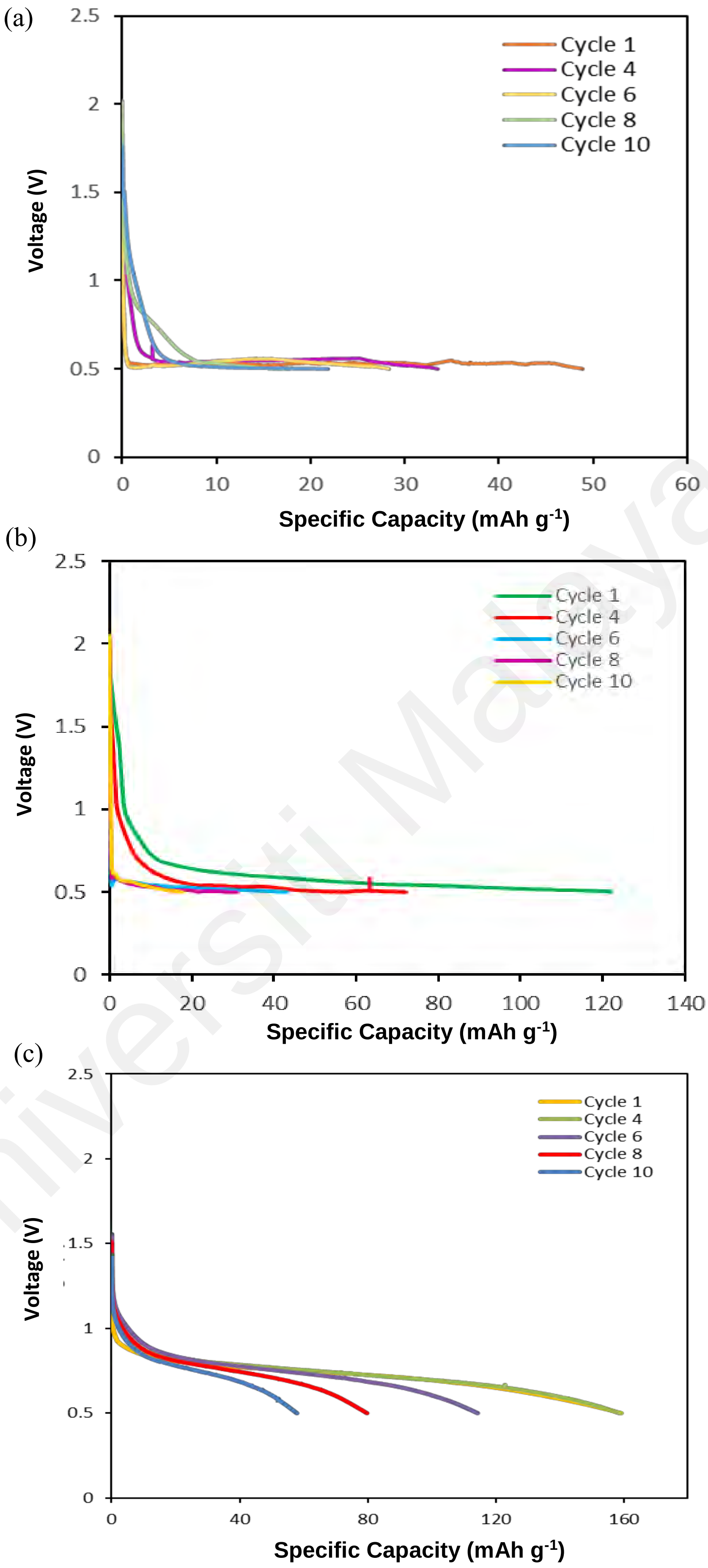

Universiti Malaya

Figure 7.2: Galvanostatic charge-discharge curves of (a) $MgMn_2O_4$, (b) $MgMn_{1.6}Ca_{0.4}O_4$ and (c) $MgMn_{1.8}Sr_{0.2}O_4$ at temperature 800°C in 1M Mg $(CF_3SO_3)_2$ electrolyte.

7.2 Electrochemical Impedance Spectroscopy (EIS)

To better understand the performance of the batteries during the charge discharge process, the cathode materials are explored by performing EIS studies on the cathode materials. In spite of the fact that EIS is a very useful method to help understand certain electrochemical behavior of materials, nevertheless, the models, that is the equivalent circuits used, is approximate in nature. The impedance was measured from 50 Hz to 500 kHz. The cells with optimized Sr and Ca doped $MgMn_2O_4$ samples with high capacity were selected to be discussed in this section. The measurements were taken before the cycle and after cycle in order to ensure the electrode-electrolyte interface cycle ability and stability of the samples during charge discharge process.

7.2.1 Impedance spectra of the Mg cells using $MgMn_2O_4$, $MgMn_{1.8}Ca_{0.2}O_4$, $MgMn_{1.8}Sr_{0.2}O_4$ at 700°C

Figure 7.3 shows the impedance Cole-Cole plot of sample $MgMn_2O_4$ at 700°C. The impedance was performed before cycling and after 10^{th} cycle. An obvious semicircle observed at high frequency region, which correspond to charge transfer resistance (Rct) at the interface and mass diffusion resistance (ZW) the bulk of active materials (Levi & Aurbach, 1997). After a few cycles, the diameter of the semicircle is reduced indicating a smaller R_{ct} and mass diffusion resistance. It is observed that the R_{ct} was decreased from 4367 Ω to 694 **Ω**.Thus, decreasing of R_{ct} are probably enhanced kinetics of Mg^{2+} within the Mg cell which is a result of easier reversible access of Mg^{2+} due to the pre-magnesiation and heat treatment step (Mesallam et al., 2018).

The Cole-Cole impedance plot of optimized Ca doped, $MgMn_{1.8}Ca_{0.2}O_4$ at 700°C before and after cycling are shown in Figure 7.4. All curves displays a small semicircle at the high frequencies region and a linear line at the low frequencies region. The semicircle part at high frequency (R_{ct}) related to the charge transfer process at the

Universiti Malaya

electrode-electrolyte interface and the straight line is corresponds to the diffusion control process of magnesium ion (Wu et al., 2016). It can be observed that the R_{ct} value of the cathode materials before and after cycling was increases from 11.35k to 17.4k Ω as shown in Table 7.1. The increasing of the R_{ct} value can be related to cumulative agglomerates, which decrease the conductive area on the surface of the cathode materials and reduces the ions transportation inside the cathode causing the capacity fading. The resistance can be related to the specific capacity in discharge profile which the capacity of before and after cycling was drop from 60 mAh g^{-1} at first cycle to 29 mAh g^{-1}, at 10th cycle.

Figure 7.5 depicts EIS spectra for the Mg ion cell with optimized Sr doped sample $MgMn_{1.8}Sr_{0.2}O_4$ at 700°C as cathode. It can be seen only the semicircle be observed at before and after cycling process for the samples. The R_{ct} seems to be increased as the number of cycle increases, R_{ct} increases from 1831 Ω to 2786 Ω as tabulated in Table 7.1. The decreased in resistance can be attributed to the enhanced of conductivity of the active materials (Satyavani et al., 2016).

Universiti Malaya

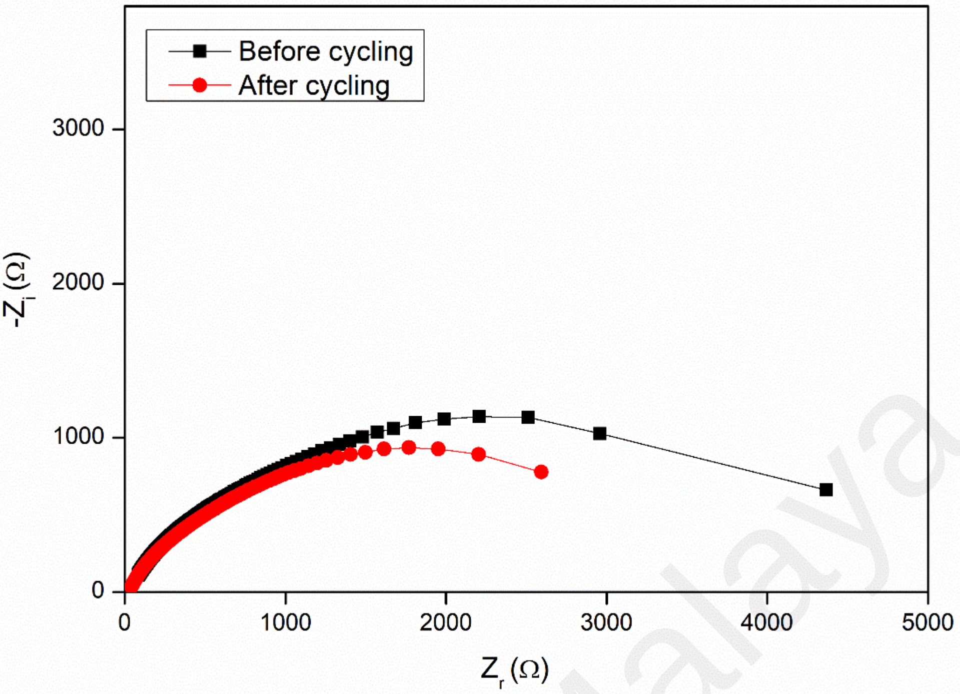

Figure 7.3: EIS spectra of the Mg cell using $MgMn_2O_4$ at 700°C before and after cycling.

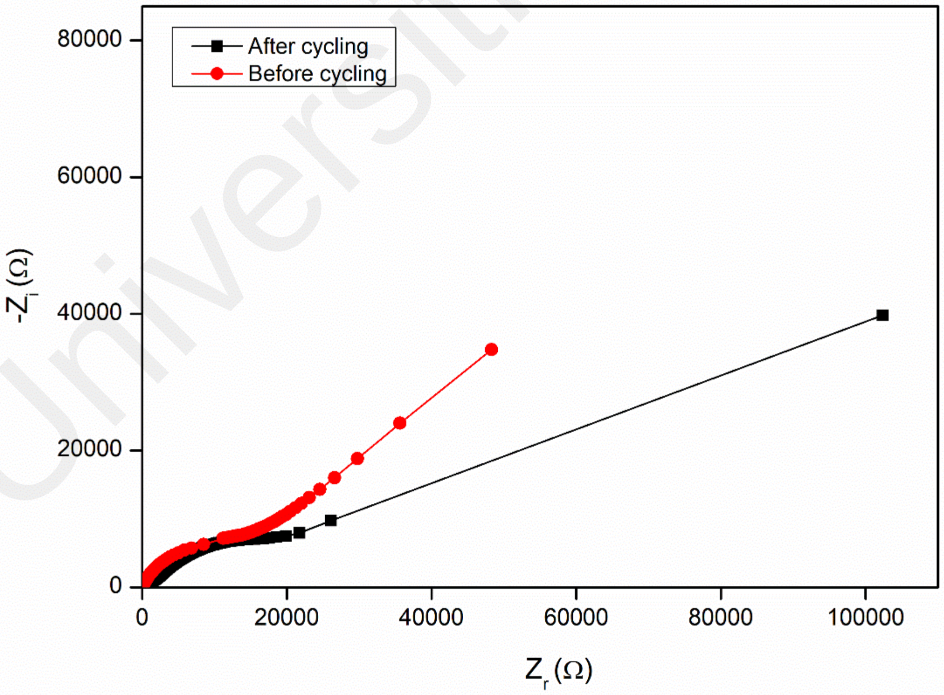

Figure 7.4: EIS spectra of the Mg cell using $MgMn_{1.8}Ca_{0.2}O_4$ at 700°C before and after cycling.

Universiti Malaya

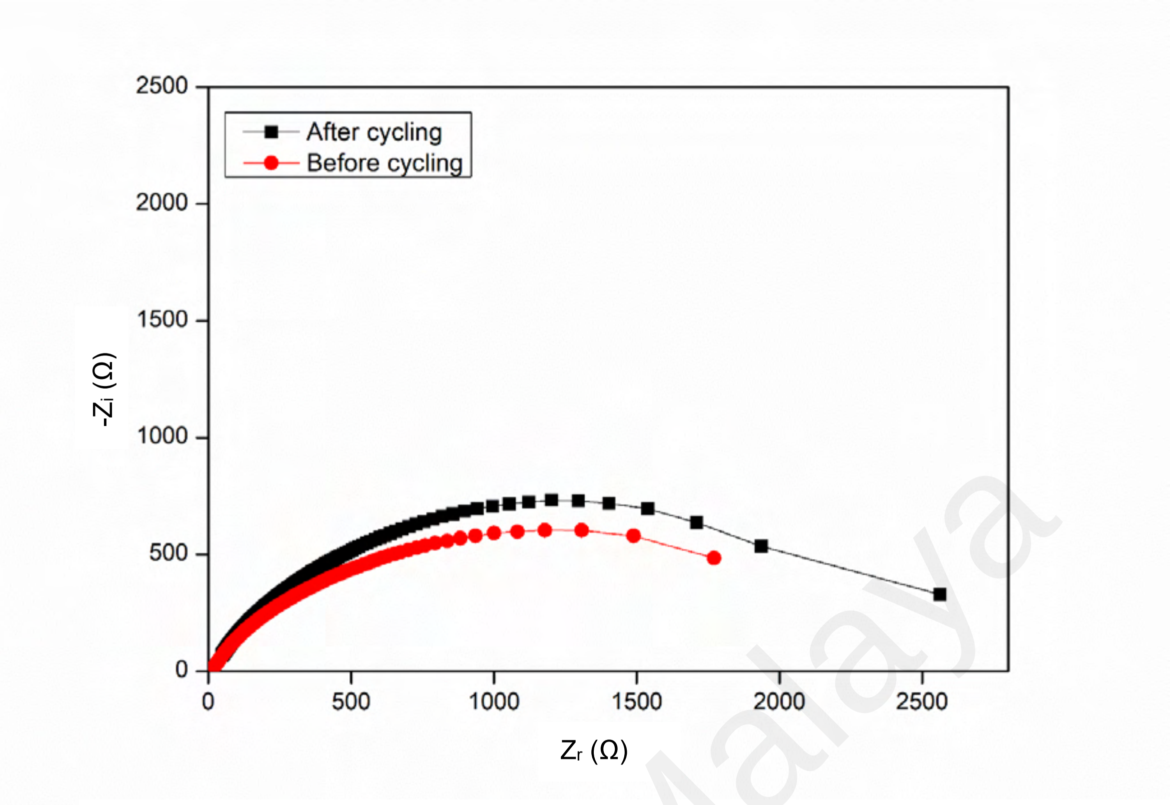

Figure 7.5: EIS spectra of the Mg cell using $MgMn_{1.8}Sr_{0.2}O_4$ at 700°C before and after cycling.

Table 7.1: Charge transfer resistance (R_{ct}) of the Mg cell using $MgMn_2O_4$, $MgMn_{1.8}Ca_{0.2}O_4$ and $MgMn_{1.8}Sr_{0.2}O_4$ obtained from EIS measurements before and after cycling of charge/discharge.

Sample	**Temperature (°C)**	**R_{ct} (Ω)**		**Δ R_{ct} (Ω)**
		Before cycling	After cycling	
$MgMn_2O_4$	700	4367	2593	1774
$MgMn_{1.8}Ca_{0.2}O_4$	700	11350	17400	6050
$MgMn_{1.8}Sr_{0.2}O_4$	700	1831	2786	955

Universiti Malaya

7.2.2 Impedance spectra of Mg cells using $MgMn_2O_4$, $MgMn_{1.6}Ca_{0.4}O_4$, $MgMn_{1.8}Sr_{0.2}O_4$ at 800°C

Figure 7.6 shows the Cole-Cole plot of the Mg cell using $MgMn_2O_4$ at temperature 800°C. Based on the results, an obvious large and small semicircle observed at high frequency region, which correspond to charge transfer resistance (R_{ct}) at the interface and mass diffusion resistance (ZW) the bulk of active materials. The diameter of semicircles are larger before the cycling process while its disseminated lower semicircles after 10 cycles. The clarifications are correlated to the R_{ct} value and discharge capacity where R_{ct} value are decreases from 4367 to 694 Ω as listed in Table 7.2.

The Cole-Cole plot of Ca doped samples, $MgMn_{1.6}Ca_{0.4}O_4$ at temperature 800°C are shown in Figure 7.7. For Ca doped samples at 800°C, the spectra observed two semicircles at low and high frequency regions. It is difficult to obtain R_{ct} value from the complex impedance plot. Hence, the data was plotted in admittance form by plotting imaginary admittance, Ai versus the real admittance Ar as shown in Figure 7.7(b). The charge transfer resistance (R_{ct}) of cells before and after cycling to be 304.41 Ω and 278 Ω respectively. The decrease in the resistance after cycling reveals the higher electrical conductivity for the Ca dopant onto $MgMn_2O_4$. High conductivity of the dopants may enhances the Mg^{2+} diffusion coefficient in the material, thus benefit in improving the battery performances (Wu, Thiben, & Jaegermann, 2002). Figure 7.8 depicts Cole Cole plot of Sr doped samples, $MgMn_{1.8}Sr_{0.2}O_4$ at 800°C. The R_{ct} of the samples before cycling are known to be 1171 Ω while after cycling the resistances increments up to 3800 Ω as arranged in Table 7.2. The expanding in resistance may cause cumulative agglomerates, which decrease the conductive area on the surface of the cathode materials and reduces the ions transportation inside the cathode causing the capacity fading.

Universiti Malaya

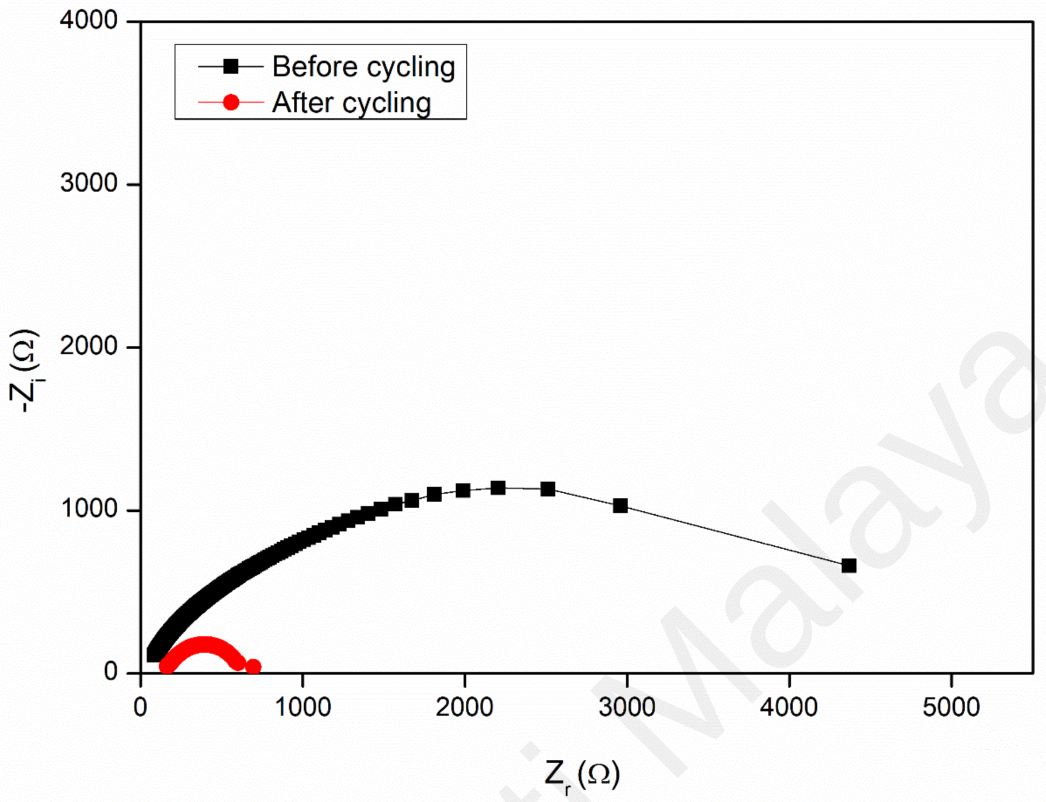

Figure 7.6: EIS spectra of the Mg cell using $MgMn_2O_4$ at 800°C before and after cycling.

Universiti Malaya

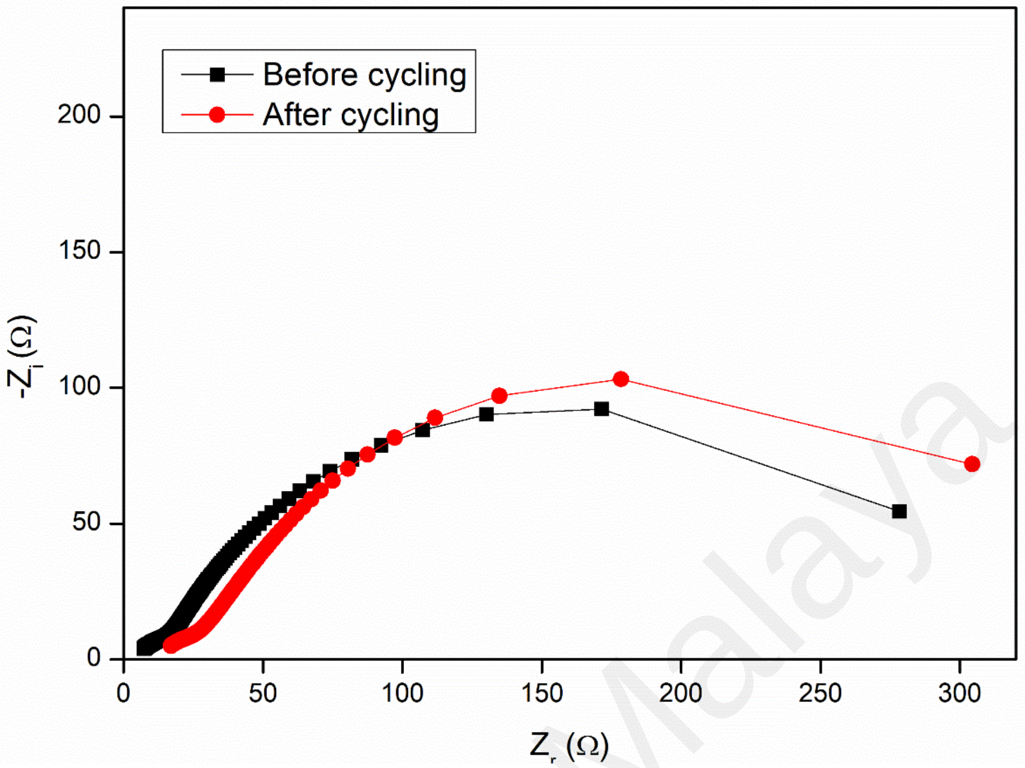

(a)

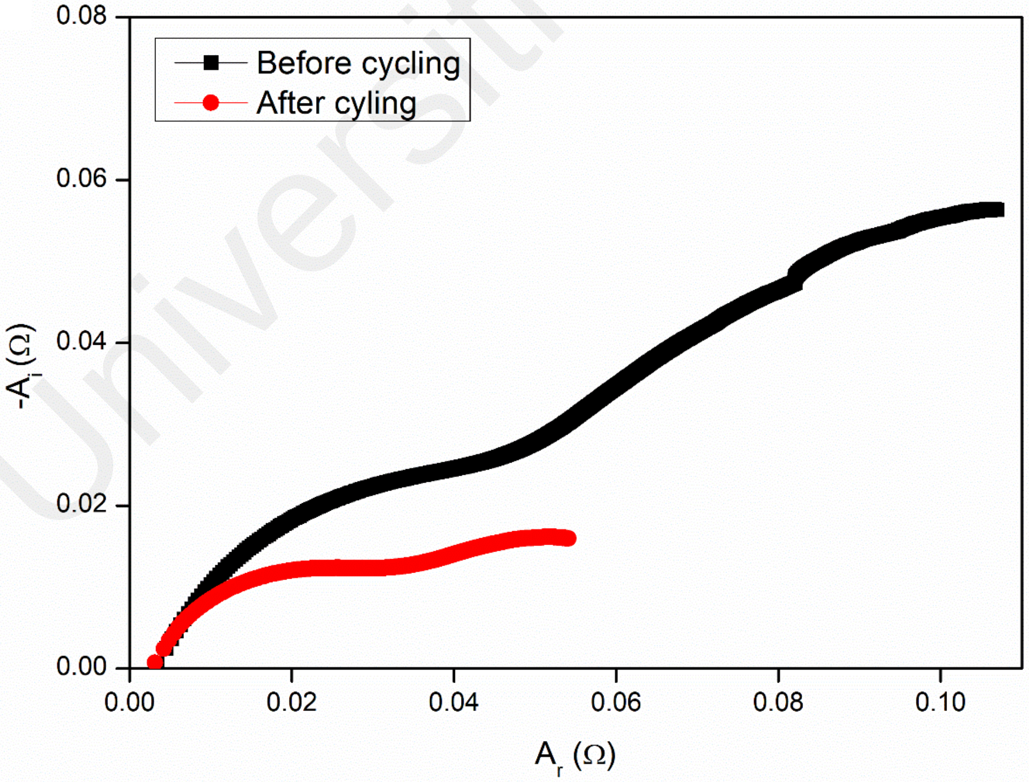

Universiti Malaya

Figure 7.7: EIS spectra of the Mg cell using $MgMn_{1.6}Ca_{0.4}O_4$ at 800°C before and after cycling (a) Admittance plot of sample $MgMn_{1.6}Ca0._4O_4$.

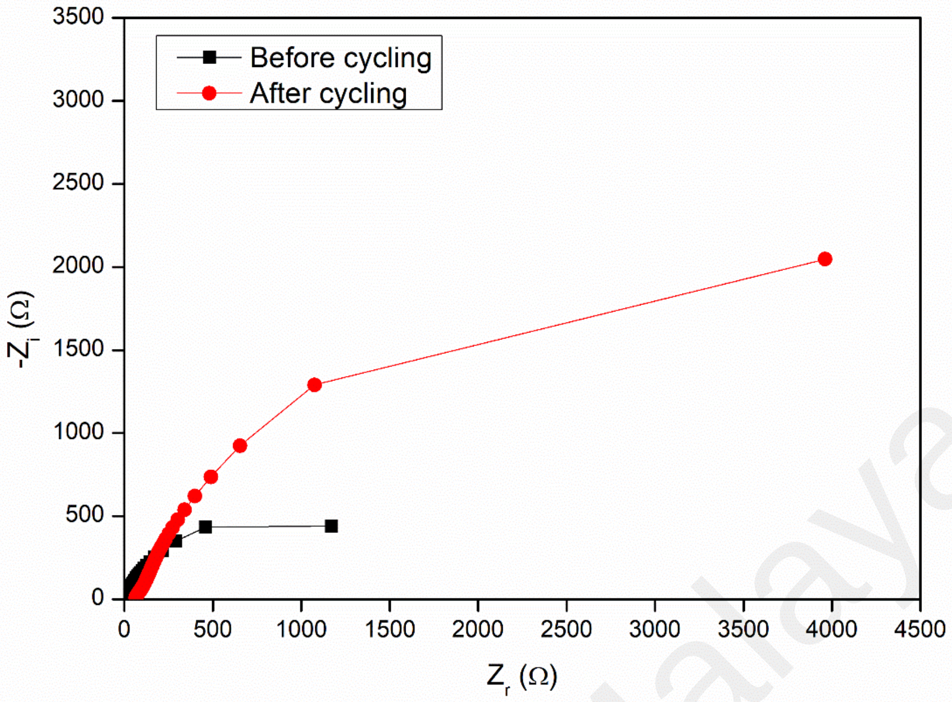

Figure 7.8: EIS spectra of the Mg cell using $MgMn_{1.8}Sr_{0.2}O_4$ at 800°C before and after cycling.

Universiti Malaya

Table 7.2: Charge transfer resistance (R_{ct}) of the Mg cells using $MgMn_2O_4$, $MgMn_{1.8}Ca_{0.2}O_4$ and $MgMn_{1.8}Sr_{0.2}O_4$ obtained from EIS measurements before and after cycling of charge/discharge.

Sample	Temperature (°C)	R_{ct} (Ω)		ΔR_{ct} (Ω)
		Before cycling	After cycling	
$MgMn_2O_4$	800	4367	694	3673
$MgMn_{1.8}Ca_{0.2}O_4$	800	278	304.41	26.41
$MgMn_{1.8}Sr_{0.2}O_4$	800	1171	3800	2629

CHAPTER 8: CONCLUSIONS AND SUGGESTIONS FOR FUTURE WORK

This works described the preparation of magnesium based cathode materials which include undoped samples, $MgMn_2O_4$ and doped samples, $MgMn_{2-X}Ca_xO_4$ and $MgMn_{2-x}Sr_xO_4$ where x=0.1, 0.2, 0.3, 0.4 and 0.5. All the samples were synthesized using self-propagating combustion method. The prepared cathode samples were annealed at 700°C and 800°C for 24 hours. Several characterization techniques have been performed in order to study the structural, morphological, thermal and electrochemical properties of the prepared cathode materials.

Thermal studies include Thermogravimetric analysis (TGA) and the Differential Scanning Calorimetry (DSC) indicates the stability of the cathode materials and the suitable annealing temperature of the precursor. In this work, temperatures at 700°C and 800°C have been chosen as a suitable annealing temperature for the cathode samples based on the stable curves observed from the results. In this manner, all the basic structural and morphological studies of undoped and doped samples were performed at 700°C and 800°C. Structural of the undoped and doped samples was decided by X-ray diffraction (XRD) analysis where $MgMn_2O_4$ exhibit a tetragonal spinel structure be indexed as 01-072-1336 in which can be clarified by Mg^{2+} and $Mn^{3+/4+}$ ions occupy tetrahedral and octahedral sites (Sinha et al., 2008). Ca and Sr doped for all compositions exhibit a most stable structure known as cubic structure could be indexed as 01-089-3684 and 01-089-4047 respectively. The structure stability of both doped samples proved that the successful interstitial doping towards $MgMn_2O_4$, which may concern was influenced in their performances as well. The intensity also can be obviously seen between these two temperatures where the tests at 800°C displayed higher intensity as compared to results at temperature 700°C. These results fulfill the objective 1 stated in section 1.2 previously.

Universiti Malaya

The micrograph obtained from FESEM provide detailed information on surface structure and morphological properties of the cathode materials. In this section, the structure was obtained from samples undoped and both doped samples with distinctive compositions between two temperatures 700°C and 800°C. Based on the results, it can be observed that the bigger porous formation was gotten from Ca and Sr doped samples at both temperatures whereas no appearances of porous in undoped sample structure. The detailed structure of Ca and Sr doped samples show a porous formation of interconnected pores. For Ca doped samples, the highest porosity is belongs to x=0.2 and x=0.4 whereas for Sr doped, x=0.2 exhibits high porosity at temperatures 700°C and 800°C respectively. The structure with high porosity crystallinity are played an important role in ion intercalations and deintercalation. The presence of calcium and strontium elements is confirmed through Energy dispersive x-ray (EDX) and EDS mapping. This revealed that both dopings has been successfully done through self-propagating combustion synthesis.

Morphological studies also are taken out with TEM analysis to investigate the detailed morphology of the cathode material samples to better understanding the structural properties and particle behavior. From TEM images, it can be seen a cubic shape from both Ca and Sr doped samples and this in line with XRD result which found to be a cubic structure. Since cubic structure is a stable structure, hence both doped samples prove that the change from tetragonal which comes from undoped samples to a cubic was influenced the performances of Mg ion cells.

In the aspect of specific surface area ,porosity was determined by BET measurements for the $MgMn_2O_4$ and optimized $MgMn_{2-x}Ca_xO_4$ and $MgMn_{2-x}Sr_xO_4$. Based on IUPAC, the adsorption isotherm of these undoped and doped samples can be classified as macroporous. The specific surface area of Ca and Sr doped is higher than undoped samples for both 700°C and 800°C. This result can be related to FESEM and TEM where

Universiti Malaya

smaller particle size gives a larger surface area which easier for ions transportation happened in and outside of the structure.

Raman spectroscopy has shown that the vibrational features with common characteristics among the samples. The successfulness of Ca and Sr dopants onto $MgMn_2O_4$ was explained by the relative intensity of the peak presence for temperatures at 700°C and 800°C. The peak between 300-600 cm^{-1} was related to cation and anion Mn-O bond lengths and polyhedral occurring in the samples. All the morphological and structural studies results meet the objective 2 stated in section 1.2.

The electrochemical aspects of the magnesium based cathode materials comprises of the investigations of LSV, CV and battery performances. All of the electrochemical studies was performed in 1M $Mg(CF_3SO_3)_2$ electrolyte. The LSV was performed in order to check the electrochemical potential window stability, which will be used in cyclic voltammetry and charge discharge studies. In this work, among all the Ca doped compositions at temperature 700°C, the higher voltage is obtained from sample with x=0.2 which obtained to be 3.15 V while at 800°C obtained from x=0.4 exhibited higher oxidation voltage which is 3.37 V among undoped and other compositions . For Sr doped, it can be concluded that the best compositions which deliver the most stable potential window and high oxidation voltage belongs to the samples with x=0.2 for both temperatures. The overall result of LSV part, it can be summarized that both Ca and Sr doped samples possess the highest voltage than undoped samples and samples at temperature 800°C. For that reason, the widest electrochemical potential window stability proves a promising result to be used in CV and Mg ion cells studies.

The cyclic voltammograms and battery performances were performed from the optimized samples obtained from LSV results. In this work, at temperature 700°C, the

Universiti Malaya

specific capacity obtained from $MgMn_{1.8}Ca_{0.2}O_4$ and $MgMn_{1.8}Sr_{0.2}O_4$ at first cycle was 60 mAh g^{-1} and 40 mAh g^{-1} respectively. At temperature 800°C, the fabricated cells conveyed a capacity of 138 mAh g^{-1} and 160 mAh g^{-1} for Ca and Sr doped samples respectively. For undoped samples at 700°C and 800°C of $MgMn_2O_4$, the specific capacity at the first cycle are 38 mAh g^{-1} and 49 mAh g^{-1} which is lower than doped samples. Therefore, it can be stated that both Ca and Sr dopants onto $MgMn_2O_4$ based cathode materials can enhances a good electrochemical properties thus improving the battery performances. This electrochemical result was in line and proved the objective 3 in section 1.2 stated in chapter 1.

There are some suggestions that could be done to improve the performances of Mg-based cathode materials in magnesium ion batteries. This includes in the aspect of electrolytes used which we can be used other electrolytes based on other Mg salts such as magnesium perchlorate ($MgClO_4$), magnesium chloride ($MgCl_2$) and magnesium nitrate ($Mg(NO_3)_2$) that may be considered in attempt to promote a good magnesium ion battery . In the present research report, for Mg ion battery, there is no commercialize electrolyte been introduced yet. Other than that, the different type of dopants such as Vanadium (V) can be used, since it has a flexible interlayer structure and good tolerance to various interstitial ions including transition metals and amines. The low compositions dopants also can used in order to achieve nanoparticles thus can improve the battery performances as well. Final suggestion is instead of magnesium metal as an anode, other material can be used as anode in the Mg cell that possibly can help in the electrochemical stability properties such as Manganese Oxide (MnO), magnesium based alloys and etc.

Universiti Malaya

REFERENCES

Anka, P. (2018). Uses of transmission electron microscope in microscopy and its advantages and disadvantages. *International Journal of Current Microbiology and Applied Sciences*, *7*(05), 743–747.

Anufrienko, V. F., & Rojo, J. M. (2002). High temperature Co-doped $LiMn_2O_4$-based spinels . structural , electrical , and electrochemical characterization. *Chemistry of Materials*, *(13)*, 1598–1605.

Arora, P., Popov, B. N., & White, R. E. (1998). Electrochemical investigations of cobalt-doped $LiMn_2O_4$ as cathode material for lithium-ion batteries. *Journal of the Electrochemical Society*, *145*(3), 807–815.

Aurbach, D., Gofer, Y., Lu, Z., Schechter, A., Chusid, O., Gizbar, H., & Cohen, Y. (2001). A short review on the comparison between Li battery systems and rechargeable magnesium battery technology. *Journal of Power Sources*, *98*, 28–32.

Baddour-Hadjean, R., & Pereira-Ramos, J. P. (2010a). Raman investigation of cathode materials for lithium batteries. In D. K. Ozawa (Eds), *Lithium ion rechargeable batteries:Materials, technology, and new applications.* Tokyo, Japan: Wiley-VCH Verlag GmbH & Co. KGaA.

Baddour-Hadjean, R., & Pereira-Ramos, J. P. (2010b). Raman microspectrometry applied to the study of electrode materials for lithium batteries. *Chemical Reviews*, *110*(3), 1278–1319.

Banerjee, D. (n.d.). *XRD 16 Phase Identification X-Ray Diffraction (XRD)*. Retrieved from https://www.iitk.ac.in/che/pdf/resources/XRD-reading-material.pdf.

Banu, A., A.Sakunthala, Thamilselvan, M., Kumar, P. S., Suresh, K., & Ashwini, S. (2019). Preparation, characterization and comparative electrochemical studies of $MgM_XMn_{2-X}O_4$ (x=0, 0.5; M= Ni/Co). *Ceramics International*, *45*(10), 13072–13085.

Barbour, L. J. (2017). Single-Crystal X-ray Diffraction. Retrieved on 2017 from https://serc.carleton.edu/research_education/geochemsheets/techniques/SXD.html.

BEL. (2013). *BELSORP-max Instruction Manual 1.3.3*. Retrieved on 2013 from https://ch2.ntust.edu.tw/ezfiles/27/1027/img/1657/651700873.pdf.

Bi, Z., Zhang, X., He, W., Min, D., & Zhang, W. (2013). Recent advances in $LiFePO_4$ nanoparticles with different morphology for high-performance lithium-ion batteries. *RSC Advances*, *3*(43), 19744–19751.

Borovinskaya, I., Ignatieva, T., & Vershinnikov, V. (2012). Self-Propagating high-temperature synthesis of ultrafine tungsten carbide powders. *Tungsten Carbide - Processing and Applications*, 1–20.

Universiti Malaya

Bragg's Law. (2009). *Dictionary of Gems and Gemology*. Retrieved on 2009 from https://serc.carleton.edu/research_education/geochemsheets/BraggsLaw.html.

Bunaciu, A. A., Udriştioiu, E. gabriela, & Aboul-Enein, H. Y. (2015). X-Ray Diffraction: instrumentation and applications. *Critical Reviews in Analytical Chemistry*, *45*(4), 289–299.

Carlo, M. (2013). Basic requirements for the XRD sample preparation. Retrieved on 2013 from http://www2.arnes.si/~sgszmera1/html/xrd/preparation2.html.

Carter, T. J., Mohtadi, R., Arthur, T. S., Mizuno, F., Zhang, R., Shirai, S., & Kampf, J. W. (2014). Boron clusters as highly stable magnesium-battery electrolytes. *Angewandte*, 3237–3241.

Chen, M., Zhao, E., Chen, D., Wu, M., Han, S., Huang, Q., Yang, L., Xiao, X., & Hu, Z. (2017). Decreasing Li/Ni disorder and improving the electrochemical performances of Ni-Rich $LiNi_{0.8}$ $Co_{0.1}Mn_{0.1}O_2$ by Ca doping. *Inorganic Chemistry*, *56*(14), 8355–8362.

Connell, J. G., Genorio, B., Lopes, P. P., Strmcnik, D., Stamenkovic, V. R., & Markovic, N. M. (2016). Tuning the reversibility of Mg anodes via controlled surface passivation by H_2O/Cl^- in organic electrolytes. *Chemistry of Materials*, *28*(22), 8268–8277.

Dutrow, B. L. (2013). X-ray Powder Diffraction (XRD). Retrieved on December 14, 2013 from http://serc.carleton.edu/research_education/geochemsheets/techniques/XRD.htm.

Elong, K., Kamarulzaman, N., Rusdi, R., Badar, N., & Jaafar, M. H. (2013). Combustion synthesis route and their electrochemical characteristics, *ISRN condensed Matter Physics,2013,*1-8.

Feng, M., Du, Q., Su, L., Zhang, G., Wang, G., & Ma, Z. (2017). Manganese oxide electrode with excellent electrochemical performance for sodium ion batteries by pre-intercalation of K and Na ions, *Scientific Reports, 4*, 1–8.

Furtak, T. E. (1983). Current understanding of the mechanism of surface enhanced Raman scattering. *Journal of Electroanalytical Chemistry and Interfacial Electrochemistry*, *150*(1), 375–388.

Gamry Instruments. (2018). Snapshot of EIS. *Surface and Interface Analysis*, *20*(10), 859–868.

Geos 306, Raman Spectroscopy. (n.d.). Retrieved from https://www.geo.arizona.edu/xtal/geos306/geos306-12.htm.

Glass, H. F. J. (2017). *Borate polyanion-based systems as Li- and Mg-ion cathode materials* (Doctoral dissertation). Retrieved from https://www.repository.cam.ac.uk/handle/1810/264940.

Universiti Malaya

Hench, L. L., & West, J. K. (1990). The sol-gel process. *Chemical Reviews*, *90*(1), 33–72.

Huie, M. M., Bock, D. C., Takeuchi, E. S., Marschilok, A. C., & Takeuchi, K. J. (2015). Cathode materials for magnesium and magnesium-ion based batteries. *Coordination Chemistry Reviews*, *287*, 15–27.

Hutchinson, D. J., & Schilt, A. A. (1999). *Adsorption Isotherm and its Types _ Chemistry Learning*. Retrieved on 1999 from http://www.chemistrylearning.com/adsorption-isotherm/.

Ichitsubo, T., Adachi, T., Yagi, S., & Doi, T. (2011). Potential positive electrodes for high-voltage magnesium-ion batteries. *Journal of Materials Chemistry*, *21*(32), 11764–11772.

Intertek (2016). Energy Dispersive X-Ray Analysis (EDX). *Intertek Group Plc*. Retrieved on 2016 from https://www.intertek.com/analysis/microscopy/edx/.

Iturrondobeitia, A., Goñi, A., Palomares, V., Gil De Muro, I., Lezama, L., & Rojo, T. (2012). Effect of doping $LiMn_2O_4$ spinel with a tetravalent species such as Si(IV) versus with a trivalent species such as Ga(III). Electrochemical, magnetic and ESR study. *Journal of Power Sources*, *216*, 482–488.

Jarusiripot, C. (2014). Removal of reactive dye by adsorption over chemical pretreatment coal based bottom ash. *Procedia Chemistry*, *9*, 121–130.

Jiang, D., Zhao, L., Shao, Y., & Wang, D. (2015). Preparation and characterization of layered $LiNi_{0.9}Co_{0.05}Mn_{0.025}Mg_{0.025}O_2$ cathode material by a sol-gel method for lithium-ion batteries. *RSC Advances*, *5*(51), 40779–40784.

Jin, W., Yin, G., Wang, Z., & Fu, Y. Q. (2016). Surface stability of spinel $MgNi_{0.5}Mn_{1.5}O_4$ and $MgMn_2O_4$ as cathode materials for magnesium ion batteries. *Applied Surface Science*, *385*, 72–79.

Julien, C. M. (2006). Local structure of lithiated manganese oxides. *Solid State Ionics*, *177*(1–2), 11–19.

Julien, C. M., & Massot, M. (2003). Lattice vibrations of materials for lithium rechargeable batteries III. Lithium manganese oxides. *Materials Science and Engineering B: Solid-State Materials for Advanced Technology*, *100*(1), 69–78.

Kanevskii, L. S., & Dubasova, V. S. (2005). Degradation of Lithium-Ion batteries and how to fight it: A Review, *Russian Journal Of Electrochemistry,41*(1), 1–16.

Kiani, M. a., Mousavi, M. F., & Rahmanifar, M. S. (2011). Synthesis of nano- and micro-particles of $LiMn_2O_4$: Electrochemical investigation and assessment as a cathode in li battery. *International Journal of Electrochemical Science*, *6*(7), 2581–2595.

Kim, D. K., Muralidharan, P., Lee, H.-W., Ruffo, R., Yang, Y., Chan, C. K., & Cui, Y. (2008). Spinel $LiMn_2O_4$ nanorods as lithium ion battery cathodes. *Nano Letters*, *8*(11), 3948–3952.

Universiti Malaya

Lee, K. T., & Cho, J. (2011). Roles of nanosize in lithium reactive nanomaterials for lithium ion batteries. *Nano Today*, *6*(1), 28–41.

Lefèvre, G., Ducros, J. B., Nestoridi, M., Renard, F., Colin, J. F., Peralta, D., & Martinet, S. (2017). Cathode materials for high energy density lithium batteries. *E3S Web of Conferences*, *16*(111), 09002.

Levi, M. D., & Aurbach, D. (1997). Simultaneous measurements and modeling of the electrochemical impedance and the cyclic voltammetric characteristics of graphite electrodes doped with lithium. *Journal of Physical Chemistry B*, *101*(23), 4630–4640.

Liden, D., & Reddy, T. (2004). *Handbook of batteries* (3rd edition). McGraw-Hill.

LISICON - Solid electrolyte example : Lithium cobalt oxide – $LiCoO_2$ (2020). Retrieved on 2020 from https://www.chemtube3d.com/lib_lisicon-2/.

Liu, G., Chen, H., Xia, L., Wang, S., Ding, L. X., Li, D., Xiao, K., Dai, S., & Wang, H. (2015). Hierarchical mesoporous/macroporous perovskite $La_{0.5}Sr_{0.5}CoO_{3-x}$ nanotubes: A bifunctional catalyst with enhanced activity and cycle stability for rechargeable lithium oxygen batteries. *ACS Applied Materials and Interfaces*, *7*(40), 22478–22486.

Liu, Q., Wang, S., Tan, H., Yang, Z., & Zeng, J. (2013). Preparation and doping mode of doped $LiMn_2O_4$ for Li-ion batteries. *Energies*, *6*(3), 1718–1730.

Lv, D., Xu, T., Saha, P., Datta, K., Netl, U. S. D. O. E., Division, M. P., & Virginia, W. (2013). A scientific study of current collectors for Mg batteries in $Mg(AlCl_2EtBu\ )_2$ / THF electrolyte. *Journal of Electrochemical society*, *160*(2), 351–355.

Malavasi, L., Galinetto, P., Mozzati, M. C., Azzoni, C. B., & Flor, G. (2002). Raman spectroscopy of AMn_2O_4 (A = Mn, Mg and Zn) spinels. *Physical Chemistry Chemical Physics*, *4*(15), 3876–3880.

Malavasi, L., Ghigna, P., Chiodelli, G., Maggi, G., & Flor, G. (2002). Structural and transport properties of $Mg_{1-x}Mn_xMn_2O_{4\pm\delta}$ spinels. *Journal of Solid State Chemistry*, *166*(1), 171–176.

Mesallam, M., Sheha, E., Kamar, E. M., & Sharma, N. (2018). Graphene and magnesiated graphene as electrodes for magnesium ion batteries. *Materials Letters*, *232*,103-106.

Michalska, M., Lipińska, L., Mirkowska, M., Aksienionek, M., Diduszko, R., & Wasiucionek, M. (2011). Nanocrystalline lithium-manganese oxide spinels for Li-ion batteries - Sol-gel synthesis and characterization of their structure and selected physical properties. *Solid State Ionics*, *188*(1), 160–164.

Michalska, M., Ziółkowska, D. A., Jasiński, J. B., Lee, P. H., Ławniczak, P., Andrzejewski, B., & Lin, J. Y. (2018). Improved electrochemical performance of $LiMn_2O_4$ cathode material by Ce doping. *Electrochimica Acta*, *276*, 37–46.

Universiti Malaya

Mizuno, F., Singh, N., Arthur, T. S., Fanson, P. T., Ramanathan, M., Benmayza, A., & Guo, J. (2014). Understanding and overcoming the challenges posed by electrode/electrolyte interfaces in rechargeable magnesium batteries. *Frontiers in Energy Research*, *2*, 1–11.

Mizushima, K., Jones, P. C., Wiseman, P. J., & Goodenough, J. B. (1981). Li_xCoO_2 (0 < x ~< 1): A new cathode material for batteries of high energy density, *Solid State Ionics*, *3–4*, 171–174.

Mohtadi, R., & Mizuno, F. (2014). Magnesium batteries: Current state of the art, issues and future perspectives. *Beilstein Journal of Nanotechnology*, *5*(1), 1291–1311.

Mosa, J., & Aparicio, M. (2015). *The Sol-Gel Handbook:Sol-Gel Materials for Batteries and Fuel Cells* (1st edition). *3*, 1071–1118.

Muldoon, J., Bucur, C. B., & Gregory, T. (2014). Quest for nonaqueous multivalent secondary batteries: Magnesium and beyond. *Chemical Reviews*, *114*(23), 11683–11720.

Murgia, F. (2018). *P-block elements as negative electrode materials for Magnesium-ion batteries.* (Doctoral dissertation). Retrieved on 2018 from https://tel.archives-ouvertes.fr/tel-01759234/document.

Nadarzinski, K., (1999). TECNAI: the Concept for Modern TEM/STEM Analytical Systems. *Microscopy and Microanalysis*, *5*(S2), 342-343.

Nie, H. W., Wen, T. L., Wang, S. R., Wang, Y. S., Guth, U., & Vashook, V. (2006). Preparation, thermal expansion, chemical compatibility, electrical conductivity and polarization of $A_{2-\alpha}A'_{\alpha}MO_4$ ($A = Pr, Sm$; $A' = Sr$; $M = Mn, Ni$; $\alpha = 0.3, 0.6$) as a new cathode for SOFC. *Solid State Ionics*, *177*, 1929–1932.

Nishi, Y. (2001). The development of lithium ion secondary batteries. *Chemical Records*, *1*(5), 406–413.

Nitta, N., Wu, F., Lee, J. T., & Yushin, G. (2015). Li-ion battery materials: Present and future. *Materials Today*, *18*(5), 252–264.

Orikasa, Y., Masese, T., Koyama, Y., Mori, T., Hattori, M., Yamamoto, K., … Uchimoto (2014). High energy density rechargeable magnesium battery using earth-abundant and non-toxic elements. *Scientific Reports*, *4*, 1–6.

Padhi, A., Nanjundaswamy, K. & Goodenough, J., (1997). Phospho-olivines as positive-electrode materials for rechargeable lithium batteries. *Journal of The Electrochemical Society*, *144*(4), 1188-1194.

Prabaharan, S. R. S., Michael, M. S., Ikuta, H., Uchimoto, Y., & Wakihara, M. (2004). Li_2NiTiO_4 - A new positive electrode for lithium batteries: Soft-chemistry synthesis and electrochemical characterization. *Solid State Ionics*, *172*(1-4), 39–45.

Universiti Malaya

Purwamargapratala, Y., Sujatno, A., Sabayu, Y. L., & Kartini, E. (2019). Synthesis of $Li_4Ti_5O_{12}$ (lto) by sol-gel method for lithium ion battery anode. *IOP Conference Series: Materials Science and Engineering*, *553*(1). doi:10.1088/1757-899X/553/1/012062.

Qu, L., Li, M., Bian, L., Du, Q., Luo, M., Yang, B., Yang, L., Fang, S., & Liu, Y. (2017). A strontium-doped Li_2FeSiO_4/C cathode with enhanced performance for the lithium-ion battery. *Journal of Solid State Electrochemistry*, *21*(12), 3659–3673.

Rahman, M. F., Gerosa, D., & Mancinelli, V. (2015). Synthesis and characterization of cathode material for rechargeable magnesium battery technology, *Optoelectronics and Advanced Materials*, *9*(9), 1204–1207.

Saha, P., Datta, M. K., Velikokhatnyi, O. I., Manivannan, A., Alman, D., & Kumta, P. N. (2014). Rechargeable magnesium battery: Current status and key challenges for the future. *Progress in Materials Science*, *66*, 1–86.

Sarkar, S., & Jou, Y. C. (2002). Adaptive control of the reverse link in cdma2000. *International Journal of Wireless Information Networks*, *9*(1), 55–70.

Satyavani, T. V. S. L., Srinivas Kumar, A., & Subba Rao, P. S. V. (2016). Methods of synthesis and performance improvement of lithium iron phosphate for high rate Li-ion batteries: A review. *Engineering Science and Technology, an International Journal*, *19*(1), 178–188.

Scanning electron microscopy (1968). Retrieved from https://www.biosciencenotes.com/scanning-electron-microscope-sem/.

Shafey, A. M. E. (2018). Enhancing the performance and life cycle of lithium–sulfur batteries by nanostructured carbon and different additives. *International Journal of Innovative Research and Development*, *7*(8), 28–54.

Shannon, R. D., & Prewitt, C. T. (1969). Effective ionic radii in oxides and fluorides. *Acta Crystallographica Section B Structural Crystallography and Crystal Chemistry*, *25*(5), 925–946.

Shiga, T., Hase, Y., Kato, Y., Inoue, M., & Takechi, K. (2013). A rechargeable non-aqueous Mg-O_2 battery. *Chemical Communications*, *49*(80), 9152–9154.

Shiu-Sing T. (2020). Atomic world - transmission electron microscope (TEM) - Principle of TEM. Retrieved from Http://Www.Hk-Phy.Org/Atomic_World/Tem/Tem02_E.Html.

Shuzhong, L. I., Chao, L. I., Yanliung, F. A. N., Jiagiung, X. U., Tao, W., & Shuting, Y. (2006). Electrochemical performance of $LiFePO_4$, cathode material for Li-ion battery. *Rare Metals*, *25*, 62–66.

Sinha, N. N., & Munichandraiah, N. (2008). Electrochemical conversion of $LiMn_2O_4$ to $MgMn_2O_4$ in aqueous electrolytes, *Electrochemical and Solid State Letter*, *11*(11), F23–F26.

Universiti Malaya

Sinha, N. N., Ragupathy, P., Vasan, H. N., & Munichandraiah, N. (2008). Electrochemical characterization of submicron size particles of $LiMn_2O_4$ in aqueous electrolytes, *International Journal of Electrochemical Science, 3*, 691–710.

Son, S., Gao, T., Harvey, S., Steirer, K., Stokes, A., Norman, A., Wang, C., Cresce, A., Xu, K. & Ban, C., (2018). An artificial interphase enables reversible magnesium chemistry in carbonate electrolytes. *Nature Chemistry*, *10*(5), 532-539.

Spotnitz, R. (2003). Simulation of capacity fade in lithium-ion batteries. *Journal of Power Sources*, *113*(1), 72–80.

Sufri, M., & Kamarulzaman, N. (2018). Comparative study between supported and doped MgO catalysts in supercritical water gasification for hydrogen production. *International Journal of Hydrogen Energy*, *44*(7), 3690–3701.

Suib, S. L. (2008). Structure, porosity, and redox in porous manganese oxide octahedral layer and molecular sieve materials. *Journal of Materials Chemistry*, *18*(14), 1623–1631.

Sun, J., & Jiang, Z. (2014). Synthesis of $MgMnSiO_4$ and its application as cathode material for magnesium battery. *Journal of New Materials for Electrochemical Systems*, *17*(1), 9–11.

Sun, X., Bonnick, P., Duffort, V., Liu, M., Rong, Z., Persson, K. A., Ceder, G., & Nazar, L. F. (2016). A high capacity thiospinel cathode for Mg batteries. *Energy and Environmental Science*, *9*(7), 2273–2277.

Sutin, N., & Gütlich, P. (1985). Comments® on inorganic chemistry: A journal of critical discussion of the current literature. *Comments on Inorganic Chemistry*, *4*(4), 263-282.

Sutto, T. E., & Duncan, T. T. (2012). Electrochemical and structural characterization of Mg ion intercalation into RuO_2 using an ionic liquid electrolyte. *Electrochimica Acta*, *79*, 170–174.

Taleghani, S. T., Marcos, B., Zaghib, K., & Lantagne, G. (2017). A study on the effect of porosity and particles size distribution on Li-ion battery performance. *Journal of The Electrochemical Society*, *164*(11), E3179–E3189.

Tang, Y., Zheng, S., Xu, Y., Xiao, X., Xue, H., & Pang, H. (2018). Advanced batteries based on manganese dioxide and its composites. *Energy Storage Materials*, *12*, 284–309.

Tao, S., Huang, W., Liu, Y., Chen, S., Qian, B., & Song, L. (2018). Three-dimensional hollow spheres of the tetragonal-spinel $MgMn_2O_4$ cathode for high-performance magnesium ion batteries. *Journal of Materials Chemistry A*, *6*(18), 8210–8214.

Tarte, P. (1967). Isomorphism and polymorphism of the compounds Li_3PO_4, Li_3AsO_4 and Li_3VO_4. *Journal of Inorganic and Nuclear Chemistry*, *29*(4), 915–923.

Universiti Malaya

Truong, Q. D., Devaraju, M. K., & Honma, I. (2017). Nanocrystalline $MgMnSiO_4$ and $MgCoSiO_4$ particles for rechargeable Mg-ion batteries. *Journal of Power Sources*, *361*, 195–202.

Truong, Q. D., Kempaiah Devaraju, M., Tran, P. D., Gambe, Y., Nayuki, K., Sasaki, Y., & Honma, I. (2017). Unravelling the surface structure of $MgMn_2O_4$ cathode materials for rechargeable magnesium-ion battery. *Chemistry of Materials*, *29*(15), 6245–6251.

Wang, Lei, Zhang, Y., Guo, H., Li, J., Stach, E. A., Tong, X., Takeuchi S. E., Takeuchi K. J., Liu, P., Marshilock, C. A., & Wong, S. S. (2018). Structural and electrochemical characteristics of Ca-Doped "flower-like" $Li_4Ti_5O_{12}$ motifs as high-rate anode materials for lithium-ion batteries. *Chemistry of Materials*, *30*(3), 671–684.

Wang, Lu, Vullum, P. E., Asheim, K., Wang, X., Svensson, A. M., & Vullum-Bruer, F. (2018). High capacity Mg batteries based on surface-controlled electrochemical reactions. *Nano Energy*, *48*(2), 227–237.

Wang, W., Liu, H., Wang, Y., Gao, C., & Zhang, J. (2013). Effects of chromium doping on performance of $LiNi_{0.5}Mn_{1.5}O_4$ cathode material. *Transactions of Nonferrous Metals Society of China (English Edition)*, *23*(7), 2066–2070.

Whittingham, M. S. (2004). Lithium batteries and cathode materials. *Chemical Reviews*, *104*(10), 4271–4301.

Wieboldt, D., & Hahn, M. (n.d.). In situ Raman Analysis of Lithium Ion Batteries. *ThermoScientific Application Note*, 52676.

Wikipedia. (2014). BET theory. *Wikipedia*. Retrieved on 2014 from https://en.wikipedia.org/wiki/BET_theory.

Williard, N., He, W., Hendricks, C., & Pecht, M. (2013). Lessons learned from the 787 dreamliner issue on Lithium-Ion Battery reliability. *Energies*, *6*(9), 4682–4695.

Wu, Q., Thiben, A., & Jaegermann, W. (2002). Electronic structure of $LiMn_2O_4$, 585–590.

Wu, X., Li, Y., Xiang, Y., Liu, Z., He, Z., Wu, X., Li, Y., Xiong, L., Li, C., & Chen, J. (2016). The electrochemical performance of aqueous rechargeable battery of $Zn/Na_{0.44}MnO_2$ based on hybrid electrolyte. *Journal of Power Sources*, *336*(December), 35–39.

Xia, H., Luo, Z., & Xie, J. (2012). Nanostructured $LiMn_2O_4$ and their composites as high-performance cathodes for lithium-ion batteries. *Progress in Natural Science: Materials International*, *22*(6), 572–584.

Yang, Z., Gu, L., Hu, Y.-S., & Li, H. (2017). Atomic-scale structure-property relationships in lithium ion battery electrode materials. *Annual Review of Materials Research*, *47*(1), 175–198.

Universiti Malaya

Yin, J., Brady, A. B., Takeuchi, E. S., Marschilok, A. C., & Takeuchi, K. J. (2017). Magnesium-ion battery-relevant electrochemistry of $MgMn_2O_4$: Crystallite size effects and the notable role of electrolyte water content. *Chemical Communications*, *53*(26), 3665–3668.

Yoo, H. D., Shterenberg, I., Gofer, Y., Gershinsky, G., Pour, N., & Aurbach, D. (2013). Mg rechargeable batteries: An on-going challenge. *Energy and Environmental Science*, *6*(8), 2265–2279.

Younesi, R., Malmgren, S., Edström, K., & Tan, S. (2014). Influence of annealing temperature on the electrochemical and surface properties of the 5-V spinel cathode material $LiCr_{0.2}Ni_{0.4}Mn_{1.4}O_4$ synthesized by a sol-gel technique. *Journal of Solid State Electrochemistry*, *18*(8), 2157–2166.

Zainol, N., Hambali, D., Osman, Z., Kamarulzaman, N. & Rusdi, R., (2018). Synthesis and characterization of Ti-doped $MgMn_2O_4$ cathode material for magnesium ion batteries. *Ionics*, *25*(1), 133-139.

Zhao, E., Chen, M., Hu, Z., Xiao, X., & Chen, D. (2016). Layered/layered homostructure ion conductor coating strategy for high performance lithium ion batteries. *Electrochimica Acta*, *208*, 64–70.

Zhao, F., Wang, S., Brinkman, K., & Chen, F. (2010). Layered perovskite $PrBa_{0.5}Sr_{0.5}Co_2O_{5+\delta}$ as high performance cathode for solid oxide fuel cells using oxide proton-conducting electrolyte. *Journal of Power Sources*, *195*(17), 5468–5473.

Zhao, H., Liu, L., Xiao, L., Hu, Z., Han, S., Liu, Y., Chen, D., & Liu, X. (2015). The effects of Co doping on the crystal structure and electrochemical performance of $Mg(Mn_{2-x}Co_x)O_4$ negative materials for lithium ion battery. *Solid State Sciences*, *39*, 23–28.

Universiti Malaya